Hiroshima University Doctoral Thesis

Study on Relationship between Very Low-Frequency Earthquake and Non-Volcanic Tremor in the Nankai Subduction Zone

(南海沈み込み帯における超低周波地震と非火山性微動の関係に関する研究)

2017

Department of Earth and Planetary Systems Science
Graduate School of Science
Hiroshima University

RASHA AMER

Table of Contents

Main Thesis

Study on Relationship between Very Low-frequency Earthquake and Non-volcanic Tremor in the Nankai Subduction Zone
(南海沈み込み帯における超低周波地震と非火山性微動の関係に関する研究)
Rasha Amer
Accepted for the publication in *Journal of Science of the Hiroshima University, Series C (Earth and Planetary Sciences*), **Volume 12***,* No. 1

Main Thesis

Study on Relationship between Very Low-frequency Earthquake and Non-volcanic Tremor in the Nankai Subduction Zone
(南海沈み込み帯における超低周波地震と非火山性微動の関係に関する研究)

A Dissertation
by
Rasha Amer

Submitted to the Earth and Planetary Systems Science,
Graduate School of Science, Hiroshima University
in fulfillment of the requirements for the degree of

DOCTOR OF SCIENCE

July 2017

Abstract

Continuous observations of repetitive seismic phenomena provide valuable information for understanding the nature and origin of these phenomena. It is difficult to observe many seismic cycles of large earthquakes because of their long recurrence intervals. However, episodic slow earthquakes, which contain slow slip events, very low-frequency earthquakes (VLFE) and nonvolcanic tremor (NVT), have recurrence intervals of several months. They occur in down-dip extension of the seismogenic zone on subducting plate interface, and are observed in subduction zones around the world especially in southwest Japan. The slow earthquakes significantly occur in the south-west Japan, thus the knowledge of the relationship between slow earthquakes types in this region would be applicable to the other subduction zone in the world. In the result, slow earthquakes observations as well as understanding their mechanisms would be important contribution towards regular earthquake prediction in subduction zones especially earthquakes prediction in Nankai Trough, which recorded occurrences of large earthquakes with estimated magnitudes as large as 8 along the trough and has been well documented in historical materials with recurrence periods are fairly constant, and are approximately from 100 to 150 years. Therefore, we have undertaken a multifaceted study of VLFE and NVT in the Shikoku region along Nankai Trough for episodic activities of slow earthquakes in 2006, 2007 and 2011-2015.

In this study, we detected VLFE in major tremor episodes using a new method. We then studied the spatio-temporal relationship between VLFE and NVT. First, we developed a new detection method for VLFE that occurred in the Shikoku region of the Nankai subduction zone, southwest Japan. The newly developed method could be applicable to a real-time, automatic monitoring system for VLFE in the future. The results showed that our method has a high capability of VLFE detection: we could detect small events that the conventional method could not detect. Then we could increase the detection number by using a dense virtual source grid.

Our new detection method depended on calculating the average cross-correlation between observed and Synthetic seismogram for all the source grids. We applied this method by using data from Hi-net stations in Nankai trough. In addition, to increasing the detection number and spatial distribution, we found that VLFEs are located near the plate interface in the zone where tremors are observed and they associate with tremor activity in most cases in time and space, we also found

that tremor and very low-frequency earthquakes not associate in space and time in all cases and their characteristics are not correlated. This suggestion challenges our previous understanding of the spatiotemporal correlation between NVT and VLFE, but we need to study this point in detail in the future to confirm these VLFE events (the events which not correlated with tremor) are real activities. We also noticed that at the same time as Rapid Tremor Reversal (RTR), VLFEs also migrate rapidly back in the opposite direction of the source movement.

This study gives a clear understanding of the characteristics of the slow earthquakes in Southwest Japan. The results bring insight into the processes responsible for the occurrence of regular small and large earthquakes in the region that might help the seismological community to develop better earthquake forecasting models in the future in Nankai and other subduction zones around the world.

Acknowledgments

Firstly, I would like to express my sincere gratitude to my advisor Prof. Naoki Suda for the continuous support of my Master and Ph.D. study and related research, for his patience, motivation, and immense knowledge. His guidance helped me in all the time of research and writing of this thesis. I would like to thank you for encouraging my research and for allowing me to grow as a research scientist. Your advice on both research as well as on my career have been priceless. I could not have imagined having a better advisor and mentor for my graduate studies.

Besides my advisor, my sincere thanks and special appreciation go to prof. Ishihara for his financial support.

I would like to thank the rest of my thesis committee for their insightful comments and encouragement.

I would like to express my special thanks to my second advisor Prof. Katayama for encouraging my research, also for the hard questions which he usually asks and which incented me to widen my research from various perspectives.

I would like to express my special appreciation to Prof.Ando for his kindness, encouraging me and the precious support.

My sincere thanks also go to my laboratory teachers Dr.Nakauki and Dr.Kita who gave precious support and also for my lab mates friends for the good times and help.

I thank all my department teachers, students and members for all the help, support and good times I spend with you during 6 years of my life in this department.

Special thanks to my family. Words cannot express how grateful I am to my mother, father, my sister, my brother- in law and my brothers for all the sacrifices that you've made on my behalf. Your prayer for me was what sustained me thus far. I would also like to thank all my friends in Japan, Syria and around the world (too many to list here but you know who you are!) who supported and incented me to strive towards my goal. At the end, I would like express appreciation to my beloved husband Osama who spent 6 years with me in Japan and sacrifice his job in Syria, he was always my support in the moments when there was no one by my side.

To my wonderful son Taim: maybe you still very small to read this, but one day I hope you read, you were the best present for me from God, whenever I was down you raised me up with your innocent smile, you gave me a precious support to finish this work. As we used to sing together (where there's a will there's a way) just remember this…

الحمدلله رب العالمين الذي قدر لي هذا واعطاني من نعمه ما لايعد ولا يحصى
اقدم شكري الى من علماني اول الحروف الى امي الغالية التي سهرت وتعبت و لها الفضل الاول في نجاحي و ابي المكافح الذي بذل حياته لاجلنا وايضا الى اختي الغالية علا و صهري حكمت و لاخوتي الاعزاء علاء و بهاء على دعمهم ووقوفهم الى جانبي, بشكل خاص اخي و صديقي الحبيب بهاء
الى اصدقائي في اليابان و سوريا و في انحاء العالم شكرا من القلب للطفكم و مساندكم واعتذر لانه لامجال لذكر الاسماء
شكري الخاص لزوجي الغالي اسامة الذي قدم لي ما لايقدر بثمن و لعائلته الكريمة
ابني الحبيب تيم, بابتسامتك الجميلة و طفولتك الشقية استطعت ان تدعمني و تعطيني القوة لاستمرار رغم كل الظروف القاسية, شكرا لوجودك في حياتي و مساندتي لاتمام هذا العمل...

I dedicate this thesis to his soul ... to my dear brother and best friend "Kanj" who I lost in November 2015 in the war, and I don't know if he still alive or not. The last words he said to me in Damascus airport 2010 while I was very worried to come to Japan:

“I trust you can do it, you will succeed”

He encouraged and supported me all the time before I lost him in the real life, and his words encouraged me all the time during this work and will live in my heart forever ... So, I dedicate this work to him ...

أهدي هذا العمل وهذا النجاح ل روح أخي و صديقي الغالي كنج أينما كان
كنج كان من شجعني على متابعة دراستي في اليابان بينما كنت متخوفة من السفر
كانت اخر مرة رايته فيها في مطار دمشق ٢٠١٠ وودعني باخر الكلمات
(رح تنجحي و ما بكفي نجاح بدنا تفوق)
اليوم و قد حصلت على شهادة الدكتوراه بفضل من الله و رضا الوالدين
اهدي هذا النجاح ل كنج الذي وقف بجانبي في كل لحظة قبل أن تغيبه الحرب في تشرين الثاني
٢٠١٥ و ظل مرافقا لي في عقلي و قلبي و في كل خطوة في هذا العمل
و كانت كلماته حافزا لي للإستمرار رغم كل الصعوبات
ستبقى دائما" رفيق الدرب و النجاحات و لن تغيب

Table of Contents

Table of Figures

Chapter 1

Introduction

Slow earthquakes have been observed in major plate boundaries worldwide, and accommodate a significant part of the plate motion through the slow slip in the transition zone of the faults. They occur down-dip of the locked zone, where large damaging fast earthquakes nucleate. The physical processes that control slow quakes, however, remain unclear, Various types of slow earthquakes (e.g., nonvolcanic tremor (NVT), very low frequency earthquake (VLF), and slow slip events (SSE) [e.g., Schwartz and Rokosky, 2007] that have been discovered in the last two decades_ and characterized as earthquake low frequency component have a long duration compared to normal earthquake of the same scale_ Recently slow earthquakes were detected as interpolate phenomena in subduction zones, formed by interactions between a descending oceanic plate and an overlying continental plate. [Obara et al., 2011]. Knowledge of slow earthquakes' types is useful for understanding subduction processes and the occurrence mechanisms of large earthquakes. Deep slow earthquakes occur more frequently than large earthquakes, and usually, they have recurrence intervals or return period in the hundreds of years. Therefore, slow earthquakes can contribute to our understanding of megathrust earthquake processes. For example, in the Nankai Trough which runs on the coast of the southwestern part of Japan, where the Philippine Sea Plate subducting beneath the overriding Eurasian Plate in the northwest direction at a rate of approximately 4.5 cm/yr. [Seno et al., 1993], as shown in Fig 1.1, magnitude 8 earthquakes recurred at intervals of 100–150 yrs. [Ando, 1975] have been reported. For this reason, studying the different slow earthquakes types and the relationship between them in this region is very important. This study will be applicable in all subduction zones for the same goal.

In this dissertation, I undertake to describe our accurate method for VLFEs detection which we applied in southwest Japan Shikoku region as well as to explain the VLFEs detection results relationship with tremor activity occurred in the same region and period which detected by Automatic Tremors Monitoring System (ATMOS) [Suda et al., 2009].

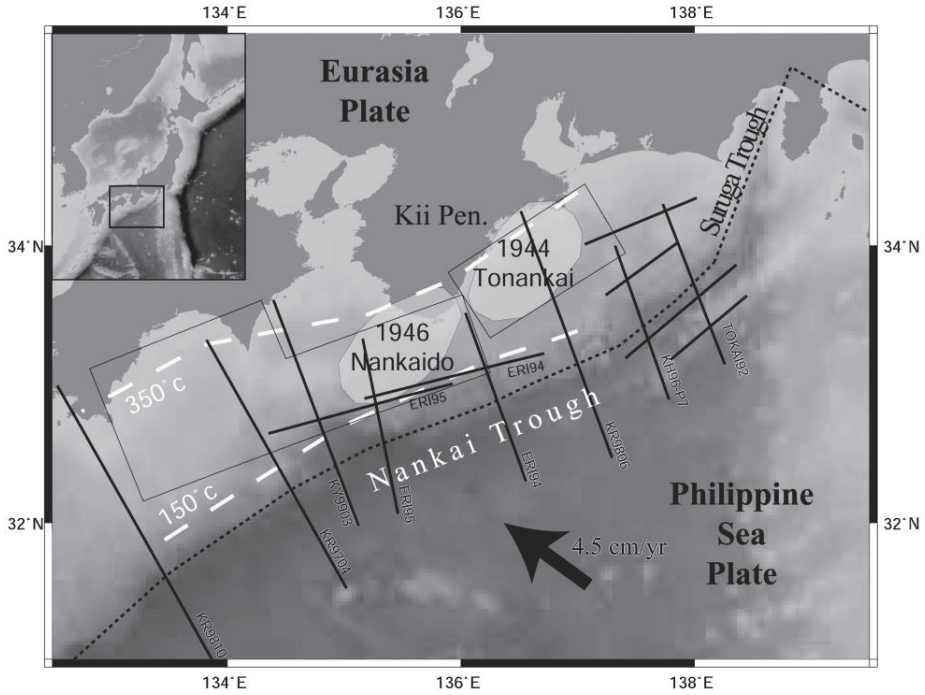

Figure 1.1: Location of the Nankai Trough. Solid black thick lines are profiles of seismic surveys. Gray-shaded ellipsoidal regions around the tip of the Kii Peninsula are the regions of aftershocks one day after the corresponding 1944 Tonankai and 1946 Nankaido earthquakes, and the surrounding thin black polygons are fault plane solutions (Ando, 1973). White dashed lines are 150 and 350 isotherms estimated by Hyndman et al. (1995). A large arrow indicates the direction of subduction of the Philippine Sea Plate at a speed of about 4.5 cm/yr (Seno et al., 1993). The original of this figure is Fig. 1 of Mochizuki and Obana (2003).

In southwest Japan, recent developments in seismic observations have enabled the discovery of slow earthquakes types, as well as the occurrence of small anomalous lower frequency earthquakes, along the Nankai subduction zone; these earthquakes have been detected are smaller than the megathrust earthquakes that are characteristic of this region. Nonvolcanic, deep low-frequency tremors and earthquakes (predominant frequencies near 0.5 s [Obara, 2002; Katsumata and Kamaya, 2003], very low frequency (VLF) earthquakes (predominant frequencies 20–200 s) [Ito et al., 2007; Ide et al., 2008], and short-term slow slip events (source duration 2–5 days) [Obara et al., 2004; Hirose and Obara, 2006] are known to occur simultaneously along the subducting plate interface.

Deep non-volcanic low-frequency tremors (NVT) that were discovered [Obara 2002] along the Nankai Trough, Japan is the most common form of slow earthquakes. [e.g., Sweet et al., 2014]; These NVT's were observed as well as very low-frequency earthquakes (VLFEs) in the Nankai Trough subduction zone are shown in Fig 1.2. Deep tremor consists of intermittent weak signals at relatively low frequency (1–8 Hz) that last as long as days to a few weeks once activity begins. epicenters of the tremors were distributed along the strike of the subducting Philippine Sea plate over a length of 600 kilometers. The depth of the tremors averaged about 30 kilometers, near the Mohorovic discontinuity. The location of the tremors within the subduction zone indicates that the tremors may have been caused by fluid generated by dehydration processes from the slab. [Obara 2002] The source of tremor is located near the down-dip limit of megathrust earthquakes in a belt-like distribution, suggesting the potential interaction with large interplate earthquakes. Many aspects of tremor, such as periodicity and migration, have been reported [Obara and Hirose, 2006]; deep tremor is already known to have several migration properties; one is migration of major activity accompanying a detectable large slow slip event [e.g. Rogers and Dragert, 2003; Obara et al., 2004], and another is minor but fast migration rapid tremor reversal (RTR) [Houston et al., 2011].

Very low-frequency (VLF) seismic signals observed in southwestern Japan are evidently radiated from shear slips on the upper surface of the subducting Philippine Sea Plate [Yoshihiro Ito et al, 2009]. Very low-frequency earthquakes (VLFEs) whose spectra have peak frequencies between 0.02 and 0.1 Hz occur in the shallow and deep transition zones on the updip and downdip sides of the seismogenic zone, respectively [Obara, 2011]. Shallow VLFEs are concentrated in clusters and are aligned on the landward side of the Nankai Trough [Obara and Ito, 2005], whereas deep VLFEs on the downdip side of the seismogenic zone are clustered in a belt-like tremor zone [Ito et al., 2007] [Akiko To, 2015]. VLFEs have been studied in the Nankai and off-Tokachi regions, Japan [e.g., Obara et al., 2004; Obara and Ito, 2005; Ito et al., 2007; Asano et al., 2008, 2015]. VLFEs have also been reported in the Ryukyu Trench [Ando et al., 2012; Nakamura and Sunagawa, 2015], Costa Rica [Walter et al., 2013], and Cascadia [Ghosh et al., 2015]. These observations suggest that VLFEs may be widely occurring events in subduction zones. Obara et al. 2004 studied VLFEs in the off-Tokachi region near the Kuril Trench and inferred that they are events on the shallow subducting plate boundary. Ito and Obara 2006 suggested that VLFEs close to the trench axis in the Nankai region may occur within the accretionary prism, based on centroid moment tensor (CMT) analysis using inland seismic stations. Ito et al. 2007 reported that VLFEs also occur at the downdip region of megathrust earthquakes in Nankai and accompany active deep low-frequency tremors and slow slip events.

Therefore, in the Nankai region, there exist both shallow VLFEs close to the trench axis and deep VLFEs at the downdip part of the seismogenic zone. A recent study with ocean-bottom seismometers showed that shallow VLFEs off the Kii Peninsula in the Nankai region occur around décollement [Sugioka et al., 2012; Matsuzawa et al., 2015].

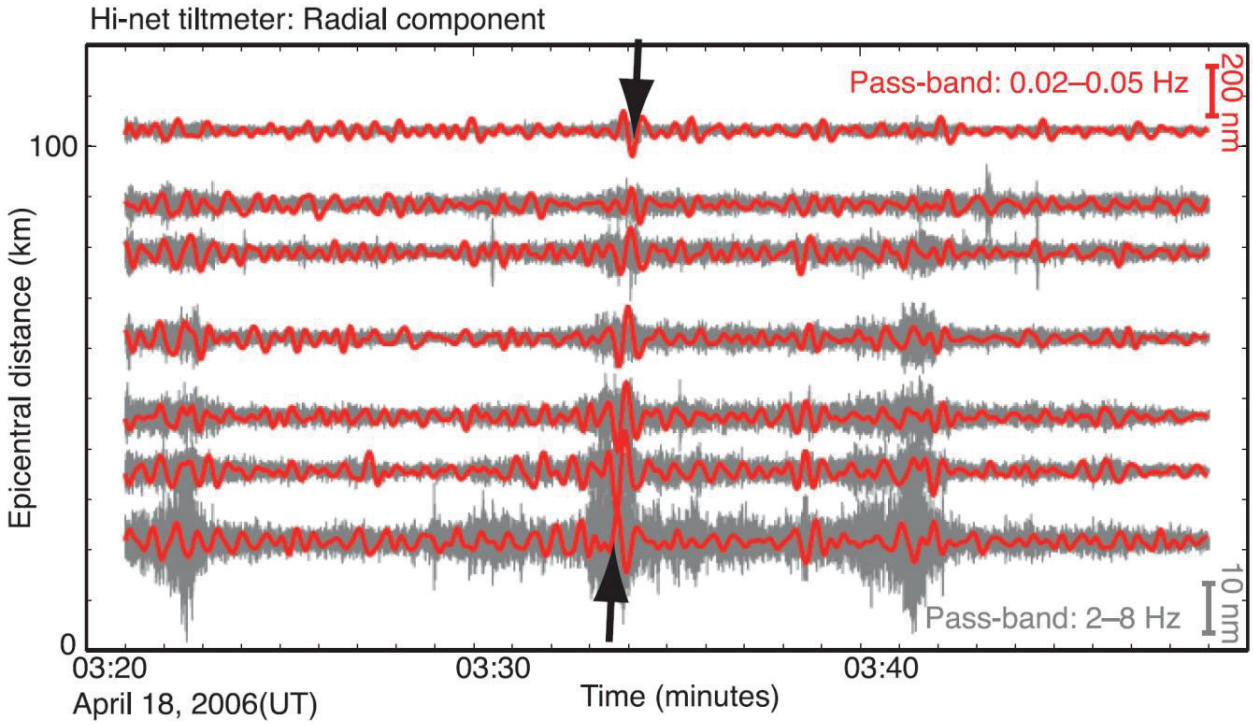

Figure 1.2: Sample seismograms of a VLF earthquake at selected sites. Radial components at seven Hi-net stations are shown. The observed waveforms are arranged in epicentral distance order from an estimated source location. The red traces indicate to VLFEs signal and black traces represent the tremor signal. The red and black represent the observed waveforms filtered for bands of 0.02 to 0.05 Hz and 2 to 8 Hz, respectively. The vertical bars on the right indicate the displacement amplitudes. The original of this figure is Fig. 1. [Ito, 2007].

Previous studies reported relationships between slow earthquakes various types occurrences Figure1.3. The short-term slow slip events which have been repeatedly observed with recurrence intervals of 3–6 months and they are shorter intervals than those of ordinary earthquakes with the same moment magnitudes [Obara and Hirose, 2006]. occur simultaneously in the transition zone from locked to aseismic slips at the downdip portion of the Nankai subduction zone in southwest Japan with Nonvolcanic deep low-frequency tremors, Deep low-frequency tremors predominantly show frequencies near 0.5 s, suggesting that the characteristic time scale of the rupture duration is on the order of 1 s, Deep low-frequency tremors and slow slip events in Japan have been detected by the seismic network of the National Research Institute for Earth Science and Disaster Prevention (NIED) [Ito et al ., 2007].

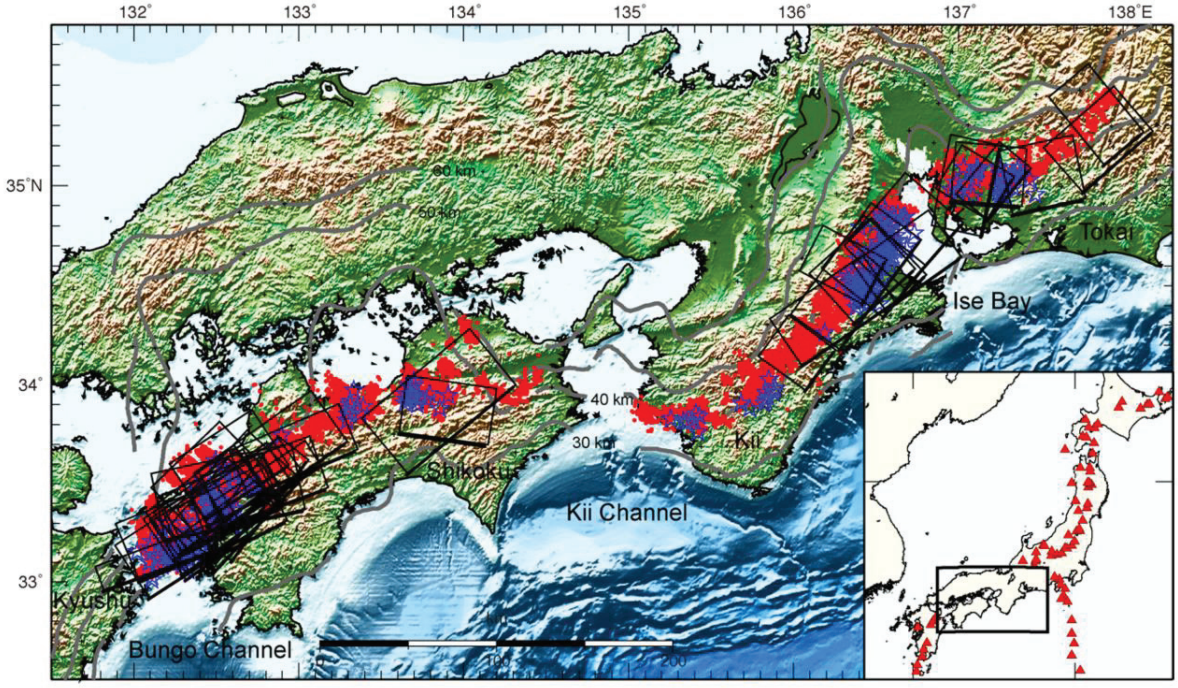

Figure 1.3: Spatiotemporal distribution of ETS (episodic tremor and slip) events: non-volcanic tremor, deep VLF (very-low-frequency) earthquakes, and short-term SSEs (slow slip events) along strike of the Nankai subduction zone in southwest Japan. Red circles and blue stars indicate tremor [Obara et al., 2010] and deep VLF earthquakes (Ito et al., 2009), respectively. Squares indicate short-term SSE fault planes, estimated from ground tilting data recorded at Hi-net stations [Sekine et al., 2010]; thick sides of the square represent the upthrown side of the fault. gray contours represent the depth of the Moho discontinuity. The original of this figure is Fig. 1 of Obara, (2011).

Also, deep tremor under Shikoku, Japan, consists primarily, and perhaps entirely, of swarms of low-frequency earthquakes (LFEs) that occur as shear slip on the plate interface. Although tremor is observed at other plate boundaries, the lack of cataloged low-frequency earthquakes has precluded a similar conclusion about tremor in those locales. [Brown.JR et al., 2009]

In addition, non-volcanic tremors (NVT) have been observed together with signals in the very low frequency (VLF) band from 0.02 to 0.05 Hz, which have been identified as VLF events in limited regions of subduction zones. The Nankai VLFEs occur in similar locations to deep tectonic tremor during episodic tremor and slow slip [Ito et al., 2007], seismic signatures especially tremor and very low-frequency earthquakes (VLFEs) are, however, difficult to detect and locate and the relationship between them still unknown and needs more studies, especially recent studies in Cascadia reported that very low-frequency earthquakes and tremor are subject to asynchronous seismic cycles [Hutchison & Ghosh,2016]. which contrasting with previous findings where tremor and very low-frequency earthquakes have a clear spatiotemporal relationship and challenging our current understanding of the dynamic relationship between the different types of slow earthquakes and their relationship to slow slip.

Because the relationship between the slow earthquakes (include VLFEs and tremor) could improve our knowledge about their characteristic activity that might be linked to huge earthquakes and because the activities of VLFEs and their spatiotemporal distribution with tremor in southwest Japan we still need more studies although many automated waveform data processing systems have been developed that use waveform inversion techniques for VLFEs detection [Hirose et al., 2008]. Some studies tried to clarify the relationship between VLF and NVT around the world [e.g. in Cascadia Ghosh et al, 2015], For all these reasons, we did a systematic search for deep VLFEs in the southwest Japan using new detection method during an episodic tremor and then study their spatiotemporal relationship with tremor.

Our detection method for VLFEs is significantly accurate compared with the conventional method. Our method could detect small events with low magnitude which previous studies could not detect. This high accuracy allowed as to increase the detection number and spatial distribution for VLFEs thus, we have enough results that allowed us to study VLFEs spatial-temporal distribution with tremor in order to clarify the unknown relationship between the two phenomena, because the knowledge of this relationship could be important toward huge regular earthquakes prediction.

This dissertation comprises two main sections: First is new deep VLFEs detection method, and second is studying the relationship of VLFEs results (results of section one) with the nonvolcanic tremor results in the same data period and region (results of ATMOS).

Chapter 2 presents explanation about study area and the earthquakes history in it in addition to explanation about the data used for both VLFEs and NVT in this study, since we aimed to detect VLFEs in the southwest Japan during an episodic tremor in several time periods in

2006 and 2007 also we applied our method for several time periods in 2011- 2015 in Shikoku region as well as we tried our method in other regions in Tokai and Kii peninsula.

Chapter 3 presents the deep VLFEs detection method which depended on calculating the average cross-correlation (cc) between observed and Synthetic seismogram for all the source grids., in this chapter I explained in details three main steps first is to prepare the observation data, second is to prepare the synthetic seismogram and third is analysis the previous two steps which depend on compare the observed waveform with the synthetic one using cross-correlation and then calculate the variance reduction and decide the detection.

Chapters 4 focus on data analysis and results for each data period, were we detected and located VLFEs and estimated their source parameters by using our new method which could detect small events that the previous methods could not detect. First, we applied our method in 2006 and 2007 using virtual source grid with an interval of 10 km then for the same data period we used dense virtual source grid was very effective in increasing the VLFEs detection number and locate new events that previous studies could not locate. The obtained VLFEs were estimated to be distributed along the Shikoku region where the events occurred on the reverse faults.

Chapter 5 presented several trials in Shikoku region, Kii, and Tokai. First, we divided Shikoku region to Western and Eastern parts to save analytic time and increase the spatial distribution, then we tested our method in two periods for Kii and Tokai region, then we applied our method using dense virtual source grid in whole Shikoku region for data from 2011 to 2015.

Chapter 6 presents the observation for our results which represented in chapter 4 and chapter 5, and discuss in detail the VLFE detection number and moment release then compared with previous results and with NVT, as well we discussed the VLFE and NVT spatiotemporal relationship.

Chapter 7 summarizes the results presented in chapter 4 and 5 and interprets these results as well presents the final conclusions and discuss the possible future work to solve the sticking points.

Chapter 8 summarizes the important points presented in each chapter.

Chapter 2

Study Area and Data

2-1. Study area

The study area (Fig. 1.1 and1.3) is where the Philippine Sea plate subducts southwest Japan along the Nankai trough. Evidence for pre-seismic changes for the 1944 earthquake was obtained, along with the Nankai trough off Southwest (SW) Japan, Earthquakes in the SW Japan region occur to a depth of 200 km under Kyushu Island and 80 km beneath Shikoku and SW Honshu. Deeper earthquakes under this region take place within the subducting Pacific slab, which is located beneath the Eurasian plate and the subducting Philippine Sea slab [Liua .X et al.,2013]. Great earthquakes have historically occurred along the Nankai Trough, for example, the 1944 Showa-Tonankai and 1854 Ansei-Tokai earthquakes, the 1946 Showa-Nankai and 1854 Ansei-Nankai earthquakes, and the 1707 Hoei and other earthquakes. It has been said that they ruptured part or whole of characteristic fault planes. However, there are several enigmas for their occurrence. Therefor Nankai trough is very important seismic study area for earthquakes predictions studies, Although it is difficult to predicate and observe large earthquakes from this Historical earthquakes because of their long recurrence intervals, but recently scientists tried to connect large earthquakes with slow earthquakes which significantly occur in Nankai trough and observed by many studies, because the fault slip mechanism of slow earthquakes is the same as that of huge quakes, so slow earthquakes have been thought to be connected to huge megathrust earthquakes.[Obara et al 2016].

For those reasons, we chose to study slow earthquakes (very low-frequency earthquakes and tremor) in Nankai trough. In this study, the Locations of the VLFE events on the subducting Philippine Sea plate interface, while the Source mechanisms of the VLF events predetermined from the subducting plate surface geometry and the plate motion. First, we analyzed data from 73 stations which distribute along Shikoku region (Fig 2.1), then we divided Shikoku region to two areas western and eastern Shikoku (Fig 5.2 and 5.6 respectively), as well, we set virtual source grids and analysis data from 41 stations in Tokai region (Fig 5.12) and 43 stations in Kii Peninsula region (Fig 5.15).

2-2. Data

2-2-1. Data for very low-frequency earthquake

In this study, we analyzed seismic records (Hi-net) that operated by the National Research Institute for Earth Science and Disaster Prevention (NIED). We used three-component broadband seismograms recorded at 73 stations as shown in Figure 2.1 (a, b) for Shikoku region for the periods from 6 January to 22 September 2006, from 10 to 21 March 2007, from7 to 31 August 2011, from 1 to 16 July 2012, from 21 to 31 May 2013, from 1 to 31 May 2014, from 1 to 30 June 2014, from to 31 July 2014 and from 1 to 11 November 2015. Also from 10 to 21 March: for each region eastern Shikoku and Wester Shikoku (dividing Shikoku for two regions), for 41 stations from 1 to 5 September for Tokai and for 43 stations from 1 to 18 July for Kii Peninsula. All these periods correspond to episodic tremor where we expected to detect VLFEs based on the previous studies [e.g., Ito et al., 2007; Ghosh et al., 2015]. Stations distribution is shown in Figure 2.1 for the Shikoku region. While Figure 5.2 for western Shikoku, Figure 5.6 for Eastern Shikoku, Figure 5.12 for Tokai and Figure 5.15 for Kii Peninsula.

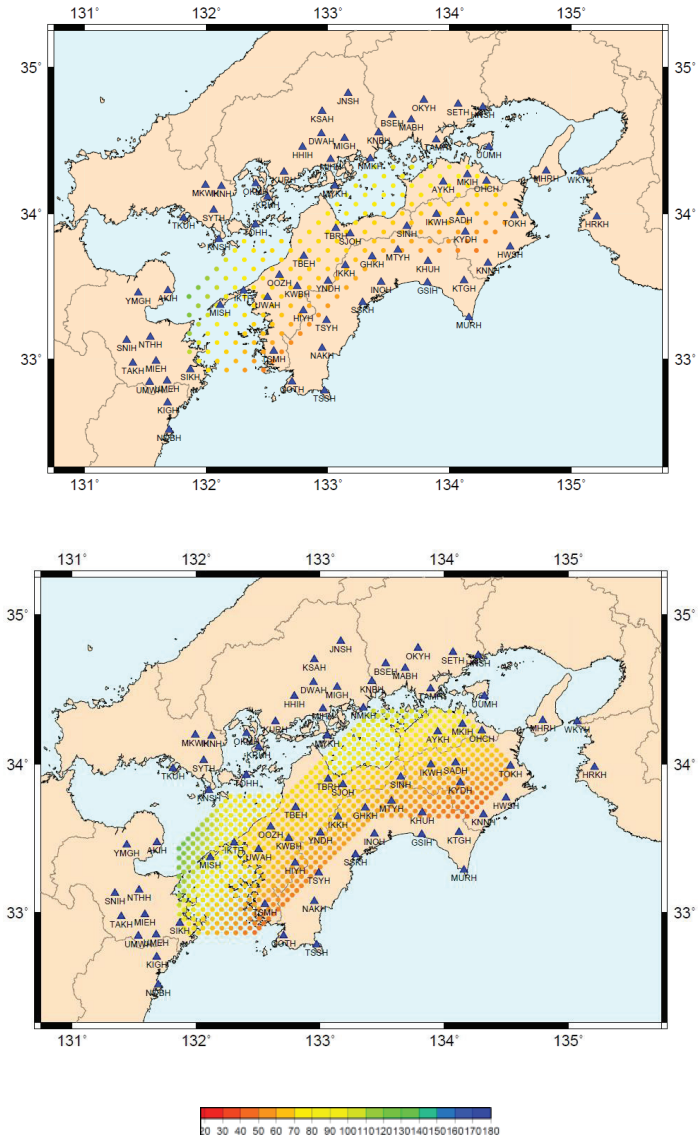

Figure 2.1: The main study area (Shikoku region) with the virtual sources grid (colored circles) and Hi-net stations (blue triangles). (a) virtual sources grid with a horizontal interval of 5 km. (b) virtual sources grid with a horizontal interval of 10 km. The color bar indicated to virtual sources depth which ranges from 10 km (red) to 80 km (blue) respectively**.**

2-2-2. Data for non-volcanic tremor

Studies at many plate boundary faults have shown that VLFEs and tremor are spatially and temporally coincident [Ide et al., 2007b; Ghosh et al., 2015]. So, we expected to detect VLFEs in tremor episodic and we chose our data where there are tremor activities, thus we can study the VLFEs and NVT relationship in details. We utilized NVT data from the results of the Tremors Automatic Monitoring System (ATMOS) published on the web: http://tremor.geol.sci.hiroshima-u.ac.jp/ [Suda et al, 2009].

Figure 2.2 is an example of tremor activity in one day for each panel (a and b) detected by ATMOS and used in this study.

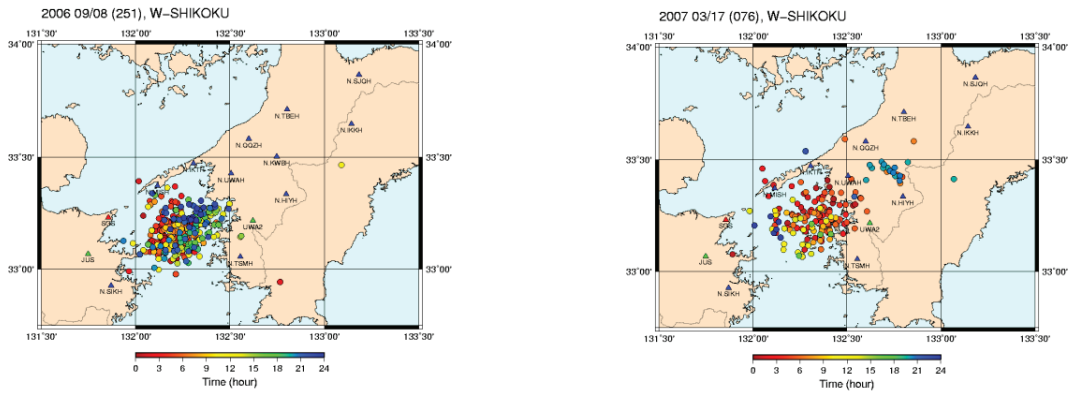

Figure 2.2: Epicenter maps examples showing tremor activity results by ATMOS [Suda at. el 2009] which used in this study. The circles represent the tremor epicenters, and the colors represent origin times (see color scale). (a) 8 September 2007, (b) 18 March 2007.

Chapter 3

Detection Method

3-1. Introduction

Until now, many studies that use inversion method to determine earthquake source mechanisms have been developed. For VLFEs, most studies used CMT analysis to locate VLFE and estimate the CMT solutions. [Ito et al., 2006, 2007, 2009] in which considerable number of small VLF events might be missed, while in this study we have developed a new method and implemented a new analysis to detect VLFE in Nankai trough, our new method depend on calculating the average cross-correlation (cc) between observed and Synthetic seismogram for all the source grids, thus this method contains 3 main steps as shown in Figure 3.1.The first step is to prepare the observation waveform, the second step is to prepare the synthetic seismogram and the final step is to analyze the final data by calculating the cross-correlation, the variance reduction (VR) and decide the final detection results of VLFEs.

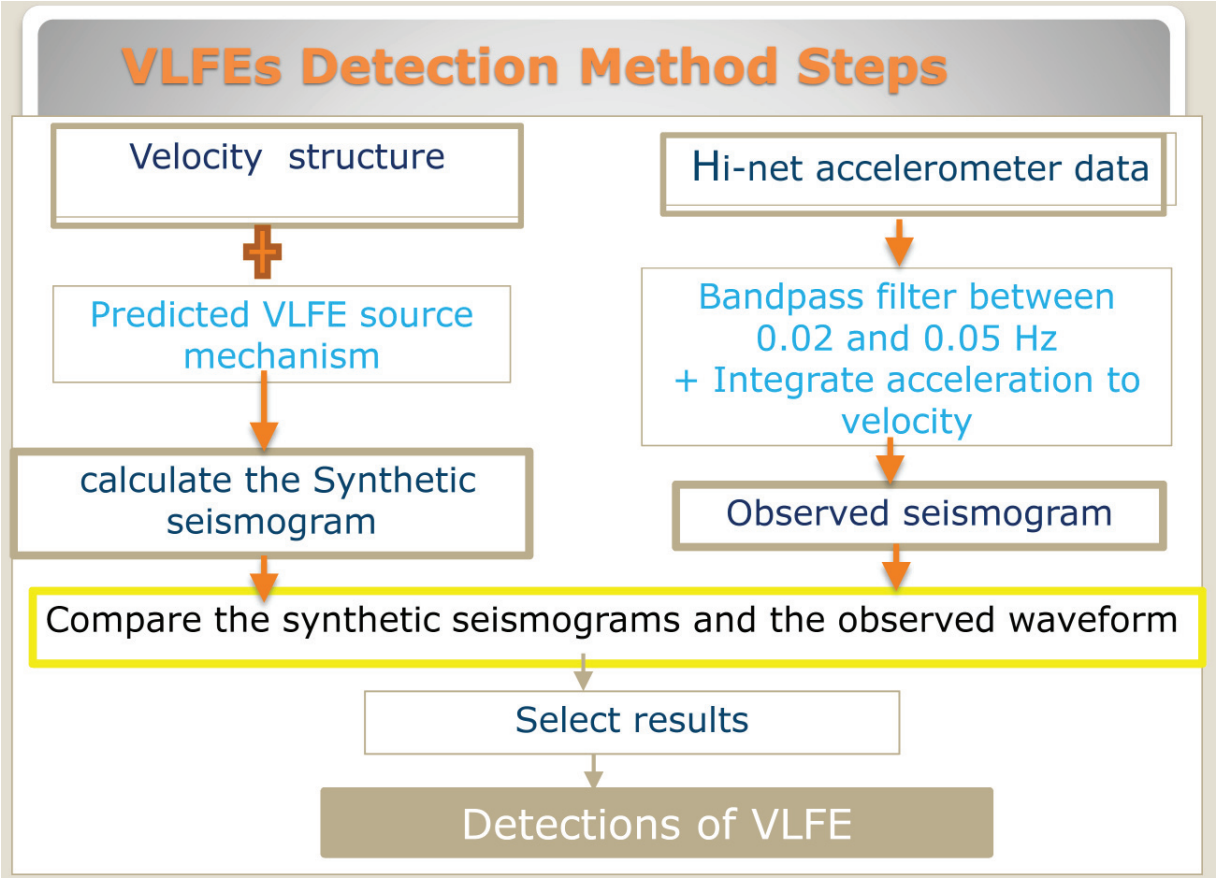

Figure 3.1: The detection steps of this method.

3-2. Obsorved seismograms

We prepared the observed waveforms by applying a band-pass filter with a passband from 0.02 to 0.05Hz to our Hi-net data, integrate the acceleration data to velocity. Figure 3.2 represents a comparison between a waveform of a VLFE event with that of an ordinary earthquake observed at F-net station [Ito et al.,2009]. Both the events have the same moment magnitude (Mw 3.4) and almost the same epicentral distance and depth. Panel b represents both events with applied band-pass filter from 0.02 to 0.05 Hz (as the filter we used for our data), while in panel c using a band-pass filter from 2 to 8 Hz, the signal of VLF is clear when the low-frequency filter is used.

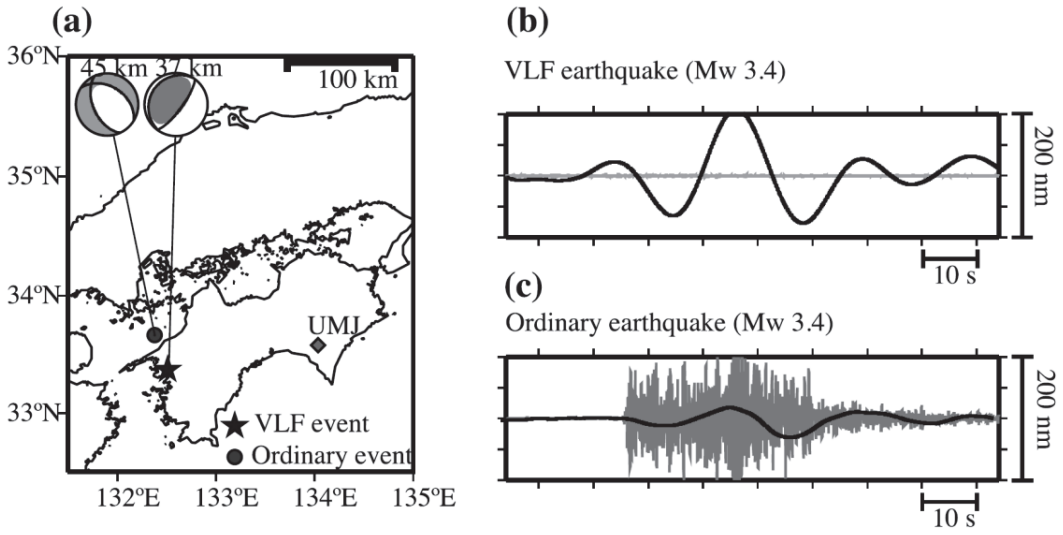

Figure 3.2: Comparison of VLFE events with ordinary earthquakes. (a) Centroid location of two events and their moment tensor solutions. The stars and solid circles indicate the centroid locations of VLF and ordinary events, respectively. (b and c) Two distinct frequency windows are apparent at 0.02–0.05 and 2–8 Hz. The solid lines and gray lines show the waveforms after the application of band-pass filters with frequencies in the ranges of 0.02–0.05 and 2–8 Hz, respectively. The original figure is figure 5 in (Ito et al, 2009)

3-3. Synthetic seismograms

In this detection method, we detect and locate VLFE by comparing the observed waveforms and synthetic seismograms. After we prepared the observed waveform, the Synthetic seismograms were calculated for all virtual sources which are set at Philippine Sea plate upper boundary. To prepare the synthetic seismograms, first we calculate the virtual sources, then we calculate the synthetic seismograms for all the virtual sources.

3-3-1. Virtual source grids

Previous studies have shown that the seismic mechanism of VLFE is consistent with the shape of the plate interface and the direction of plate convergence [Ito et al., 2007; 2009]. Based on this, we created new grid –based detection method to detect VLFE and estimate their locations in the Nankai subduction zoon. We set the virtual source grids depending on a velocity structure model [Kreemer et al., 2003. Sella et al., 2002. Miyazaki and Heki.,2001. Nakajima and Hasegawa,2007]. We created virtual source data following several steps:

First, we computed grid values of plate boundary depth from depth contour data, then we set plate boundary data and computed the grid value of plate interface depth [Baba et al 2002. Nakajima and Hasegawa 2007. Hirose et al 2008]. Figure 3.3 represents depth contours map for Nankai trough where we incorporated the data to have smooth data to get the interface data, so it became easy to estimate the depth of the plate interface.

After getting the plate boundary depth, we computed the grid values of strike and dip angles from this depth contours, it was determined by calculating the average normal vectors of the local plane of the plate boundary. Figure 3.4 represents the strike and dip data in Nankai trough were determined from plate boundary model, small blue lines with half cross indicate to strike direction and the red lines indicate to the depth contours.

The next step was to compute the grid values of rake angle from plate boundary depths by use plate motion vectors (in which plate velocity is evaluated) and computed plate convergence at the plate boundary (get the components of plate velocity), then computed trajectories of plate motion and rake angles along trajectories. Trajectories can be seen in Figure 3.5. which represents the motions lines on the subducting plate boundary calculated from plate motion model [Miyazaki and Heki, 2001], so the rake can be determined from motion lines, finally, we computed grid value of rake angle by using the raw data of rake, rake angles can be seen in Figure 3.6, which represents Nankai map with depth boundary in red color and rake contours with blue color.

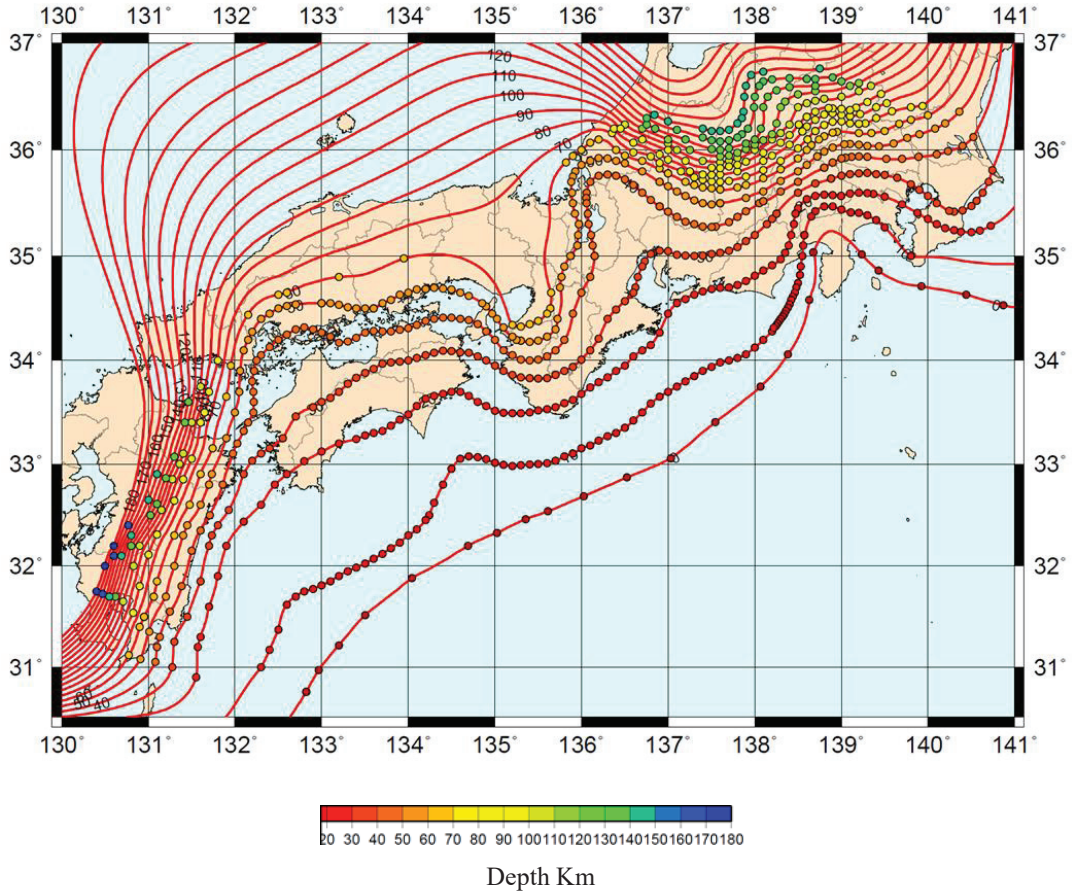

Figure 3.3: Nankai trough map with depth contours distribution the small circles in the contours because we incorporated data to have smooth data then get the interface data, so we could estimate the depth of the plate interface, color bar indicates depth km.

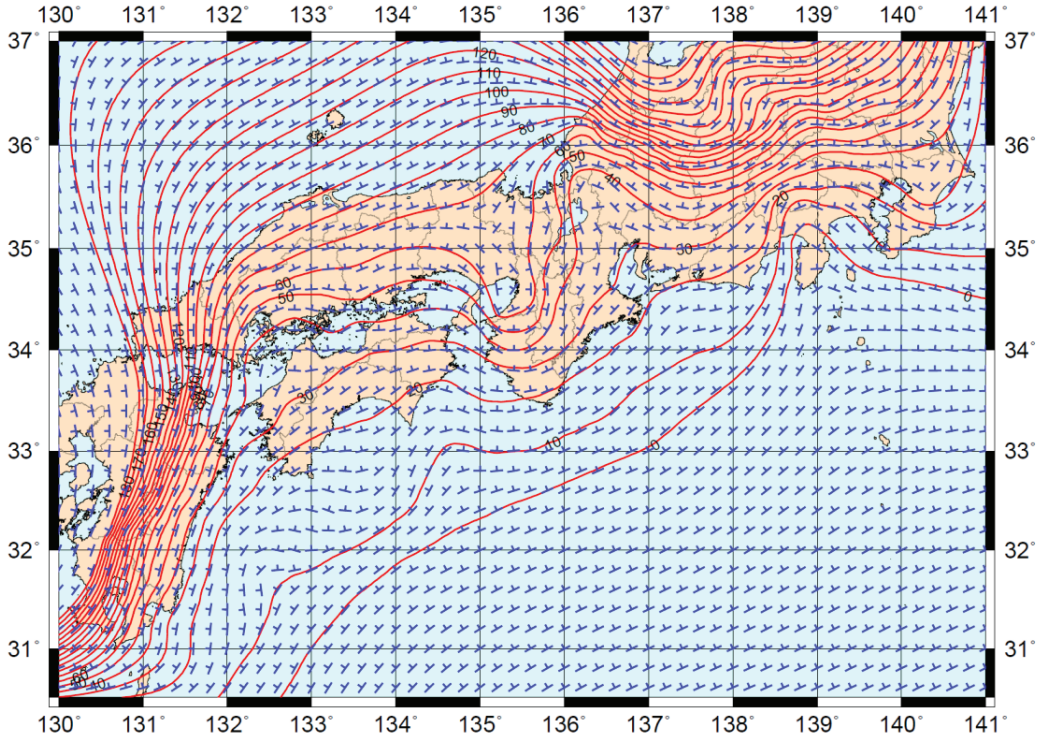

Figure 3.4: Nankai map with Strike and dip angles were determined from plate boundary models, Small blue lines with half cross indicate to strike direction, while red lines indicate to Depth contour of the Philippine Sea Plate, (Baba et al., 2002) (Hirose et al., 2008) (Nakajima& Hasegawa., 2007)

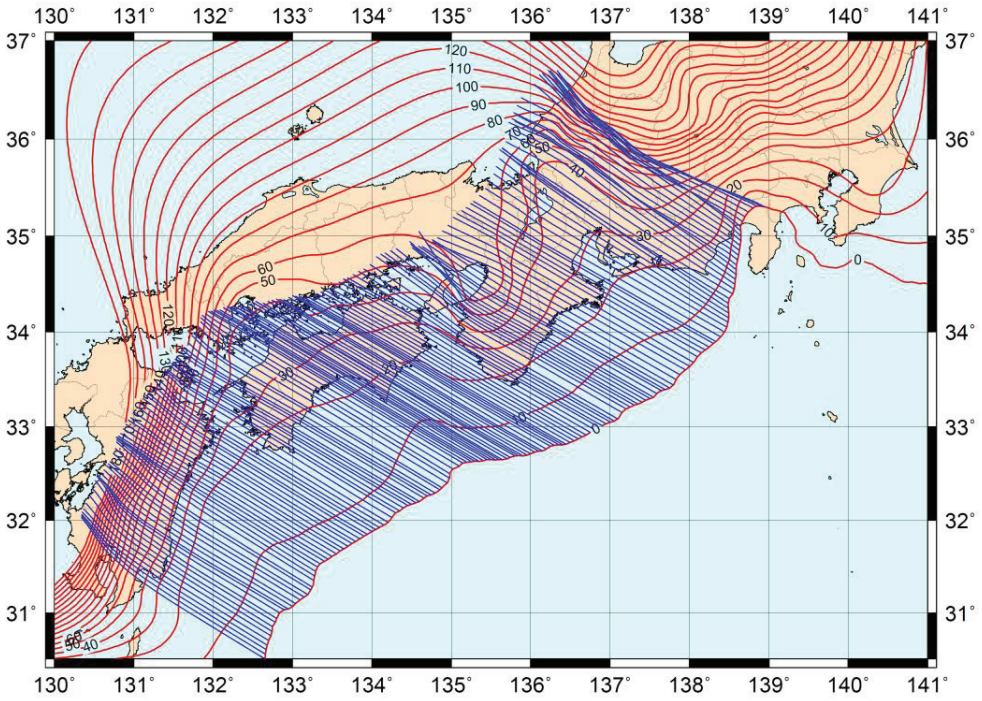

Figure 3.5: Nankai map with the trajectories of plate motion, blue lines represent Motions lines on the subdducting plate boundary calculated from Plate motion model, (Miyazaki and Heki, 2001), red lines represent depth contour of the Philippine Sea Plate.

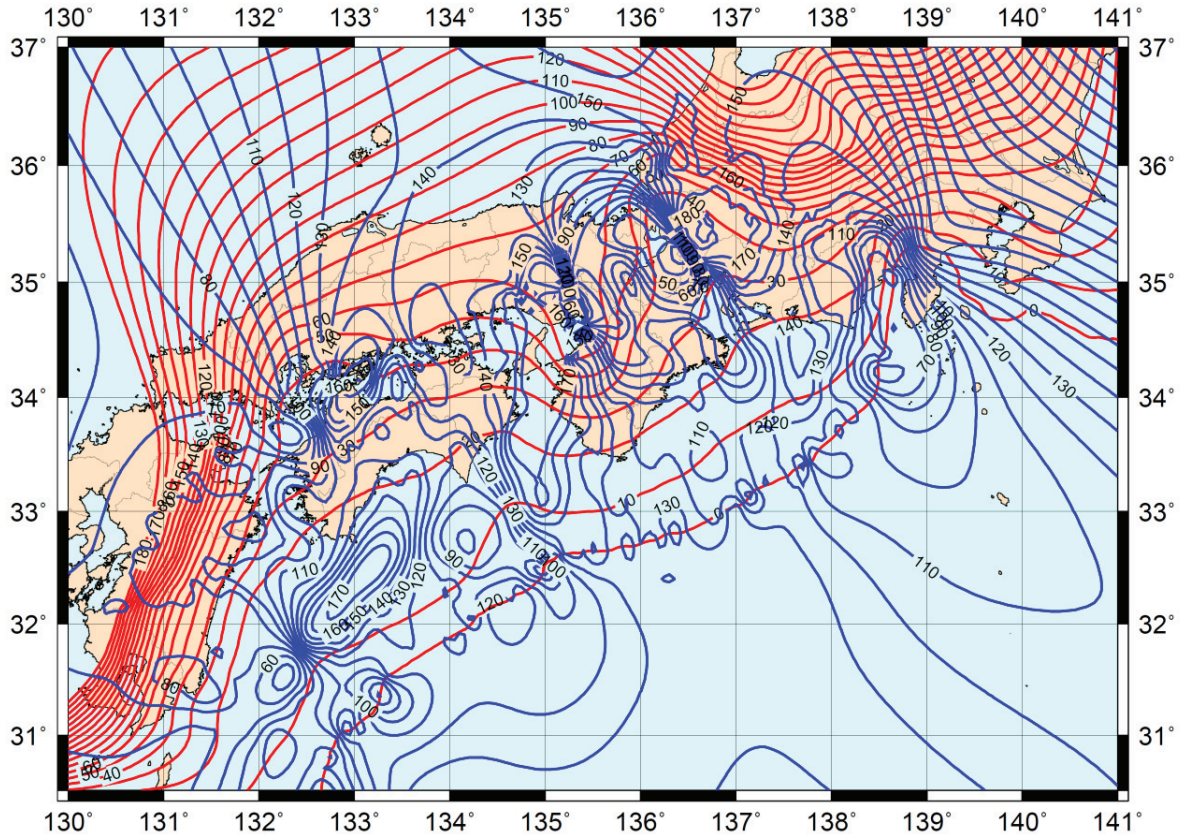

Figure3.6: Nankai map with depth boundary in red color and rake angles contours with blue color.

After computing the grid values of strike, dip and rake angles from plate boundary depth, we created virtual sources grids for Shikoku (whole Shikoku region), Western Shikoku, Eastern Shikoku, Kii and Tokai region by preparing a set of epicenters, then extracted the marginal epicenters of virtual sources which used later in data analysis, and computed the focal mechanisms at the virtual sources by interpolated strike, dip and rake angles at the source epicenter, the final results of this step is used as a sources for calculating the synthetic seismograms.

For the first trial, we created a virtual sources grid for whole Shikoku region with grid interval distance of 10 km horizontally (198 virtual sources) as shown in Fig 3.7 (a). Then for the second trial, we used a dense virtual source grid with interval grid distance of 5 km (816 virtual sources) for the same region as shown in Fig 3.7 (b), we wanted to know if we can increase the detection number of VLFE and spatial distribution in order to improve our method to apply for our later analysis. Based on this, we used dense virtual sources grids for other regions using a horizontal interval of 5 km, we created grids for Western Shikoku using 429 virtual sources as shown in figure 5.1. For Eastern Shikoku using 407 virtual sources as shown in figure 5.6. In Kii using 436 virtual sources as shown in Figure 5.14. and 352 virtual sources in Tokai as shown in Figure 5.11.

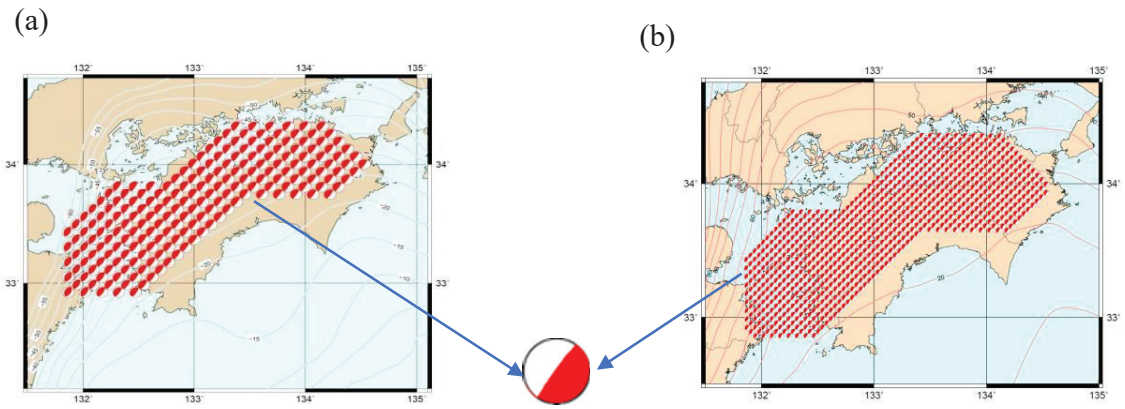

Figure3 .7: Virtual sources grid distribution on Shikoku region and their focal mechanisms, beach balls in both panels is virtual sources (a) grid with interval 10 km and total virtual sources number 198. (b) grid with interval of 5 km and total virtual sources number 816

3-3-2. Calculation of synthetic seismograms

For each virtual epicenter, we calculated the theoretical waveform. So, we could compute the Synthetic Seismograms by applying several Procedures as shown in Fig3.8. and as follows;

We prepared the station's data which contains station name longitude and latitude for every station. We selected stations based on the epicentral depth. We created the list of stations with epicentral distance less than or equal to 80 km. The stations distribution in Shikoku region with virtual sources locations and depth represented in figure 2.1. while stations distribution in Western Shikoku, Eastern Shikoku, Kii and Tokai represented in Figures (5.2), (5.12) and (5.15). Then we prepared the grid data for source mechanism by using depth, strike, dip and rake angles data which are the results of (3-3-1). We got the moment tensor, write the source parameters, and got the epicentral distance. The moment-tensor function represented by the formula 1 [Pasyanos et al., 1996] where the moment-tensor difference function μ define as the root mean square of the differences of the moment tensor elements normalized by their respective seismic scalar moment M0. Here is a Mij '= Mij/M0, ij component of the moment tensor M. M0 is the seismic moment Mij. Moment tensor of the two matches exactly when μ = 0, match basically when <0.25 μ, [Pasyanos et al., 1996] and significantly different when 0.5 <μ.

$$\mu = \sqrt{\frac{\sum_{i=1}^{3}\sum_{j=1}^{3}(M_{ij}^{(1)\prime} - M_{ij}^{(2)\prime})^2}{8}} \qquad (1)$$

Then we prepared the sources data which are the final results of (3-3-1), the source grid list contains the longitude, latitude and focal mechanism information for each virtual source. When the virtual sources data and stations information were ready, we computed the synthetic seismograms using Green function formula 2:

$$d_i(t) = \sum_k G_{ik}^s(t) m_k^s \qquad (2)$$

where

i	i-th trace
k	k-th component of moment tensor

Where m is the moment tensor, **i** is the observation point synthetic seismograms, **k** represents the component of the moment tensor, **G** Green's function **di (t)**.

For the calculation of the Green's function, Ito et al, 2009 and 1984. Fukao.1977. Ueno et al., 2002., used a combination of models of seismic velocity structure to get Green Function as shown in Fig 3.9. Ito et al. 2009 used the velocity structure where there is a layer boundary velocity structure to 33km depth, the amplitude of the theoretical waveform is largely different on the top and bottom of the layer. the wavenumber discretized using [Saikia, 1994] method in this study.

The Green function has been computed Using CPS commands (Computer Programs in Seismology) [Herrmann, 2013 for example] as follows; hprep96-cps commands for preparing the input file of hprep96, hpsepc-cps commands for computing Green function, hpulse96 commands for convolving source time function, and hpulse96 -v-i for velocity seismogram. We got the synthetic seismogram with three components (EW, NS, UD) for each station based on [Minson and dreger, 2008], no isotropic components were assumed. The bandpass filter of the SAC (Seismic Analysis Code) a subroutine was applied from 0.02 to 0.05 Hz which is the dominant frequency range of VLFE.

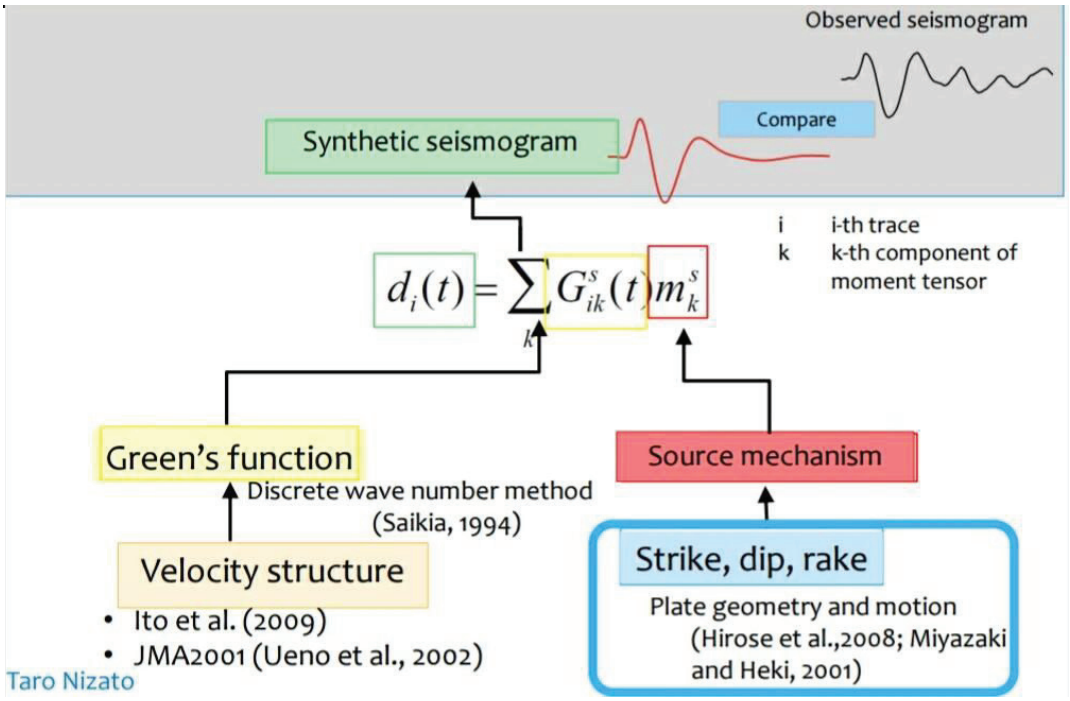

Figure 3.8: Synthetic seismogram calculation steps using Green function

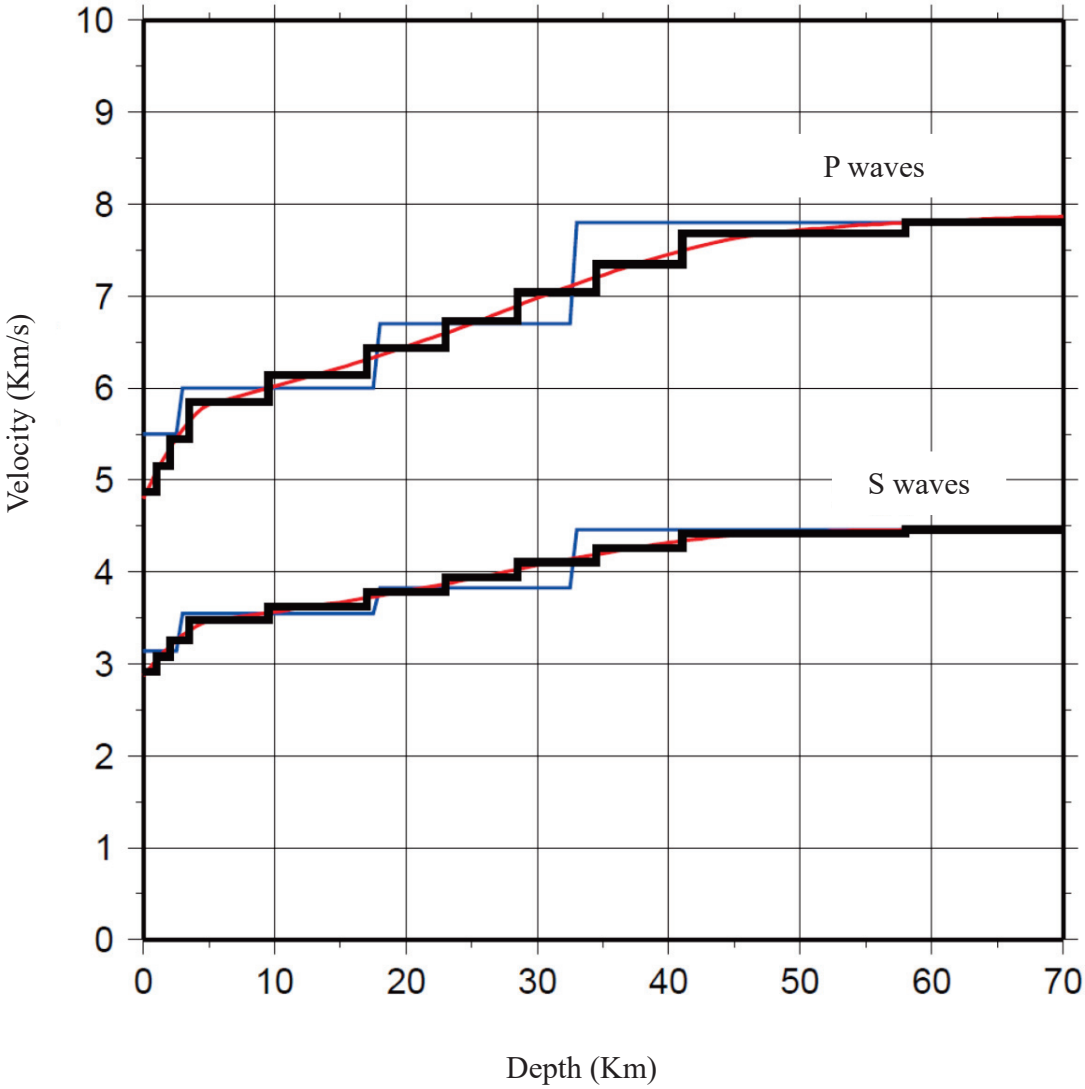

Figure 3.9; Seismic wave velocity structure (red) used for calculation of theoretical waveform. Blue used in Ito et al. [2009], The velocity structure being used, red is JMA 2001 [Ueno et al., 2002]. original figure is (figure 2-7 0 by (Nizato, T. ,2014., Master thesis)

3-4. Event detection

We analyzed the data by repeating several processing steps every second, these processing steps represented in Figure 3.10. We detected VLFE by using one-hour SAC files and this process assumes the sampling interval of one second for seismogram.

We used Fortran programs to compute the cross-correlations and the variance reduction from one hour observed and synthetic seismograms, then we used several programs to decide the final detections based on VR effective waveforms, noise waveforms and improve the detection results by removing the redemand and the isolated detection. The main parameters decided depending on tremor locations, the final parameters set using trial and error method by repeated varied attempts which are continued until success to increase the detection number of VLFEs with the minimum false events number.

3-4-2. Amplitude information

We set the window size for the mean absolute amplitude of 120 seconds, first we compute the mean absolute amplitude in the preceding in the window size for the mean absolute amplitude of 600 seconds and computed the percentage of the noisy waveform in 120 seconds

The threshold of the amplitude (100*6.20) percent. Which is the amplitude index value of the observed waveform, 6.20 here is the result of the length of the time window of the waveform divided by the total number of 120 seconds the observed waveform. When the time is greater than 120 seconds, the amplitude of the waveform which detected in this period will remove. We used this procedure to reduce the artificial detection events because sometimes in the case of performing detection by using only the time series of VR, it is possible to affect by seismic noise such as regular earthquakes signals if they are exist.

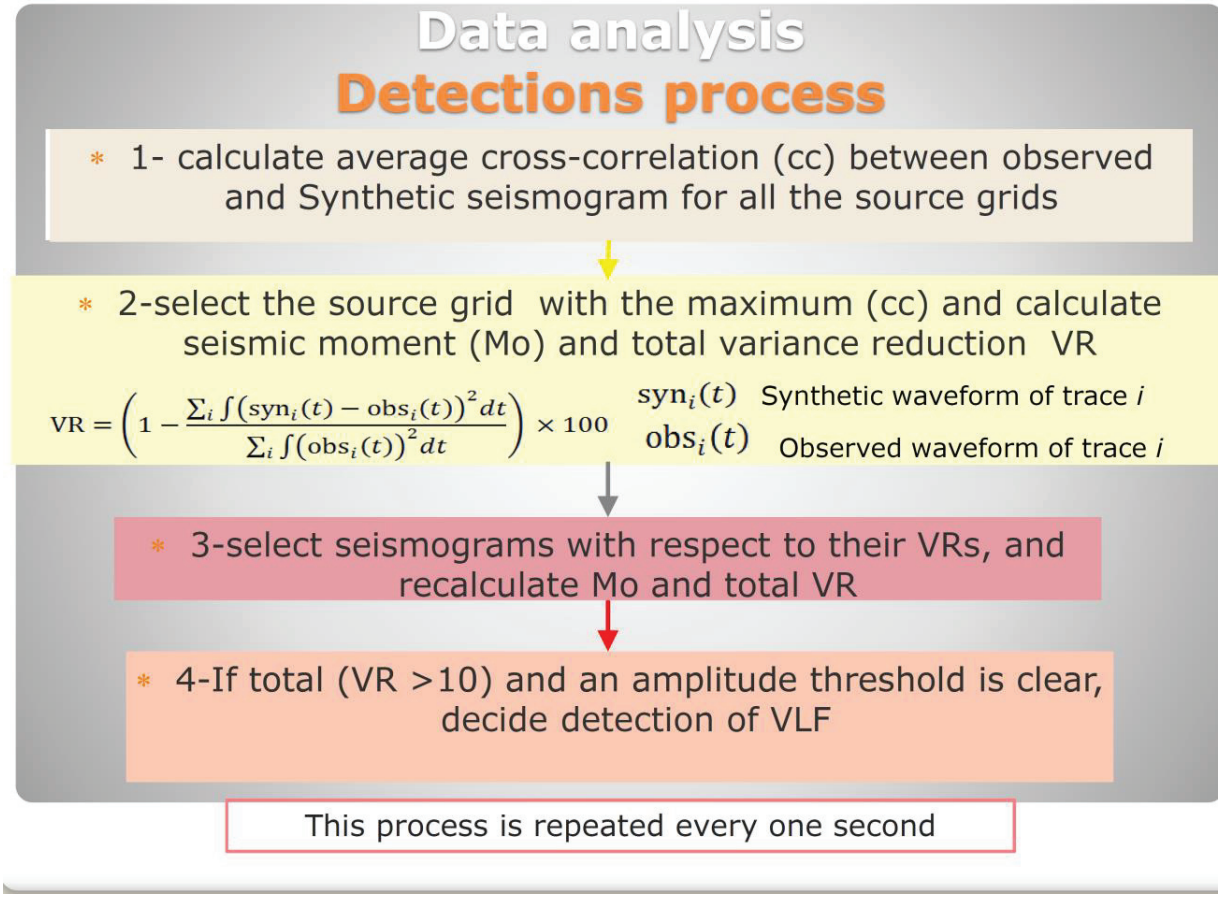

Figure 3.10: Detection processes procedures which used in this study

3-4-2. Cross correlation

We calculated the cross-correlation (CC) between every one-hour record of observed waveforms and synthetic seismogram. We used a minimum cross- correlation threshold of 0.2. We selected the grid source with the maximum CC and calculated the seismic moment Mo from the amplitude ratio. For the calculation of the cross-correlation between the theoretical waveform and the observed waveform, we set the threshold of epicentral distance of 80.0 Km, so we used only the record at the observed point which has an epicentral distance of 80 km or less from the virtual source. As well the time window of P waves has travel time of 60 seconds after the travel time of S waves. The cross-correlation value calculated for each combination of waveforms is weighted by the maximum value of the absolute amplitude of the theoretical waveform and the average value is taken as the cross-correlation value at the virtual source.

3-4-3. Variance redaction

We calculated the variance reduction (VR) between the synthetic and the observed waveforms to compare them at each virtual grid source, we calculated (VR); as expressed in follows:

$$\mathrm{VR} = \left(1 - \frac{\sum_i \int \left(\mathrm{syn}_i(t) - \mathrm{obs}_i(t)\right)^2 dt}{\sum_i \int \left(\mathrm{obs}_i(t)\right)^2 dt}\right) \times 100 \qquad (3)$$

Where $\mathrm{syn}_i(t)$ is the synthytic waveform of trance i
$\mathrm{obs}_i(t)$ is the observed waveform of trance i

With a time widow of 120 s. The grid intervals are 5 km in horizontal, Less than 8 km in depth (Upper surface of the Philippine Sea plate), and 1 s in time. For our main analysis, we chose VR to be greater than 10%. Although we set VR threshold of 10 in this method which is very low compared with the previous study, for example, [Tsuruoka et al., 2009] which is an analysis method for ordinary earthquakes, VR threshold was 65, in [Ito et al. 2007, 2009] VR was 40, and in [Takeo et al.2010] VR was 30, and generally, as the threshold value of VR decreases, the number of detections increases the artificial events number also increases, [Tsuruoka et al., 2009]. But in this method, we solved this problem by assuming the mechanism of the virtual hypocenter beforehand, and by eliminating false events using the index value of the amplitude as I explained in the previous steps. For analyzing data in Western Shikoku, Eastern Shikoku, Kii and Tokai we chose VR of minimum 25 % because of the limited stations and in the result the limited data.

Although we didn't consider detection criteria of VLFE, we decided the parameters depending on previous studies, tremor occurrences and using trial and error method by repeated varied attempts which are continued until we succeed to improve our results by increasing the detection numbers and spatial distribution with decreasing the artificial events numbers.

3-4-4. Detection criterion

To decide and improve the detection results, we did additional analysis procedures toward the final results.

First, we selected the output based on VR, the effective waveform and the percentage of the noisy waveform and by using the list of virtual marginal sources which are the results of (3-3- 1). The output removed if the final Variance Redaction VR is small (smaller than 10 for our main analysis), if the number of effective waveforms is small (smaller than 20), if the percentage of the noisy waveform is large (larger than 44 %), and if they are located on the marginal grids.

Second, we selected the output of the previous step by removing the redcurrant detection and using minimum time difference between two events, because of the long – period waves, the same VLFE is usually detected in continues several seconds. In this step, we selected one result only with largest variance reduction from such detection, so the detection removed of the occurrence shortly after the previous and it has smaller VR.

The third and final data process to get the final detection was to select the output of the second step by removing the isolated detections. Although the detection of the previous two steps is almost correct, sometimes it is desirable to remove spatially isolated detections. In this step, we removed such detections by using the maximum distance between the nearby stations and a minimum number of detections at the nearby source grid, so the detection removed on one source grid if the very source grid has a small number of detection or the nearby source grid has a small number of detection.

After the final detection decided so we plot the final results using GMT as shown in the following Chapters.

Chapter 4

Data Analysis and Results

4-1. Sparse virtual source grids

For the first trial to apply our new method, we chose to set the virtual sources grid with horizontal interval of 10 km and less than 8 km in depth (Fig 3.8 (a)) using seismic records from 73 Hi-net stations (Fig 2.2. (a)) in two data periods, from 6 to 22 September 2006 and from 10 to 21 March 2007, we used trial and error to decide the parameters, we set VR to be minimum 10%, we detected and located 258 events distributed in 28 locations0 for data from 6 to 22 September, and 277 events distribute on 34 locations for data from 10 to 22 March.

In the result, we could detect new and small events which the previous methods could not detect or locate, furthermore, the detection number is 10 times more than the previous studies results. Figure 4.1 (b) and Figure 4.2 (a) (lower part) represents space – time plot for VLFE results for this method using 198 virtual sources and tremor detected by ATMOS in two periods from 6 to 22 September 2006 and from 10 to 21 March 2007 respectively, the red dots in both figures represents the VLFEs activates while the black dots represents the tremor activities, the upper part represent Shikoku map with the detected events locations represented by red circles, the color scale indicates the number of the detection in the same location.

Figure 4.3 (a, b) represents the temporal cumulative number of VLFEs' seismic moment with respect to tremor's RD (Reduced Displacement of tremor) on September 2006 and March 2007 respectively. Using 198 virtual sources grid for VLIEs detection, we noticed a linear relationship, in general.

Figure 4.4 (a, b) represents the hourly and the cumulative number of detections per the analysis periods of VLFE detected using 198 virtual sources grid and tremor detected by ATMOS in September 2006 and March 2007 respectively.

4-2. Dense virtual source grids

Although our previous results using sparse virtual source grid showed very high detection numbers compared with the previous studies, we wanted to improve our method to get even better results, so we modified our method by set the virtual source grid with horizontal interval of 5 Km instead of 10 km0, and we applied all the other procedures as usual , we set virtual source grid contains 816 virtual sources (Fig 3.8 (b)) instead of 198 ,we used the same data as the previous step with the same stations, the virtual sources with stations distributions is shown in Figure (Fig 2.1 (b)), we detected 298 events for 100 locations using data from 6th to 22nd September 2006 , and 286 events for 102 locations for data from 10th to 21st March 2007. It is noticeable that we could increase the detection number since we could detect 40 VLFEs event more by using dense virtual source grid than using the sparse grid for data in 2006, also we could detect 11 events more in data 2007. As well as we could increase the spatial distribution by using dense virtual sources grid, because we could increase the locations of the events to be 72 locations more than using sparse grid for data in 2006 and 70 locations for the data in 2007. So, by this modification we could make our method more accurate in time and space, therefore, we decided to use a dense virtual source grid for our later analysis.

Figure 4.1 (a) and Figure 4.2 (b) (lower part) 0represents space–time plot for VLFEs results for this method using dense virtual sources and tremor detected by ATMOS in two periods from 6 to 22 September 2006 and from 10 to 21 March 2007 respectively. The red dots in both figures represents the VLFEs activates while the black dots represent the tremor activities, the upper part represent Shikoku map with the detected events locations represented by red circles, the color scale indicates the number of the detection in the same location. From competence between Figure 4.1 (a) and (b) as well competence between Figure 4.2 (a) and (b), It is noticeable that using a dense virtual source grid could increase the detection number as well the spatial distribution.

Figure 6.4 (a) and (b) represents the temporal cumulative number of VLFE seismic moment with respect to tremor's RD (Reduced Displacement of tremor) on September 2006 and March 2007 respectively. Using dense virtual sources grid for VLIE detection, while Figure 6.6 (a) and (b) represents the hourly and the cumulative number of detections per the analysis periods of VLFE detected using dense virtual sources grid and tremor detected by ATMOS in September 2006 and March 2007 respectively.

Figure 4.5 (a) and (b) represents the maxim cross correlation for the detection events for data 2006 and 2007 respectively, Figure 4.6(a) and (b) represents the variance reduction for the detection results in 2006 and 2007 respectively, and Figure 4.7 (a) and (b) represents

the total and final variance reduction for every event detected sing dense sources grid in 2006 and 2007 respectively.

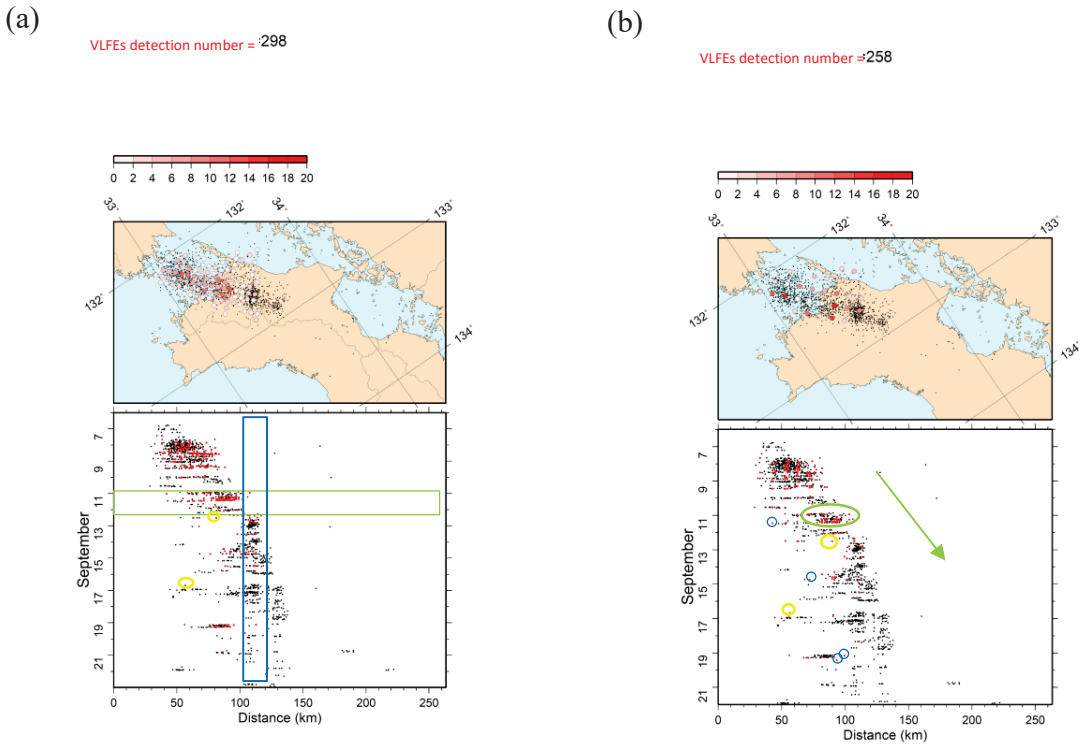

Figure 4.1: space- time plot for data 2006(September 6 to 22) (a) dense virtual source grid with horizontal interval of 5 km (816 virtual source), (b) virtual source grid with horizontal interval of 10 km (198 virtual source). Spatial distribution of tremor (black) and VLF (red). The color of the distribution is varied according with the number of VLF detection for each virtual source. Green (triangle in a and ellipse in b) are where RTR of tremor and rapid reversal of VLFE are seen, the green arrow in b is the direction of migration along strike direction, blue rectangle refers to tremor occurrence in the same cluster for a long time. Small blue circles represented examples of VLFE evens which are not correlate with the tremor is both space and time. Small yellow circles in both panels indicate to uncorrelated VLFE with tremor which repeated in both analyses in the same time and location.

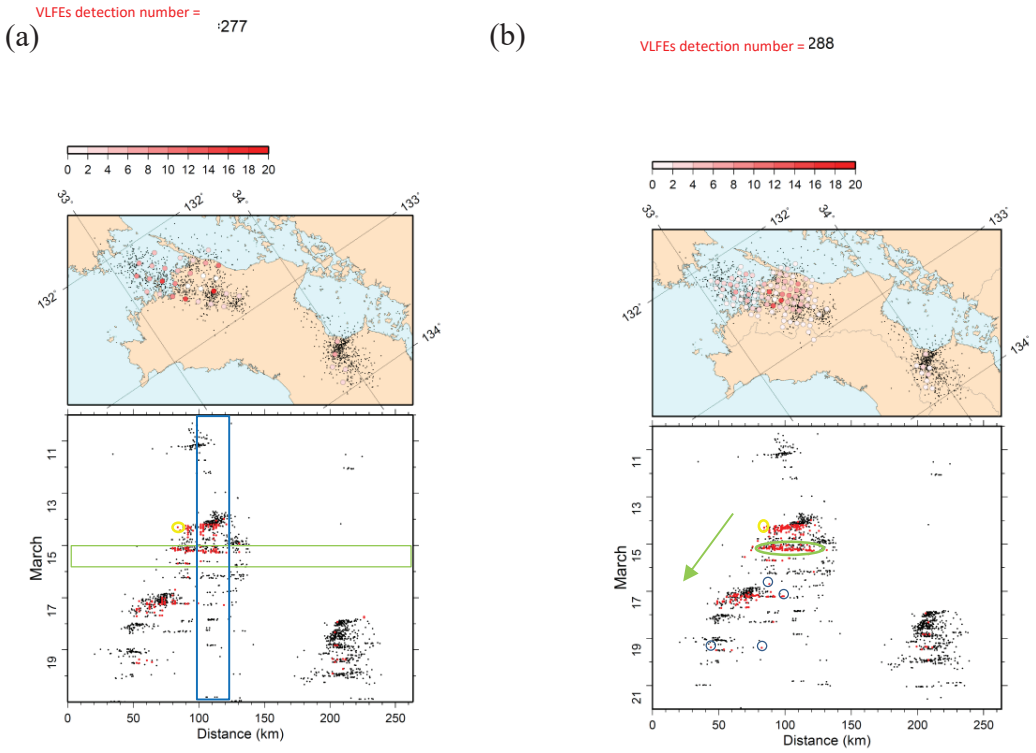

Fig 4.2: Same as Figure 3. However, the period is from March 10 to 21, 2007

(a)

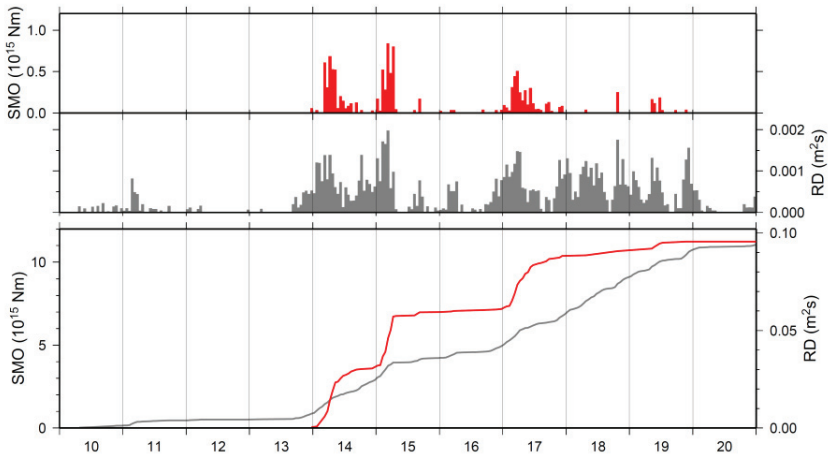

(b)

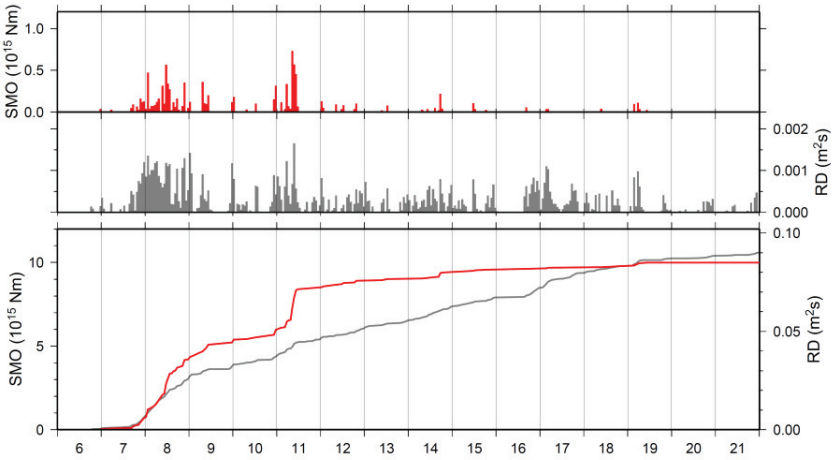

Figure 4.3: VLFEs seismic moment detected using 198 virtual sources grid and tremor RD (a) Data from 6th to 22nd September 2006, (b) Data from 10th to 21st March 2007. the red line is VLFEs' moment while the gray line is tremors' RD. The bars in the upper panel represents the cumulative number in each active day while the lower panel represents the cumulative number curve for all the analysis periods.

(a)

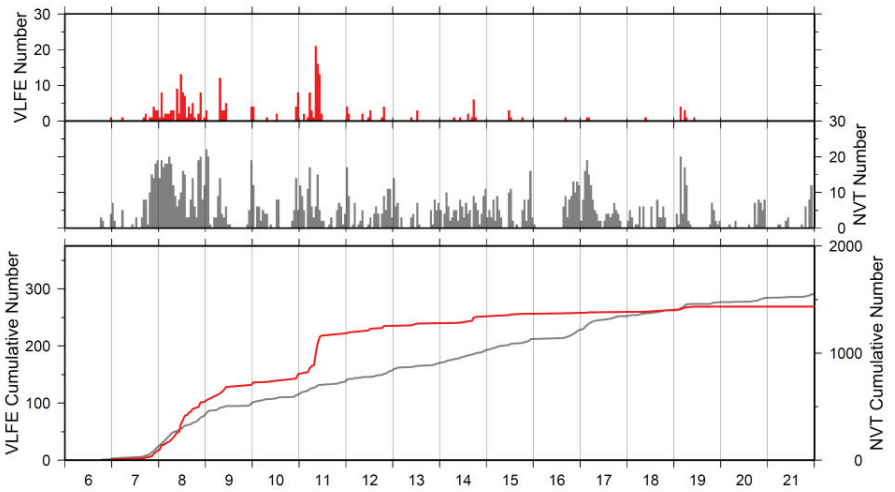

(b)

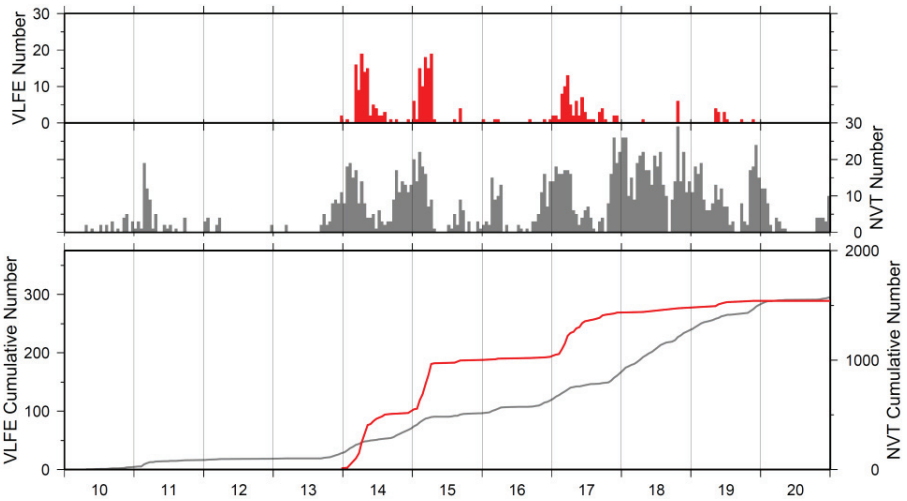

Figure 4.4: VLFE detection number which events detected using 198 virtual sources with tremor detection number for the same period (a) data from 6 to 22 September 2006, (b) data from 10 to 21 March 2007, the red line is VLFE' while the gray line is tremor cumulative detection number. The bars in the upper panel represents the cumulative number in each active day while the lower panel represents the cumulative number curve for all the analysis periods.

(a)

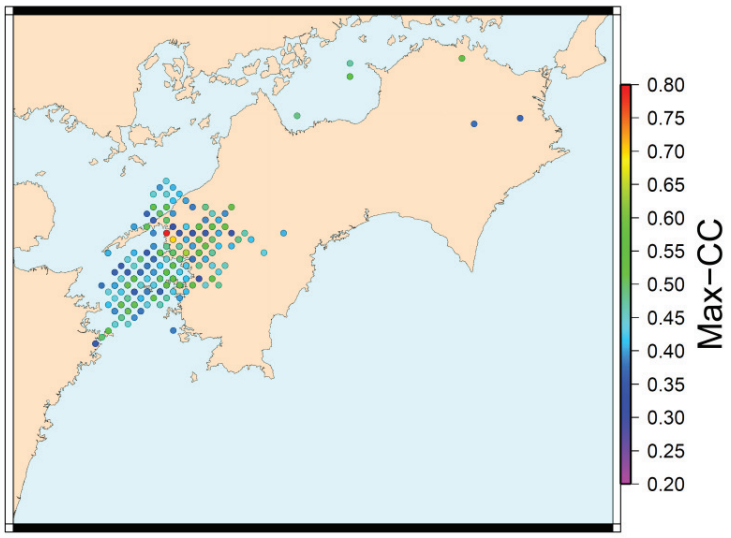

(b)

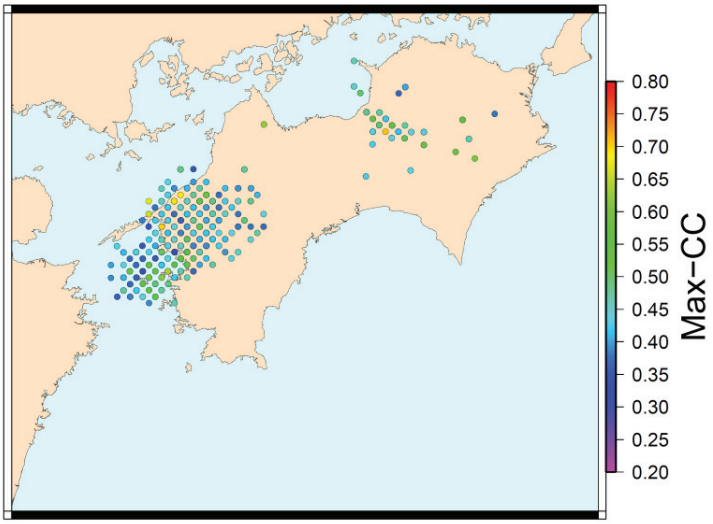

Figure 4.5: Shikoku map with maximum cross-correlation for the detection events, the color skill indicates to the cross-correlation value which decided to be minimum 0.2 in the analysis, in this method we chose the detection based on the maximum cross-correlation between synthetic and observed waveform (a) data from 6 to 22 September 2006, (b) data from 10 to 21 March 2007, this got results using dense virtual sources grid.

(a)

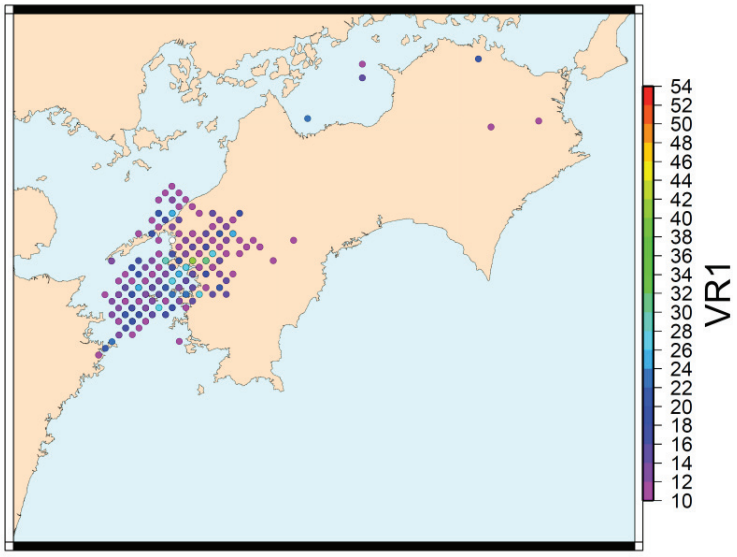

(b)

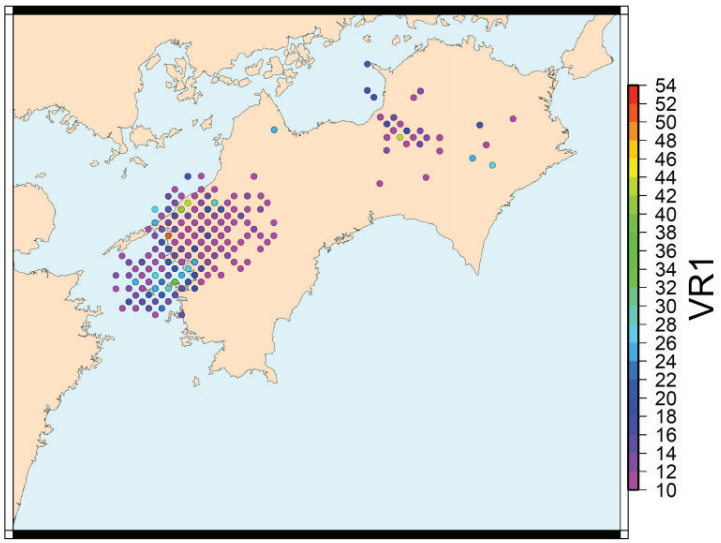

Figure 4.6: Shikoku map with maximum variance reduction for the detection events, the color skill indicates to the VR value which decided to be minimum 10 in the analysis, in this method we chose the detection based on the VR between synthetic and observed waveform (a) data from 6 to 22 September 2006, (b) data from 10 to 21 March 2007, this got results using dense virtual sources grid.

(a)

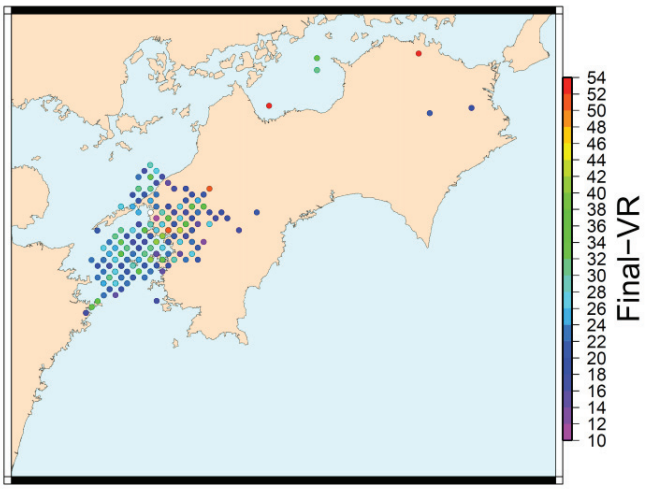

(b)

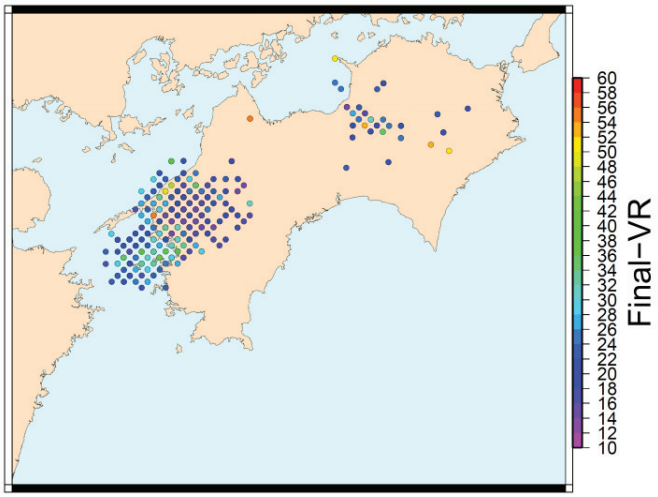

Figure 4.7: Shikoku map with total variance reduction for the detection events, the color skill indicates to the VR value which decided to be minimum 10 in the analysis, in this method we chose the detection based on the VR between synthetic and observed waveform (a) data from 6 to 22 September 2006, (b) data from 10 to 21 March 2007, this got results using dense virtual sources grid.

Chapter 5
Results for western and western Shikoku, Kii Peninsula, Tokai and whole Shikoku between 2011 and 2015

After we got a high VLFEs detection number by using dense virtual source grid, we decided to use dense virtual source grid with horizontal interval of 5 km for all our analysis, we applied our method in Shikoku region by dividing the region for West and East, we thought that this procedure could give more accurate results since we notice that tremor activity occur independently in each part of Shikoku region. As well we applied our method as a first trial in Kii peninsula and Tokai region. We also applied our method for whole Shikoku region again but by using several time periods from 2011 to 2015, we used dense virtual source grid and the same stations as in data 2006 and 2007.

5-1. Eastern and western Shikoku for 2007 data

5-1-1. Western Shikoku

We divided Shikoku region into western and eastern regions by setting dense virtual source grids for each region separately. We set the western part virtual sources grid with a horizontal interval of 5 km and we got grid consisting of 429 virtual sources with depth less than 8 km shown in Fig. 5.1. Then we calculated the synthetic seismograms as usual. For observed data, first, we chose data from 73 Hi- net station Fig. 5.2 (a), the data period from 10 to 21 March 2007 then we process the data as I explained in the previous chapters, we decided to use variance reduction of 10 as in our analysis for 2006 and 2007, we detected 267 events in 62 locations as shown in Fig. 5.3 represents the spatial distribution of tremor (black) and VLF (red) from 10 to 21 March 2007 from 73 Hi-net in Western Shikoku in the upper part, while in the lower part represents spatiotemporal distribution for the same results. The height and color of the bars are varied according to the number of VLFE detection for each virtual source. We noticed that there are many artificial events even we used the same procedure in the analysis reducing the false detection by using the amplitude index. We thought that because we used data from very far stations so the noise signals increased, so we decided to decrease the station's numbers based on the distance from the grid sources. Therefore, we re-do the analysis for western Shikoku religion using same data period from 10 to 21 March but from 40 Hi-net stations Figure 5.2 (b), and we increase the variance reduction to be 25 instead of 10. We could detect 51 events in 18 locations. Figure 5.4 represents the Spatial distribution of tremor (black) and VLF (red) from 10 to 21 March 2007 from 40 Hi-net stations in Western Shikoku in the upper part, while in the lower part represents spatiotemporal distribution for the same results. The height and color of the bars are varied according with the number of VLFE detection for each virtual source. We noticed that the false detection deleted but the detection number decrees about 5 times. Figure 5.5 represents competence between the both situations in Figure 5.5 (a) using 73 stations and in (b) using 40 stations for the same region and same data period but with different VR value, (10 in a for using 73 stations and 25 in b by using 40 stations). When we used a grid for one part from the region we must order data from only the surrounding stations to get good results.

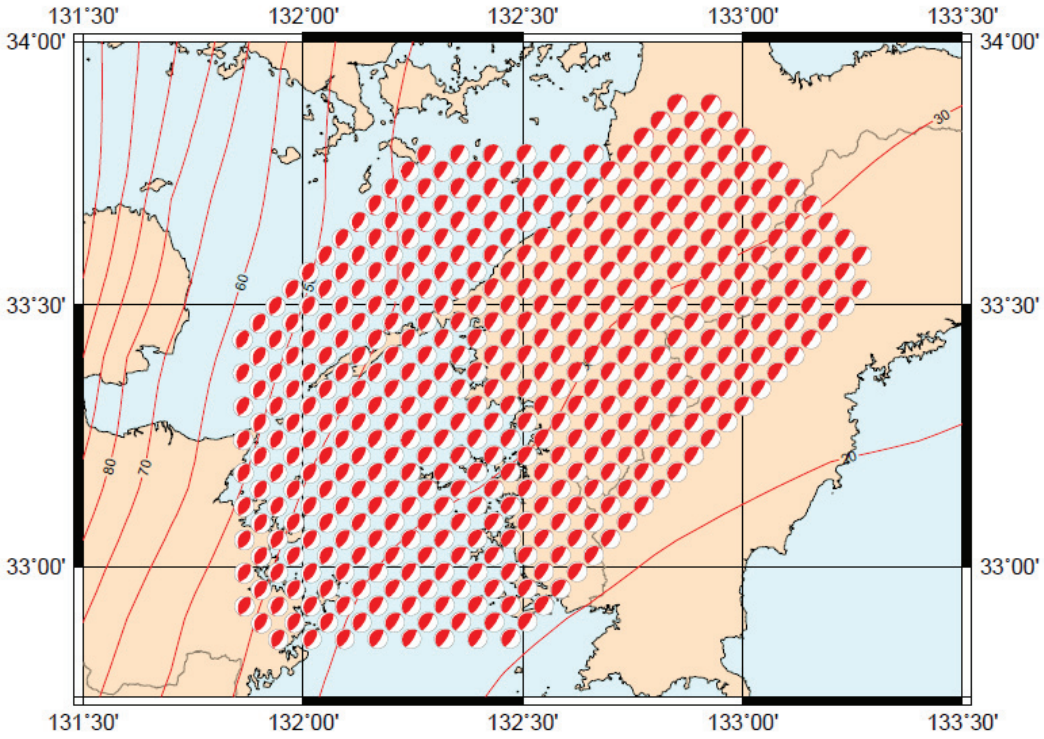

Figure 5.1: Virtual source grid in Western Shikoku region, we used a horizontal interval of 5 Km and less than 8 Km in depth, the grid consists of 425 virtual sources, the beach balls indicate to the focal mechanism.

(a)

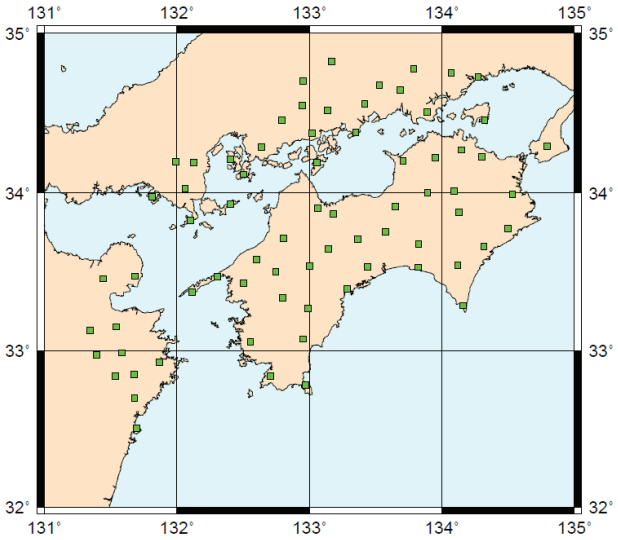

(b)

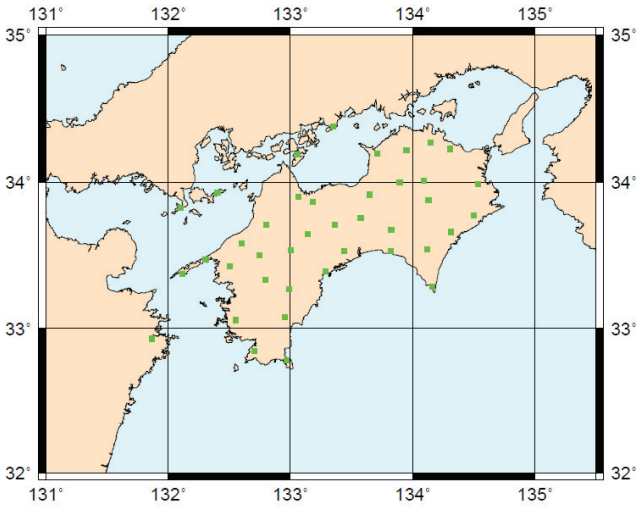

Figure 5.2: Stations distribution for the analysis in Western Shikoku, the green square indicates to the station location (a) 73 Hi-net station (b) limited stations (40 Hi- net station).

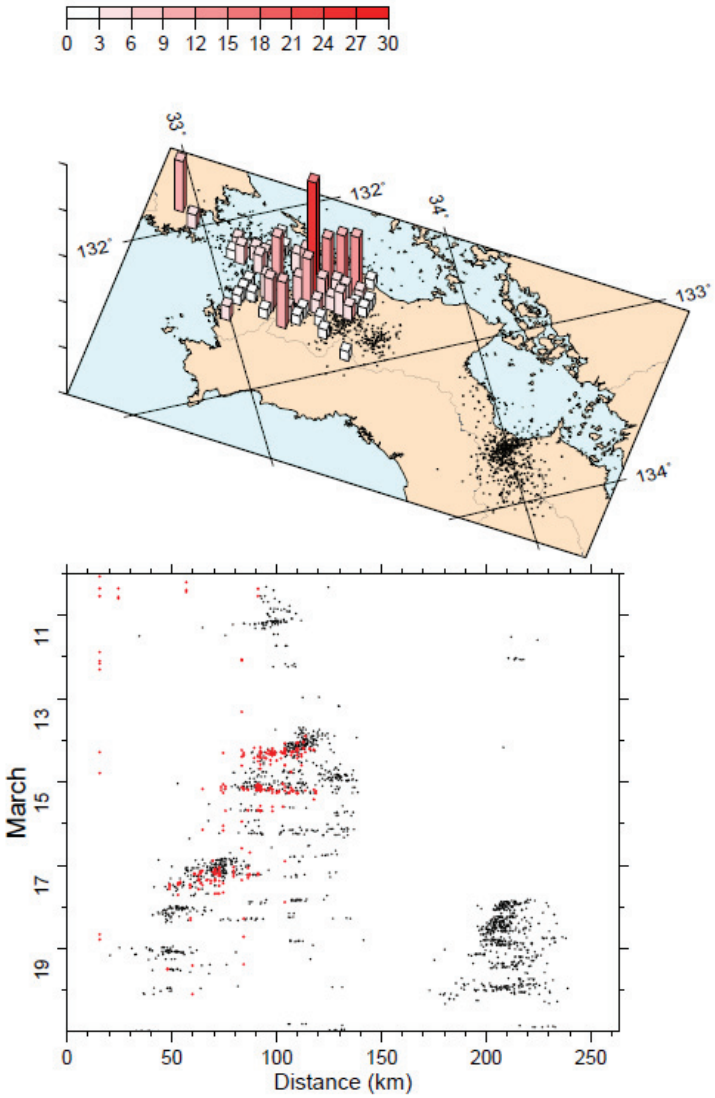

Figure 5.3: Spatial distribution of tremor (black) and VLFE (red) from 10 to 21 March 2007 from 73 Hi-net in Western Shikoku in the upper part, reduced while in the lower part represents spatiotemporal distribution for the same results. The height and color of the bars are varied according to the number of VLFE detection for each virtual source, the detection number is 267 events in 62 locations.

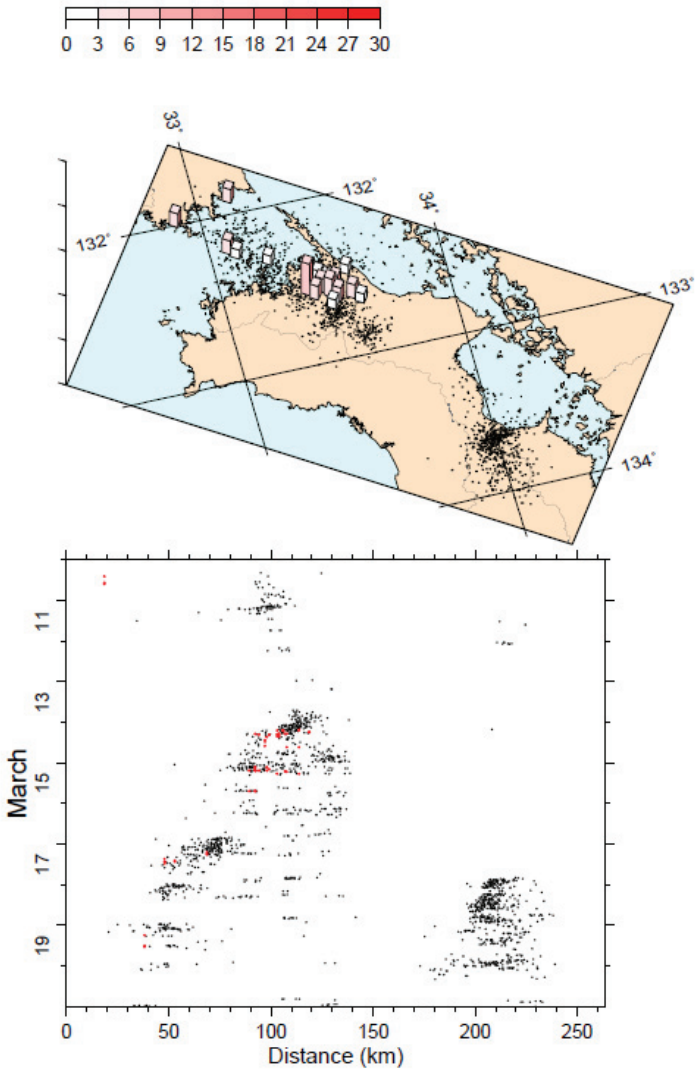

Figure 5.4: Spatial distribution of tremor (black) and VLFE (red) from 10 to 21 March 2007 from 40 Hi-net in Western Shikoku in the upper part, reduced while in the lower part represents spatiotemporal distribution for the same results. The height and color of the bars are varied according to the number of VLFE detection for each virtual source. The detection number is 51 events in 18 locations.

(a)

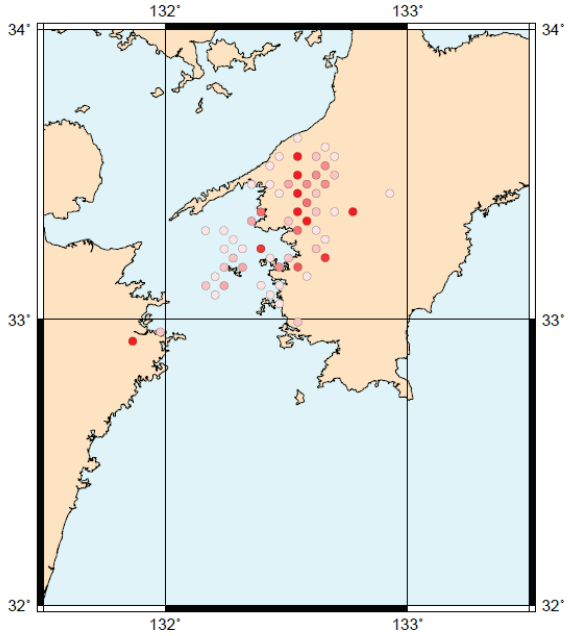

(b)

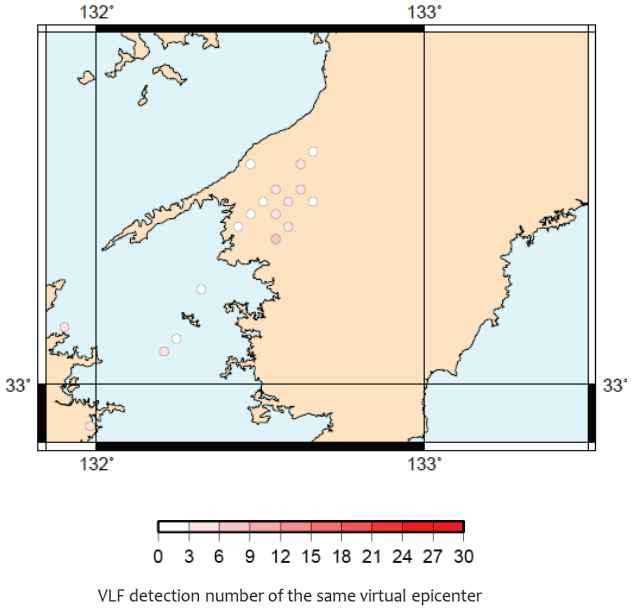

Figure 5.5: Comparison between the both situation in (a) using 73 stations the detection number is 267 for 62 locations and (b) using 40 stations for the same region and same data period but with different VR value, (10 in a for using 73 stations and 25 in b by using 40 stations). The detection number is 51 for 18 locations, the circles are the events locations while the color indicates the detection number in the same virtual source.

5-1-2. Eastern Shikoku

We applied our method for Shikoku Eastern part by set a dense virtual sources grid with 5 km in horizontal and less than 8 km in depth, we got grid consist of 407 virtual sources as shown in Figure 5.7. First, we used data from 73 Hi-net stations for data period from 10 to 21 March and VR of 10 as shown in Figure 5.2. (a), then we used data from limited stations number (34 station surrounding the virtual source only) for the same period and VR of 25 as shown in Figure 5.6., for the first trial we detected 13 events for 6 locations and for the second we detected 10 events for 5 locations as shown in figure 5.8. and figure 5.9. respectively. The upper part of both figures represents the Spatial distribution of tremor (black) and VLFE (red) in Eastern Shikoku from 10 to 21 March 2007 from 73 Hi-net stations and VR of 10 and for data from 34 stations using VR of 25 respectively. while in the lower part of the both figures represent the spatiotemporal distribution for the same results. The height and color of the bars in both figures are varied according to the number of VLF detection for each virtual source.
We noticed that the 3-false detection deleted. Figure 5.10. represents comparison between the both situations in (a) using 73 stations and in (b) using 34 stations for the same region and same data period but with different VR value, (10 in a for using 73 stations and 25 in b by using 34 stations). This ensured our previous result, when we divide Shikoku region for two parts, we must order data from only the surrounding stations to get good results. In addition, this trial didn't increase the detection number or spatial distribution compared with using same parameters (VR=10) for same data period in whole Shikoku region, although we could save analyzing time when we divided the study area, but we decided to continue our later analysis for Shikoku using whole region virtual source grid Figure 3.7 (b).

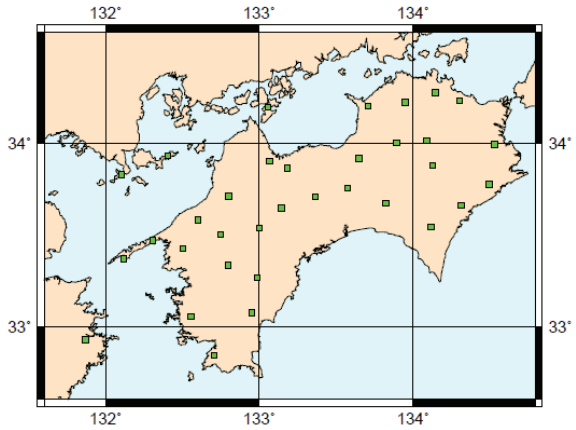

Figure 5.6: Stations distribution for the analysis in Eastern Shikoku, the green square indicates to the station location for limited stations (34 Hi- net station)

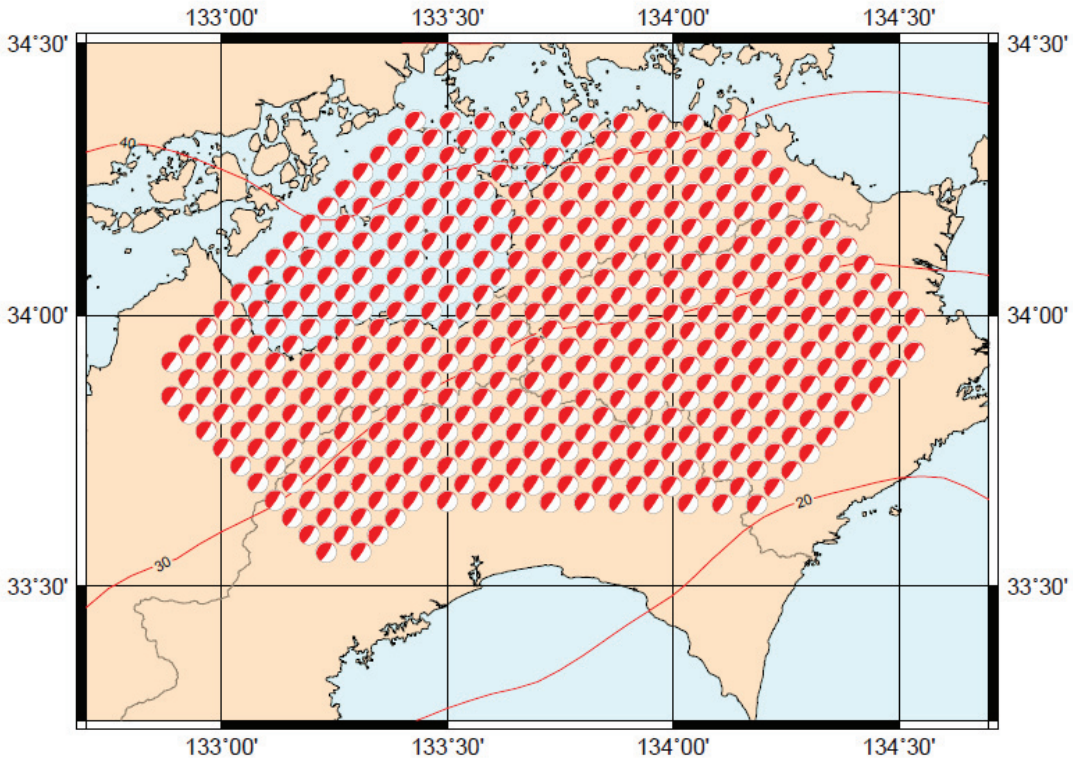

Figure 5.7: Virtual sources grid in Eastern Shikoku region, we used a horizontal interval of 5 Km and less than 8 Km in depth, the grid consists of 407 virtual sources, the beach ball indicates to the focal mechanism.

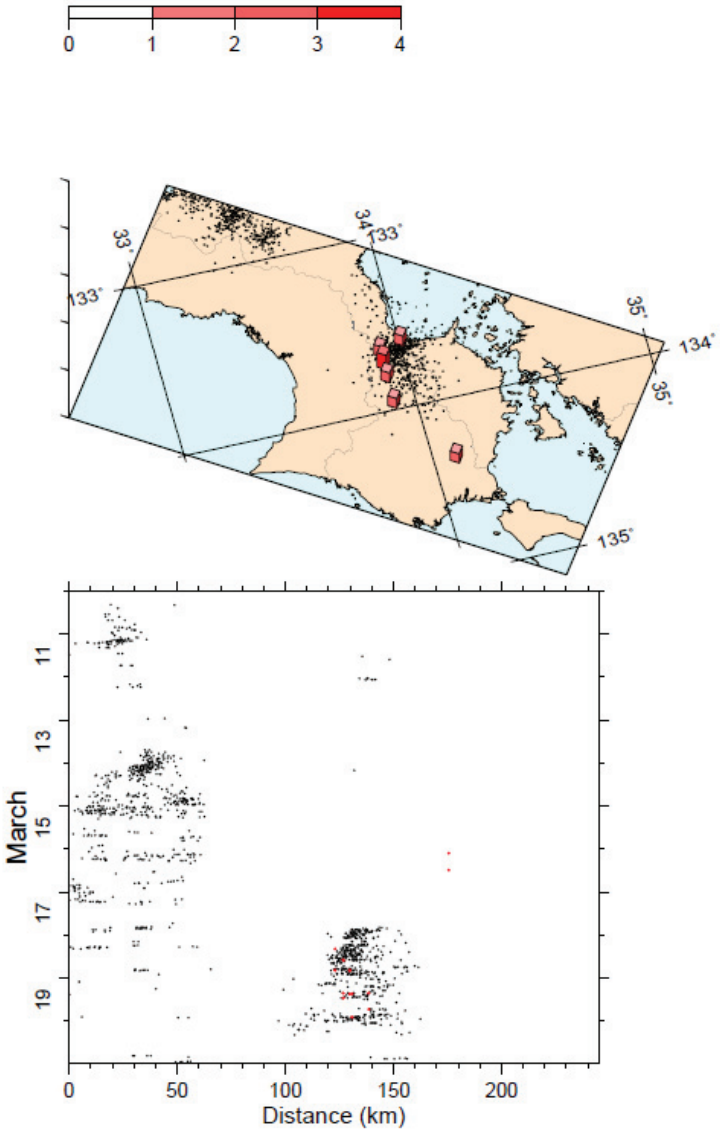

Figure 5.8: Spatial distribution of tremor (black) and VLFE (red) from 10 to 21 March 2007 from 73 Hi-net in Eastern Shikoku in the upper part, while the lower part represents spatiotemporal distribution for the same results. The height and color of the bars are varied according to the number of VLFE detection for each virtual source, the detection number is 13 events in 6 locations.

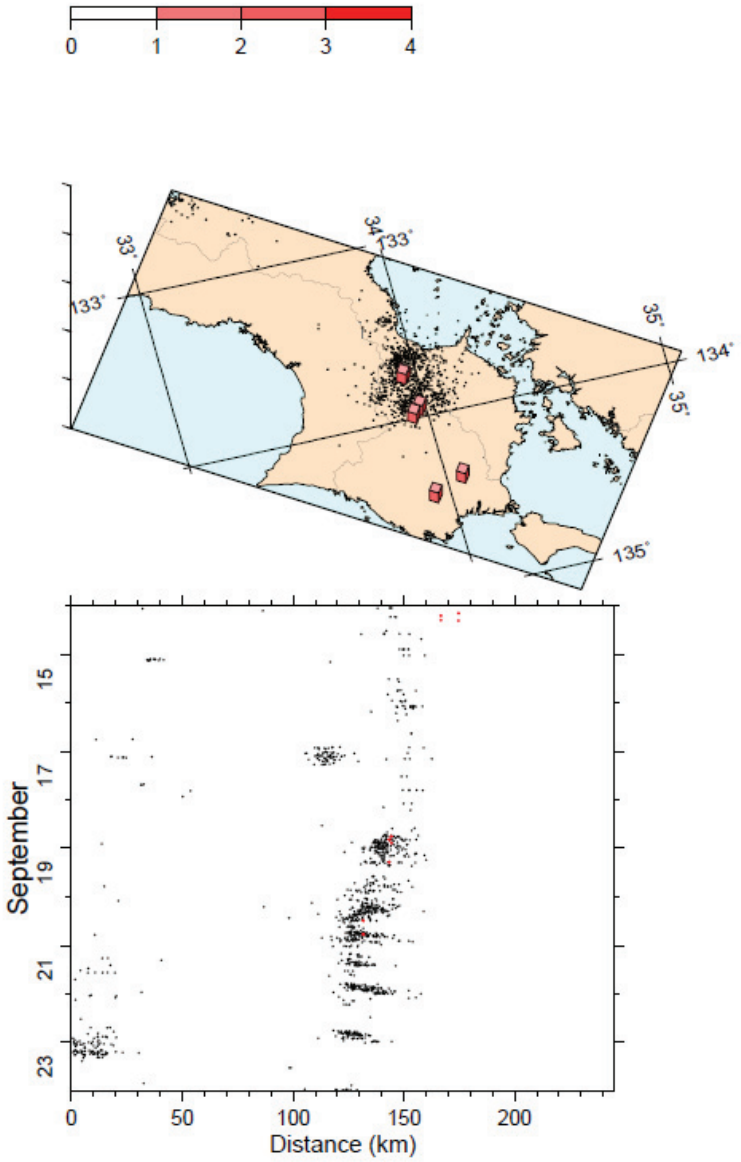

Figure 5.9: Spatial distribution of tremor (black) and VLFE (red) from 10 to 21 March 2007 from 34 Hi-net in Eastern Shikoku in the upper part, while the lower part represents spatiotemporal distribution for the same results. The height and color of the bars are varied according to the number of VLFE detection for each virtual source. The detection number is 10 events in 5 locations.
.

(a)

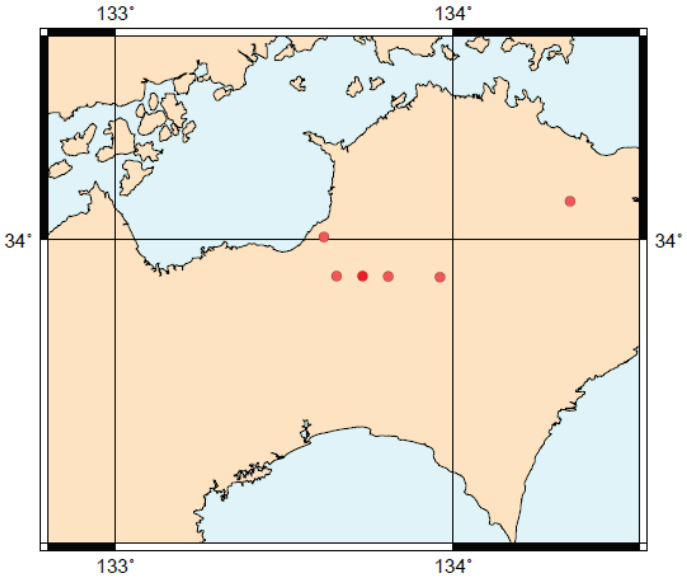

(b)

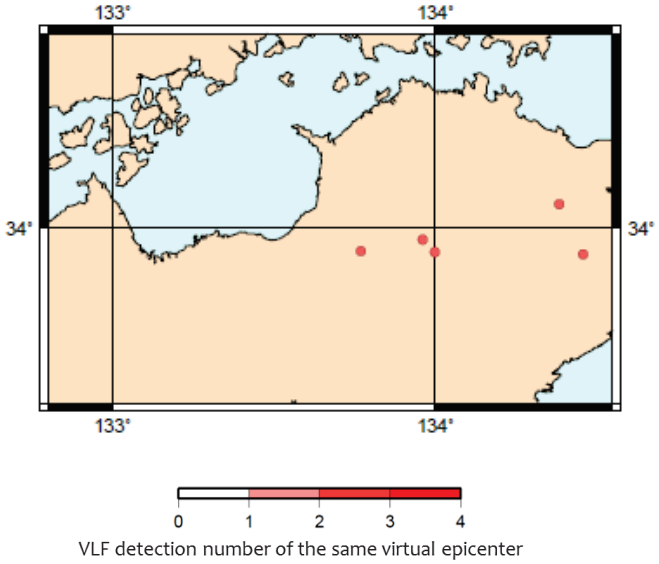

Figure 5.10: Comparison between the both situation in (a) using 73 stations the detection number is 13 for 6 locations and (b) using 34 stations for the same region and same data period but with different VR value, (10 in a for using 73 stations and 25 in b by using 40 station). The detection number is 10 for 5 locations, the circles is the events locations while the color indicate to the detection number in the same virtual source.

5-2. Tokai and Kii Peninsula

5-2-1. Tokai region

Since the aim of this study is to detect VLFE and study their relationship with NVT in whole Nankai trough region, we applied our method in Tokai region as a first trial other than Shikoku region.
We set dense virtual sources grid using an interval of 5 km horizontally and less than 8 km in depth and consist of 352 virtual source Figure 5.11. We chose data period depending on NVT occurrences from 1 to 5 September 2014 from 41 Hi- net stations. Figure 5.12. shows the stations distribution in Tokai. We set the Total Variance reduction VR >20 in the data analysis. We detected 9 VLFE events in 4 locations, Figure 5.13. represents the Spatial distribution of tremor (black) and VLF (red) from 1 to 5 September 2014 from 41 Hi-net stations in Tokai region in the upper part of the figure, while in the lower part represents spatiotemporal distribution for the same results. The height and color of the bars are varied according to the number of VLFE detection for each virtual source.

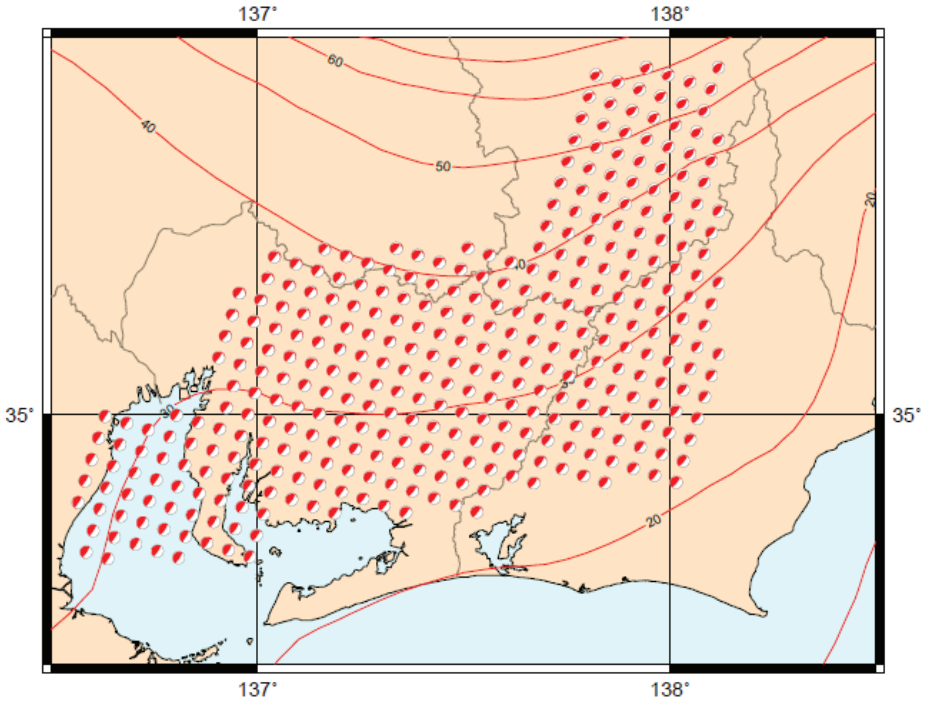

Figure 33, Virtual sources grid in Tokai region, we used horizontal interval of 5 Km and less than 8 Km in depth, the grid consists of 352 virtual sources, the beach ball indicates to the focal mechanism.

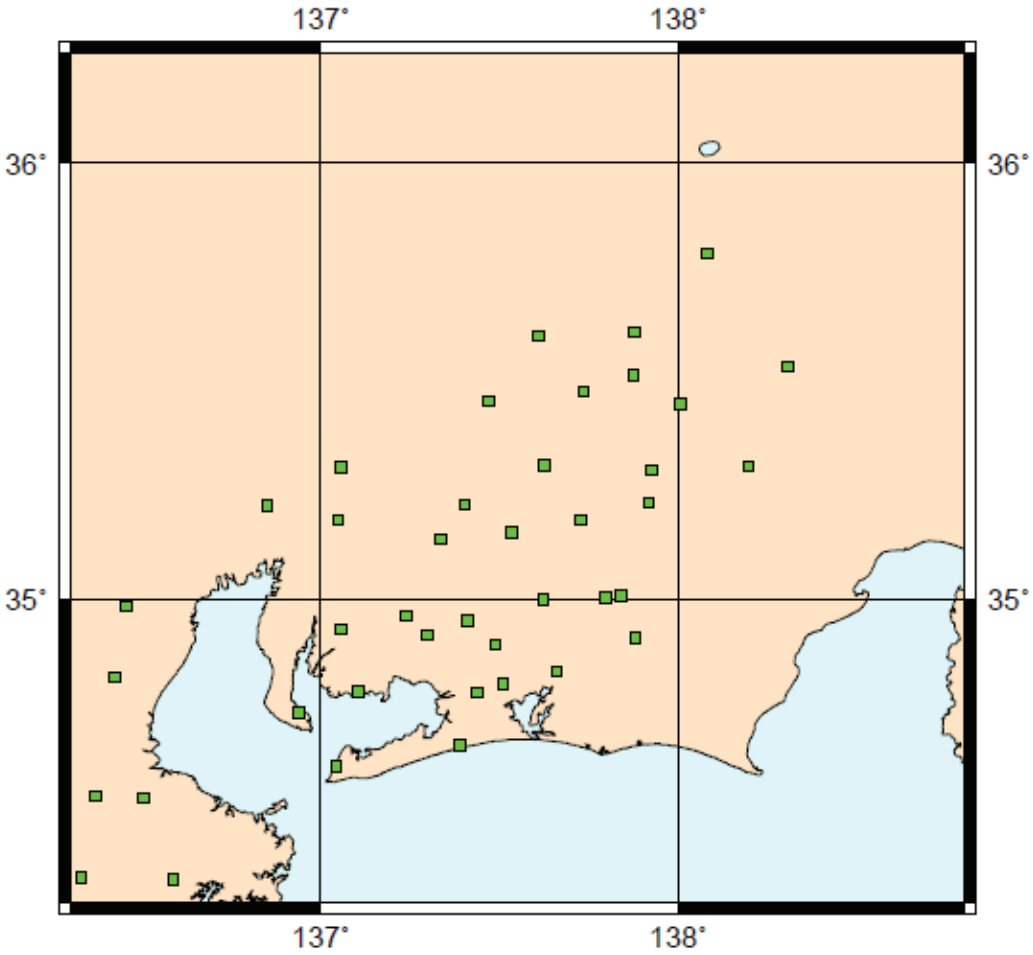

Figure 5.12: Stations distribution in Tokai region, the grin square indicates to the station location (41 Hi- net stations)

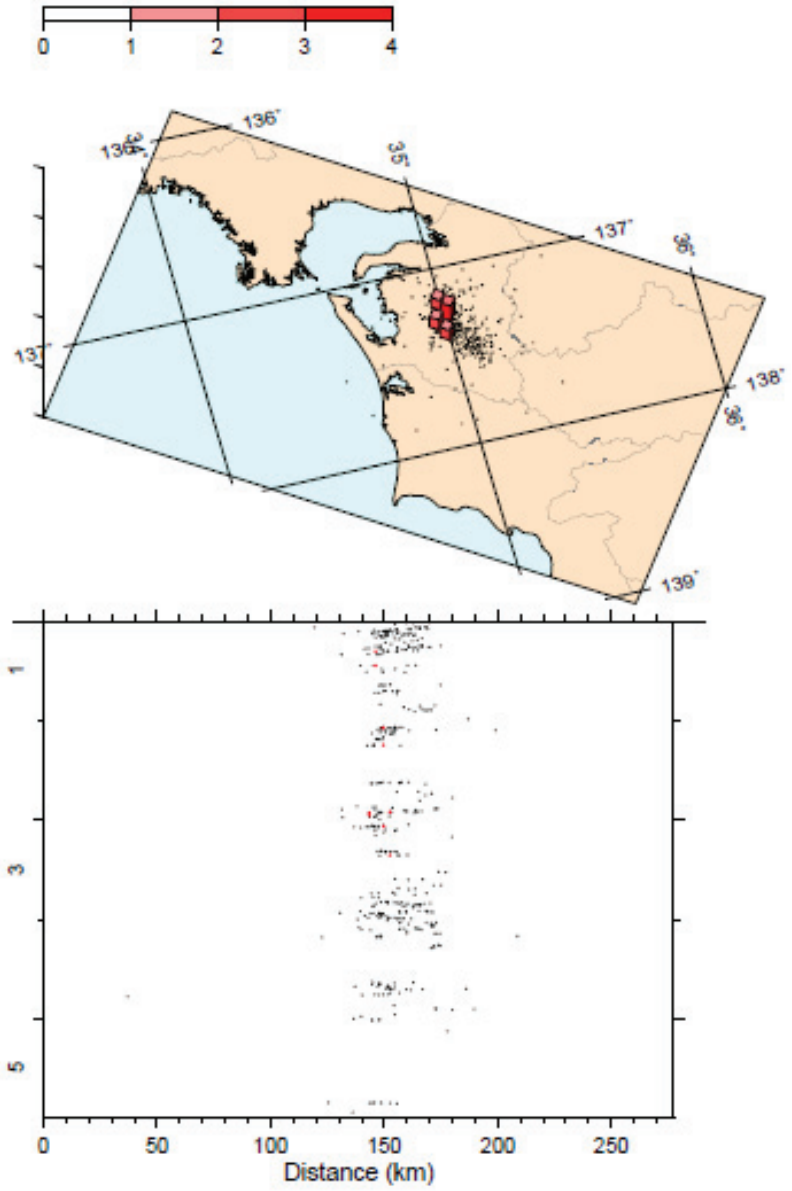

Figure 5.13: Spatial distribution of tremor (black) and VLFE (red) from 1 to 5 September 2014 from 41 Hi-net in Tokai region in the upper part, while in the lower part spatiotemporal distribution for the same results. The height and color of the bars are varied according to the number of VLFE detection for each virtual source. The detection number is 9 events in 4 locations.

5-2-2. Kii Peninsula

We applied our method as a second trial other than Shikoku region in Kii peninsula, we set a dense virtual sources grid using interval of 5 km horizontally and less than 8 km in depth and consist of 436 virtual source Figure 36, we chose data period depending on NVT occurrences from 5 to 15 July 2014 from 43 Hi- net stations. Figure 37 show the stations distribution in Kii. We set the total variance reduction (VR) >20 in the data analysis. We detected 46 VLFE events in 20 locations. Figure 5.16 represents the Spatial distribution of tremor (black) and VLFE (red) from 1 to 5 September 2014 from 41 Hi-net stations in Kii region in the upper part of the figure, while in the lower part represents spatiotemporal distribution for the same results. The height and color of the bars are varied according to the number of VLFE detection for each virtual source. It is noticeable that there are a lot of artificial detection in this result, so in the future analysis, we must change the parameters to eliminate such detection in this region.

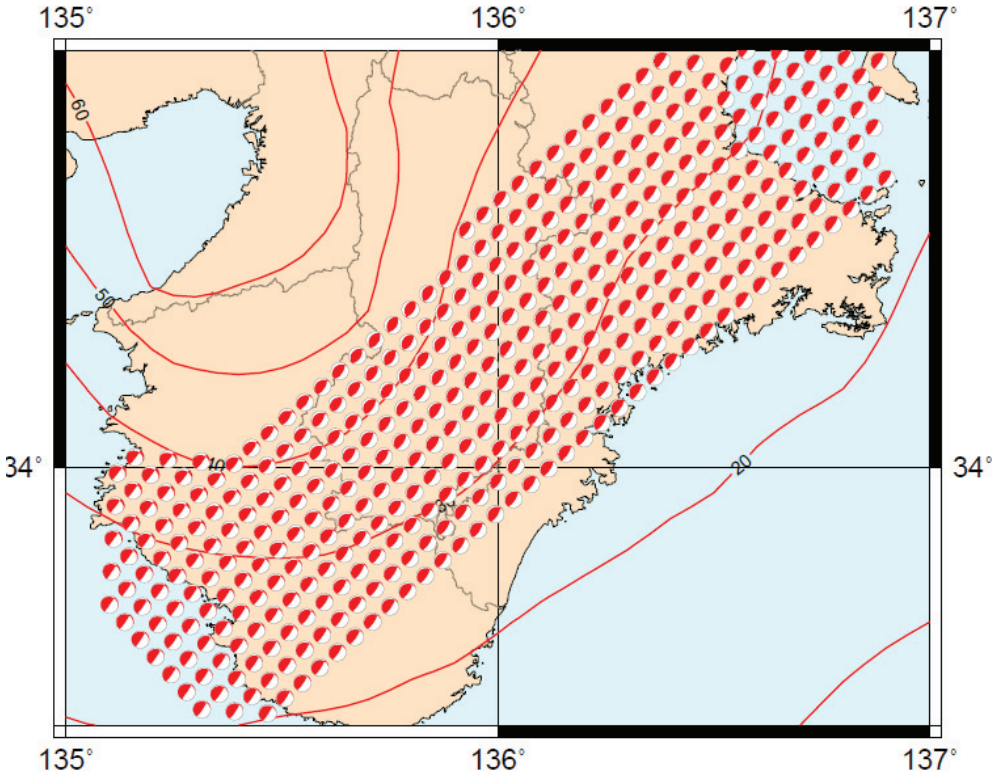

Figure 5.14: Virtual sources grid in Kii region, we used a horizontal interval of 5 Km and less than 8 Km in depth, the grid consists of 436 virtual sources, the beach ball indicates to the focal mechanism.

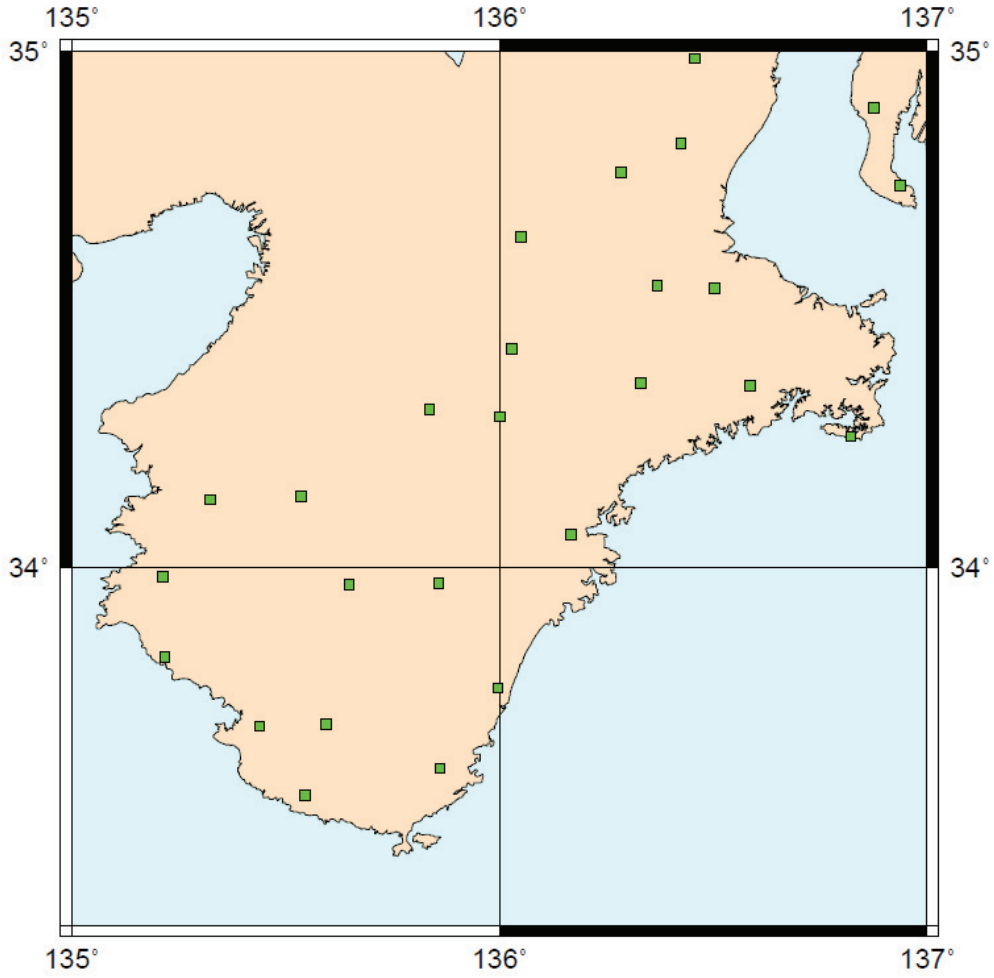

Figure 5.15: Stations distribution for the analysis in Kii region, the green square indicates to the station location (43 Hi- net station)

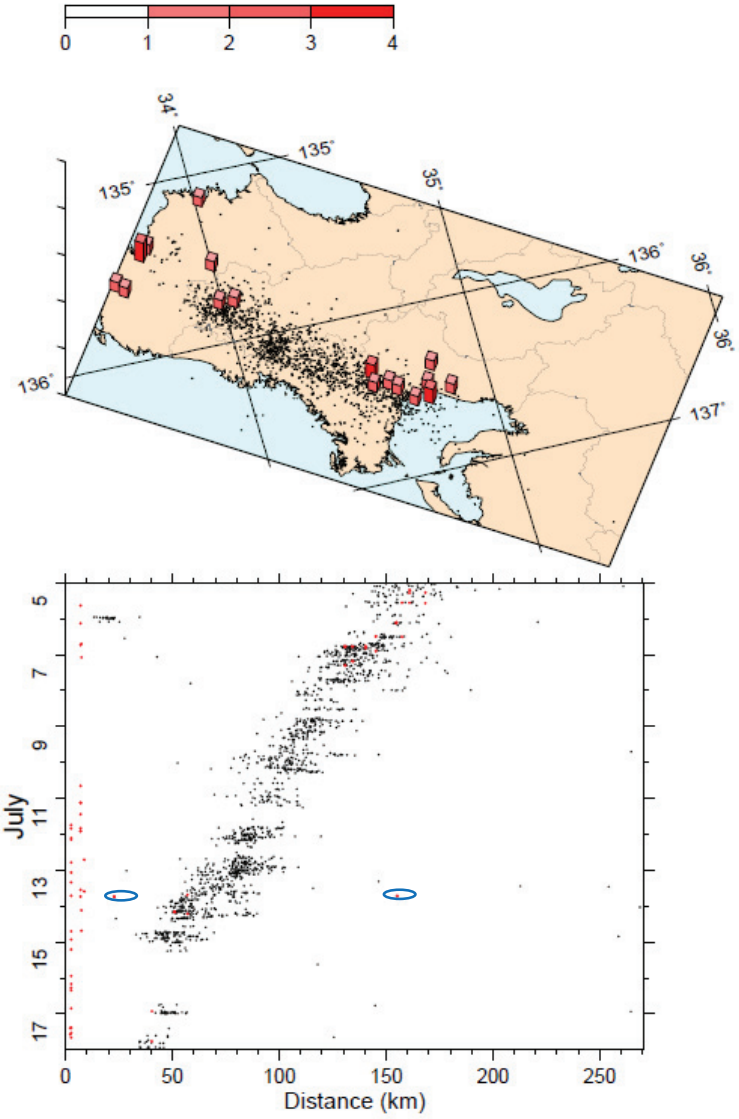

Figure 5.16: Spatial distribution of tremor (black) and VLFE (red) from 1 to 5 September 2014 from 41 Hi-net in Kii region in the upper part, while in the lower part spatiotemporal distribution for the same results. The height and color of the bars are varied according to the number of VLF detection for each virtual source. The detection number is 9 events in 4 locations.
.

5-3. Results using dense virtual source grids for data between 2011 and 2015

After testing our method for several periods and several regions in Nankai trough, we decided to use dense virtual source grid for whole Shikoku region as shown in Finger 3.7 (b), and using the same parameters that we used in data 2006 and 2007 for the same region (minimum VR of t 10) we used 73 Hi- net stations Figure 4 (b) and data periods from 7 to 31 August 2011 ,from 1 to 16 July 2012, from 21 to 31 May 2013, from 1 to 31 May 2014, from 1 to 30 June 2014 , from to 31 July 2014 and from 1 to 11 November 2015 which all are NVT active periods.
We could detect 88 events in 53 locations for data from7 to 31 August 2011 Figure 5.17, 18 events for 12 locations for data from 1 to 16 June 2012 Figure 5.18, 81 events for 47 locations for data from 21 to 31 May 2013 Figure 5.19, and 93 events for 44 locations for data 1 to 11 November 2015 Figure 5.20. As well we analysis continues data from May 1st to July 30th 2014 Figures 5.21 which we could detect 209 events for 95 locations, and for data from 1 to 30 May, Figure 5.22 which we could detect 65 events for 42 locations for data from 1 June to 29, and Figure 5.23. for data from 1 to 30 July, we could detect 119 events for 61 locations.

Figures from 5.17. to 5.23. (lower part for each figure) represents space–time plot for VLFE results for this method using dense virtual sources and tremor detected by ATMOS in periods from7 to 31 August 2011, from 1 to 16 June 2012, from 21 to 31 May 2013, from 1 to 11 November 2015, from 1 to 31 May 2014, from 1 to 30 June 2014 and from to 31 July 2014 respectively, the red dots in both figures represents the VLFE activates while the black dots represents the tremor activities, the upper part represents Shikoku map with the VLFE events locations represented by red circles, the color scale indicates the number of the detection in the same location.

Figure 6.1 (a-j) represent the temporal cumulative number of VLFE seismic moment with respect to tremor's RD (Reduced Displacement of tremor) on periods from7 to 31 August 2011, from 1 to 16 June 2012, from 21 to 31 May 2013, from 1 to 11 November 2015, from 1 to 31 May 2014, from 1 to 30 June 2014 and from to 31 July 2014, respectively. Using dense virtual sources grid for VLIE detection, although we noticed linear relationship, in general, the scale of VLFEs moment is very small compared with our previous results in 2006 and 2007.

Figure 5.25 (a-j) represents the hourly and the cumulative number of detections per the analysis periods of VLFE detected using dense virtual sources grid and tremor detected by ATMOS on periods from7 to 31 August 2011, from 1 to 16 June 2012, from 21 to 31 May 2013, from 1 to 11 November 2015, from 1 to 31 May 2014, from 1 to 30 June 2014 and from to 31 July 2014, respectively. it is noticeable that the detection number for each of these results is small componence with the detection number for our previous results in 2006 and 2007, we thought that maybe if we changed the parameters the results could improve but we couldn't improve them, we tried to change the amplitude factor but also the detection number still small, we think that maybe this result because of artificial reason, or the noise level became higher after Tohoku earthquake or because of a natural phenomenon, to make sure about these we will analyses this data period again using F-net data in the future.

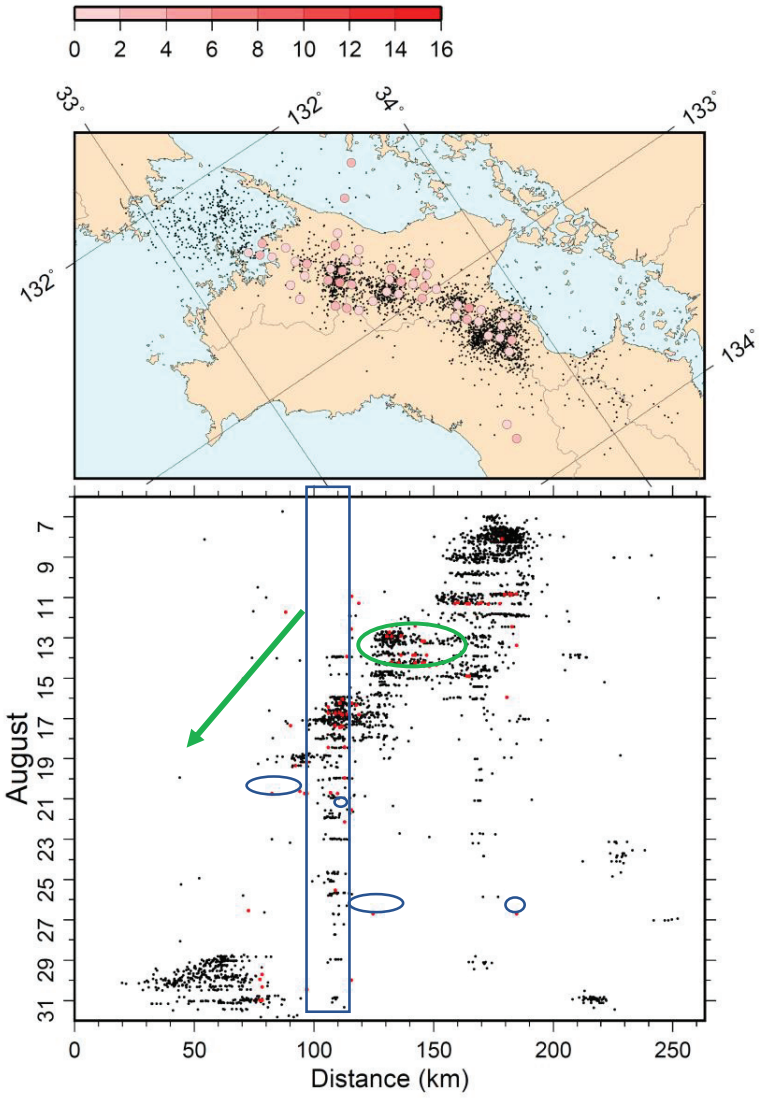

Figure 5.17: Space- time plot for data 2011(August 7 to 31) using dense virtual source grid with a horizontal interval of 5 km (816 virtual sources). Spatial distribution of tremor (black) and VLFE (red) The color of the distribution is varied according to the number of VLFE detection for each virtual source. The detection number is 88 VLFEs events in 53 locations. Green ellipse is where RTR of tremor and rapid reversal of VLF are seen, the green arrow in b is the direction of migration along strike direction, blue rectangle refers to tremor occurrence in the same cluster for a long time. Small blue circles represented examples of VLFE events which are not correlated with the tremor is both space and time.

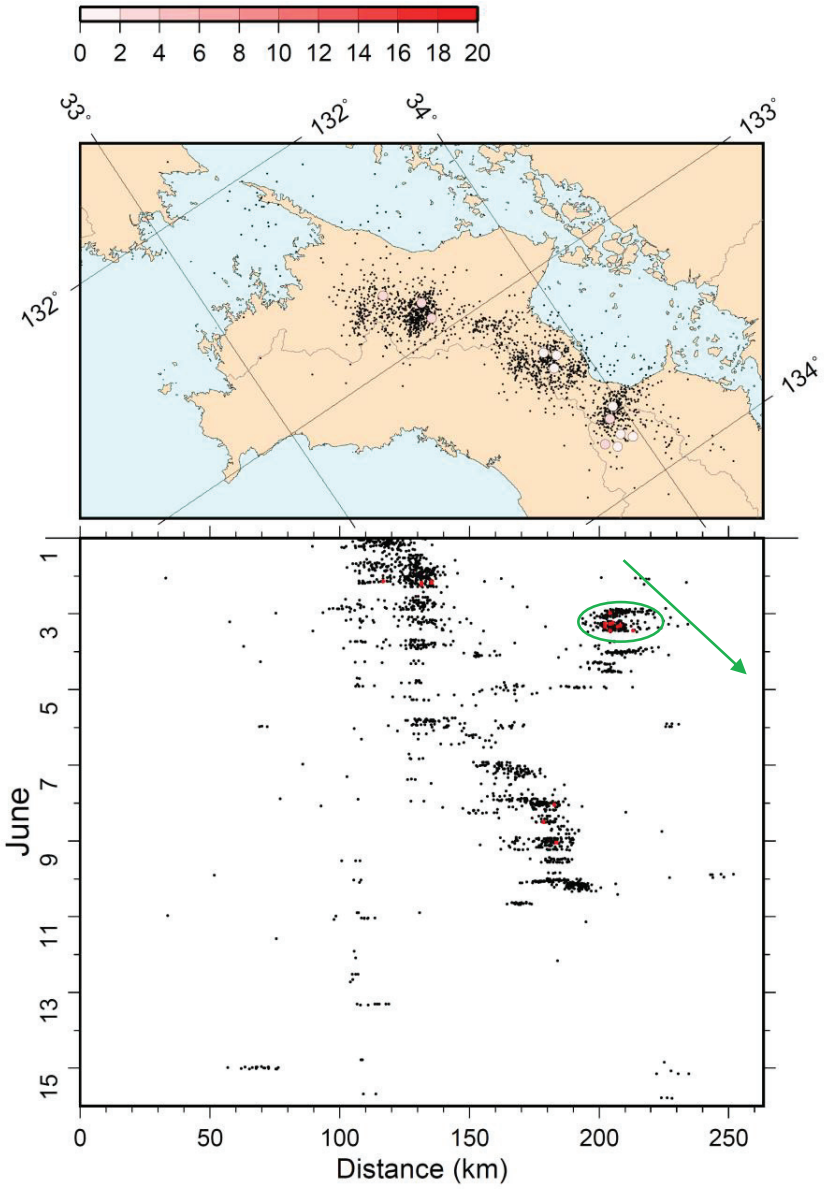

Figure 5.18: Same as in figure 5.17 but for data from June 1 to 15, 2012 detection number is 18 events in 12 locations

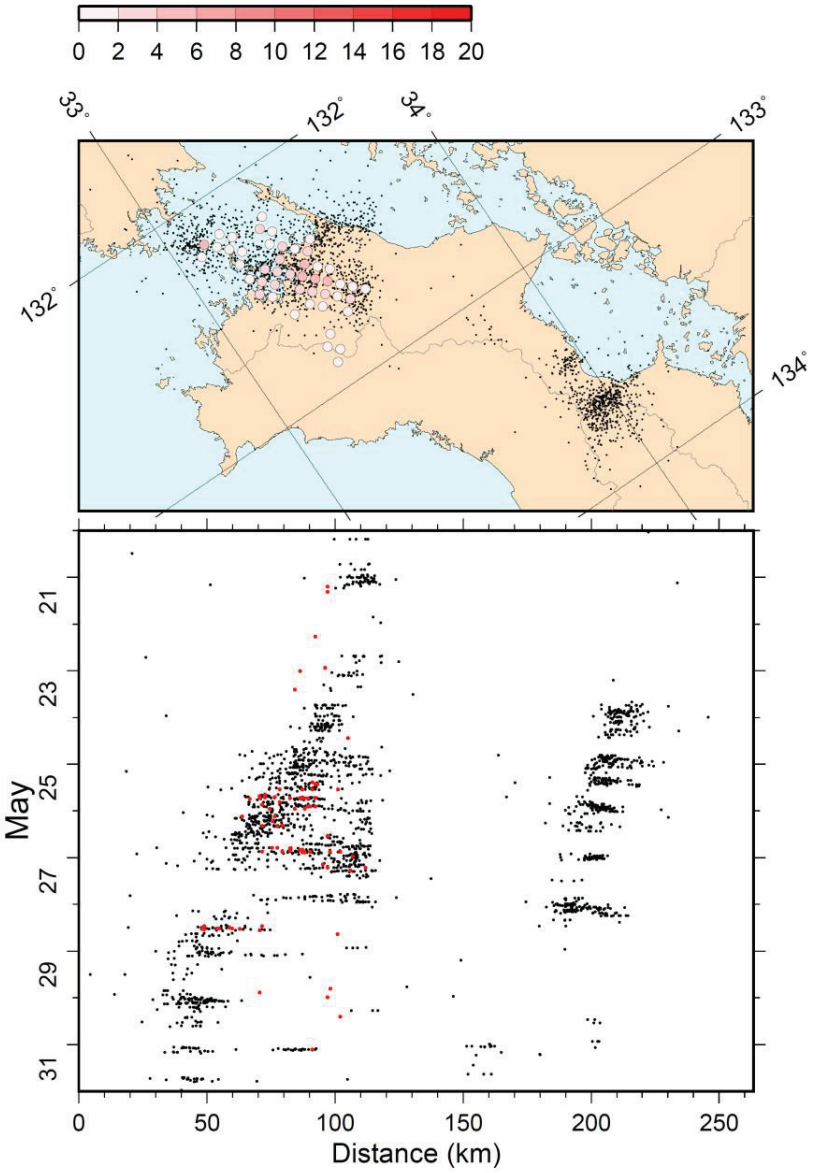

Figure 5.19: Same as in figure 5.17 but for data from 21 to 31May 2013 detection number is 81 events in 47 locations.

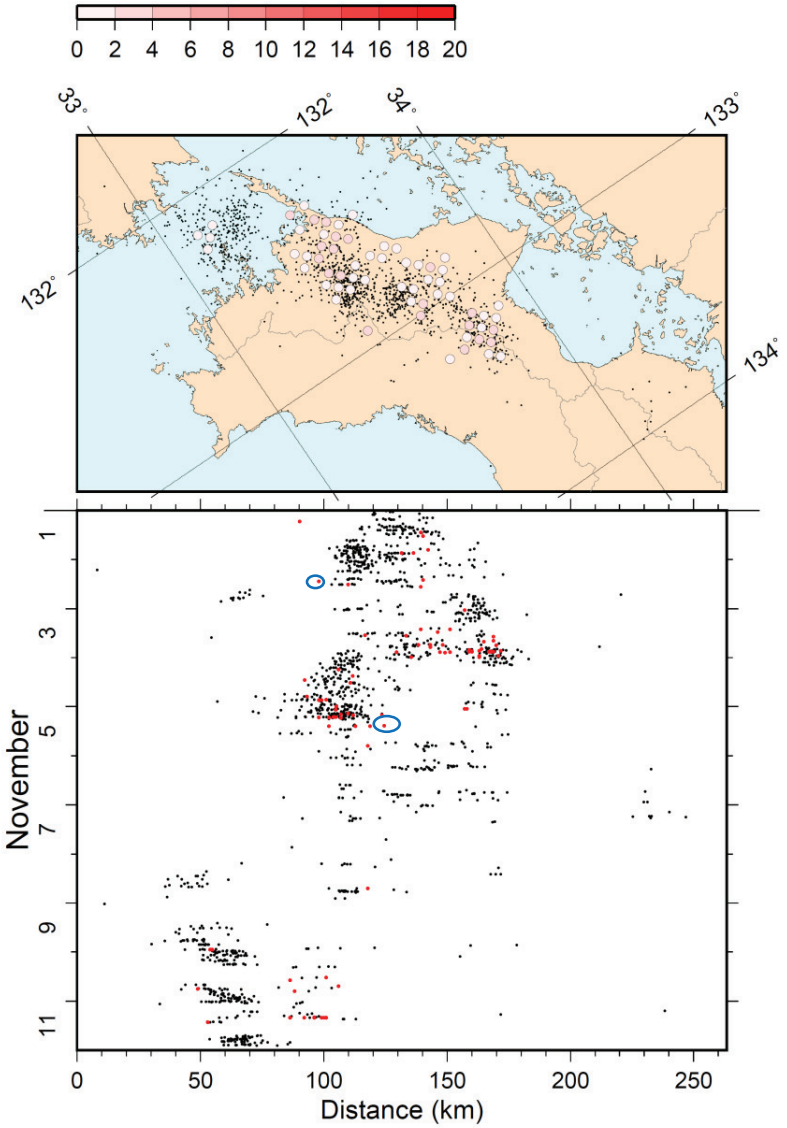

Figure 5.20: Same as in figure 5.17 but for data from 1 to 11 November 2015 detection number is 81 events in 47 locations.

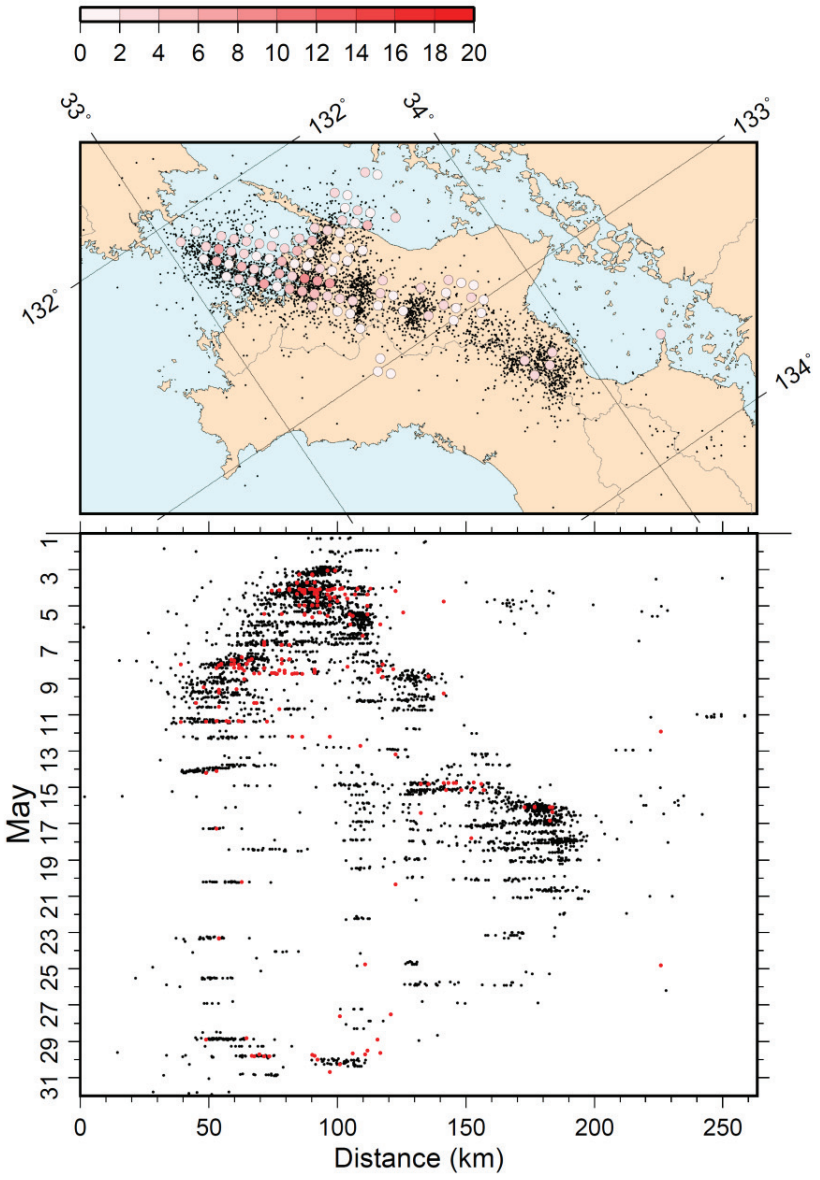

Figure 5.21: Same as in figure 5.17 but for data from 1 to 31 May 2014 detection number is 209 events in 95 locations**.**

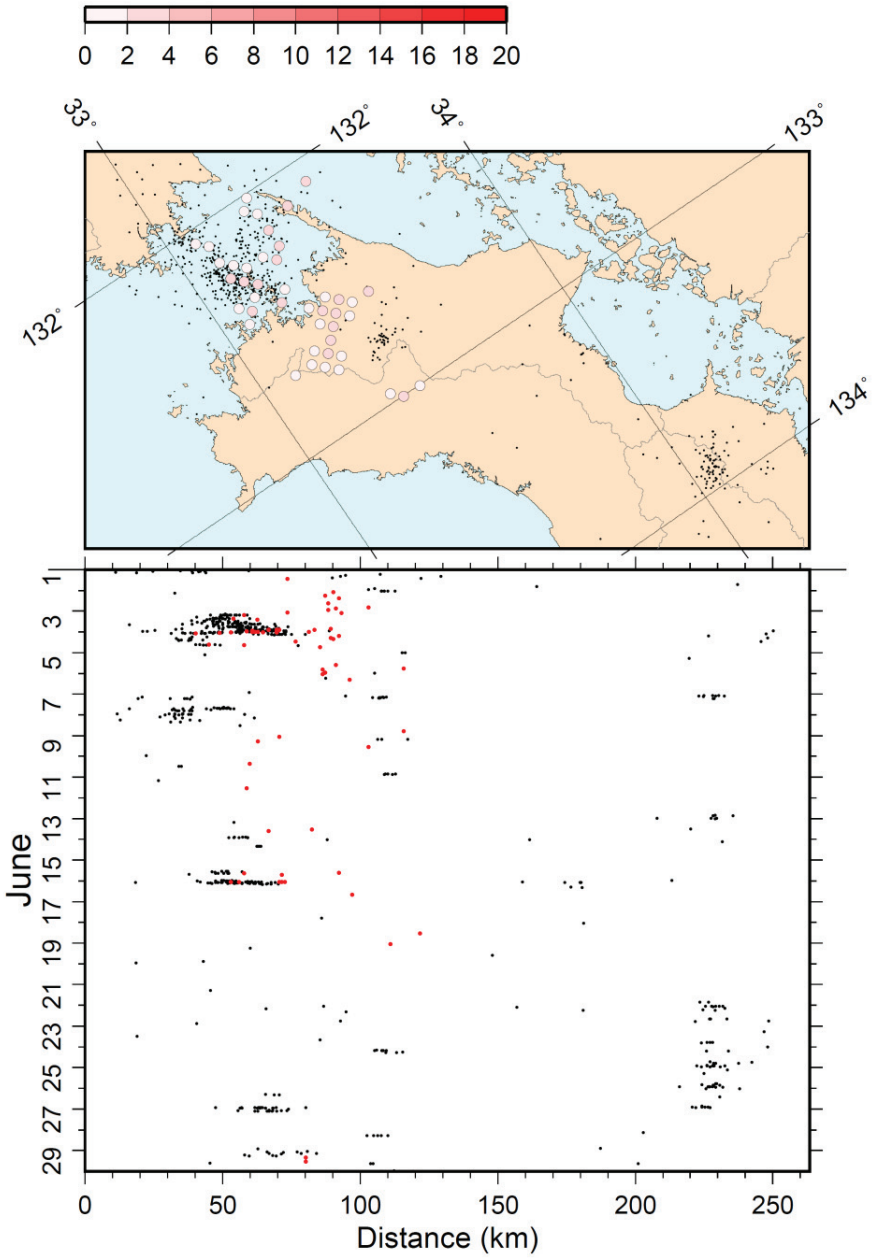

Figure 5.22: Same as in figure 5.17 but for data from 1 to 29 June 2014 detection number is 65 events in 42 locations**.**

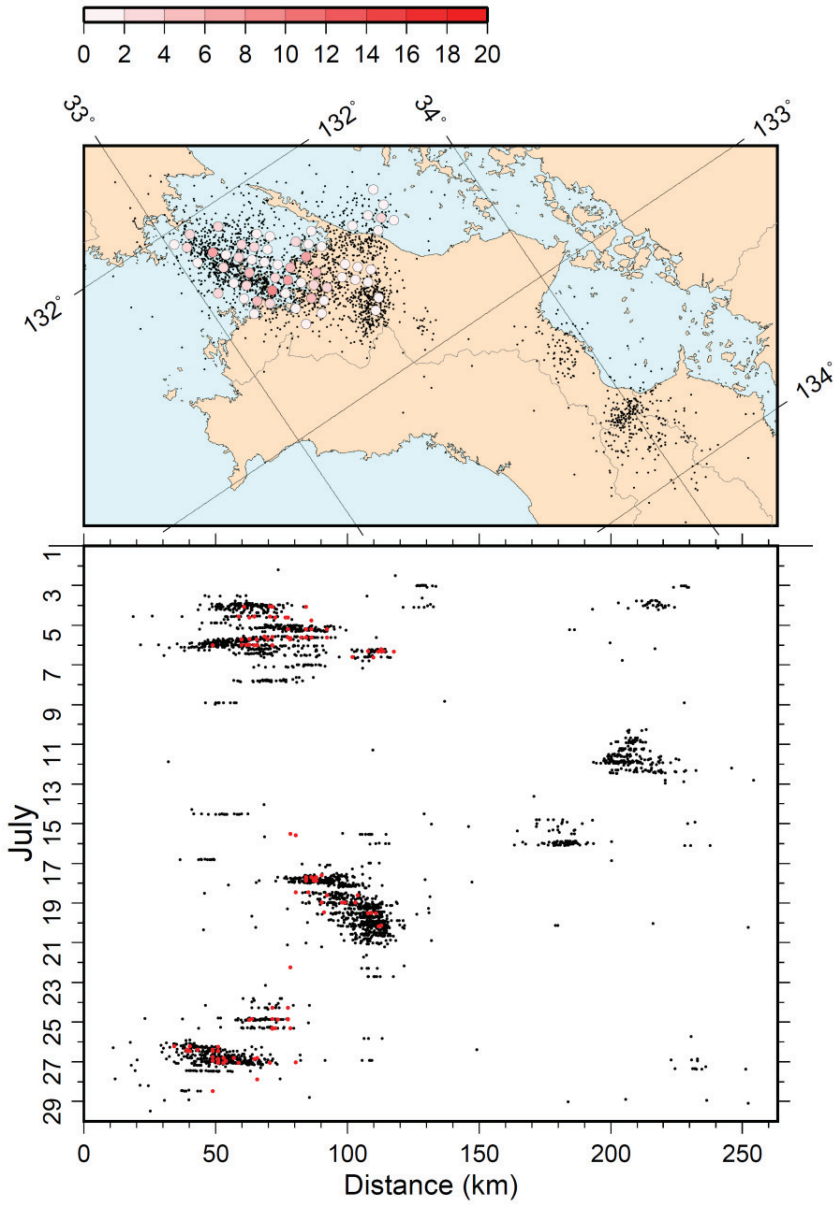

Figure 5.23: Same as in figure 5.17 but for data from 1 to 29 June 2014 detection number is 119 events in 61 locations**.**

Chapter 6
Results

6-1. Very low-frequency earthquake

6-1-1. Number of detections

Until now, many studies that use inversion method to determine earthquake source mechanisms have been developed [Ito et al., 2007-2009], but in this study, we have developed a new method and implemented a new analysis to detect VLFE in Nankai trough. By applying our accurate new method for several data periods, we could detect and locate large numbers of VLFE events in the study area for two periods in 2006 and 2007 for our initial analysis.

In the first trial using data period from 11 to 22 Sep 2006 we could detect 258 events for 28 locations by applying the old version method that used virtual sources grid with a horizontal interval of 10 km, and 298 events for 100 locations by applying the new version method that used dense grids with a horizontal interval of 5 km. We ensured our new version method results by using different data period, we used data from 10 to 21 March 2007, we could detect 277 events for 34 locations using the old version method as shown in Fig 4.1(a, b respectively) and 288 events for 102 locations for the new version method as shown in Fig 4.2(c, d respectively), we can say that we could increase the detection number and the spatial distribution using dense grid of virtual sources, we improved our results by changing the parameters, these parameters could be changed for other analysis for new data periods or new regions.

For the analysis in the Western Shikoku, Eastern Shikoku, Kii, and Tokai, we could detect more VLFE events when we used the dense grid of virtual sources. We saved analyzing time and gave clearer spatially results, but we got the same detection number as when we analysis whole Shikoku by using the same parameters. When we used data from limited stations (only in the Area of study) the detection number of VLFE decrease for about 5 times less than the detection number of VLFE when we used extended stations in the surrounding area around the study region. Changing the parameters as variance reduction is very important when we use a different number of stations and different data.

For the analysis from 2011 to 2015 in whole Shikoku region Figures 5.17-23. We noticed in all these results that the detection number decreased compared with the analysis from 2006 and 2007, We thought that is could be because of the parameters, but by changing the parameters many times we couldn't increase the detection numbers, then we thought that maybe because the amplitude factor so we re-calculate the amplitude factor for all the data and did the analysis again, but also we couldn't increase the detection number, we think these results may because artificial reason or because the noise level became higher after Tohoku earthquake or because of a natural phenomenon, to make sure about this suggestion we will analyze the same data periods using F-net data in the future, if we could not increase the detection number by this procedure, then we will interpret these abnormal results as natural phenomena which will be very important result for earthquake prediction in this region.

6-1-2. Comparison with the results from previous studies

We calculated in detail the characteristics of VLFE. We considered our results from data 2006 and 2007 as the mean results since other results need more analysis to confirm the final detections. From 2006 and 2007 results; It noticeable that the accuracy of this method is very high compared with the previous studies. We could achieve a high temporal resolution of VLFE detection with preservation of clear spatial distribution as shown in Figure 6.1 (a) and (b). In the result, we detected and located small and new events, and we could increase the detection number about 10 times more than the previous studies. Although we set VR threshold of 10 in this method which is very low compared with the previous study. For example, [Tsuruoka et al., 2009] which is an analysis method for ordinary earthquakes, VR threshold was 65, in [Ito et al. 2007, 2009] VR was 40, and in [Takeo et al.2010] VR was 30, and generally, as the threshold value of VR decreases, the number of detections increases the artificial events number also increases, [Tsuruoka et al., 2009], but in this method, we solved this problem by assuming the mechanism of the virtual hypocenter beforehand, and by eliminating false events using the index value of the amplitude.

In fact, many newly detected events in this method are not false events means that the frequency distribution with magnitude shows a clear distribution as shown in Figure 6.2 (a) and (b) and Figure 6.3 (a)-(d) which represent the frequency distribution with the magnitude for data from Sep 2006, Mar 2007, May 2014, June 2014 July 2014 and for long period from May 1st, 2014 to July 30th, 2014 in addition, although Mw 2.9 is the lower than the previous studies, Mw 2.7 can be detected by this method. It can be said that this method can detect events with small Mw that the previous studies could not detect even when considering that the average Mw is smaller than results in the previous studies.

(a)

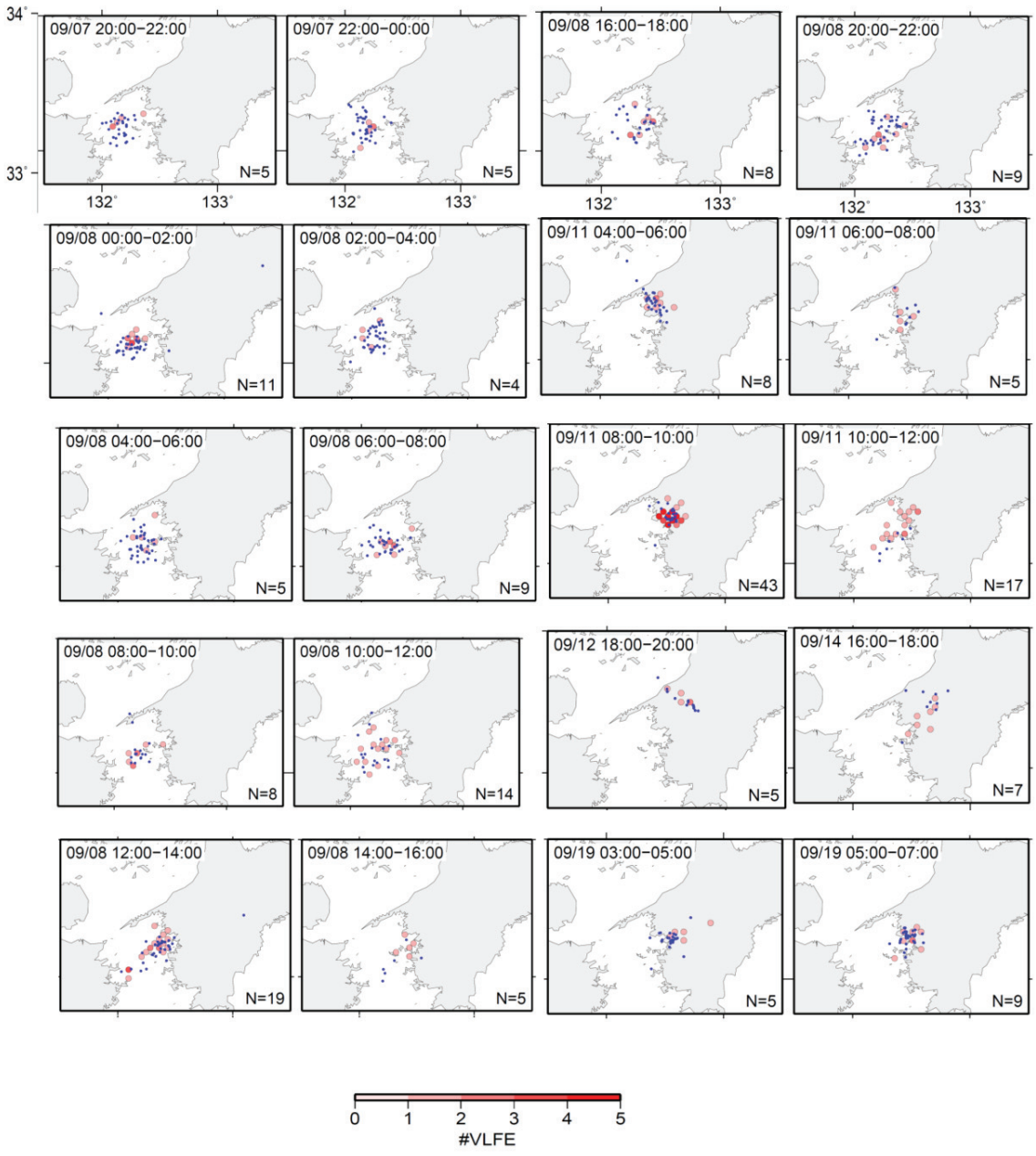
34°
33°
132°
133°
09/07 20:00–22:00
N=5
09/07 22:00–00:00
N=5
09/08 16:00–18:00
N=8
09/08 20:00–22:00
N=9
09/08 00:00–02:00
N=11
09/08 02:00–04:00
N=4
09/11 04:00–06:00
N=8
09/11 06:00–08:00
N=5
09/08 04:00–06:00
N=5
09/08 06:00–08:00
N=9
09/11 08:00–10:00
N=43
09/11 10:00–12:00
N=17
09/08 08:00–10:00
N=8
09/08 10:00–12:00
N=14
09/12 18:00–20:00
N=5
09/14 16:00–18:00
N=7
09/08 12:00–14:00
N=19
09/08 14:00–16:00
N=5
09/19 03:00–05:00
N=5
09/19 05:00–07:00
N=9
0 1 2 3 4 5
#VLFE

(b)

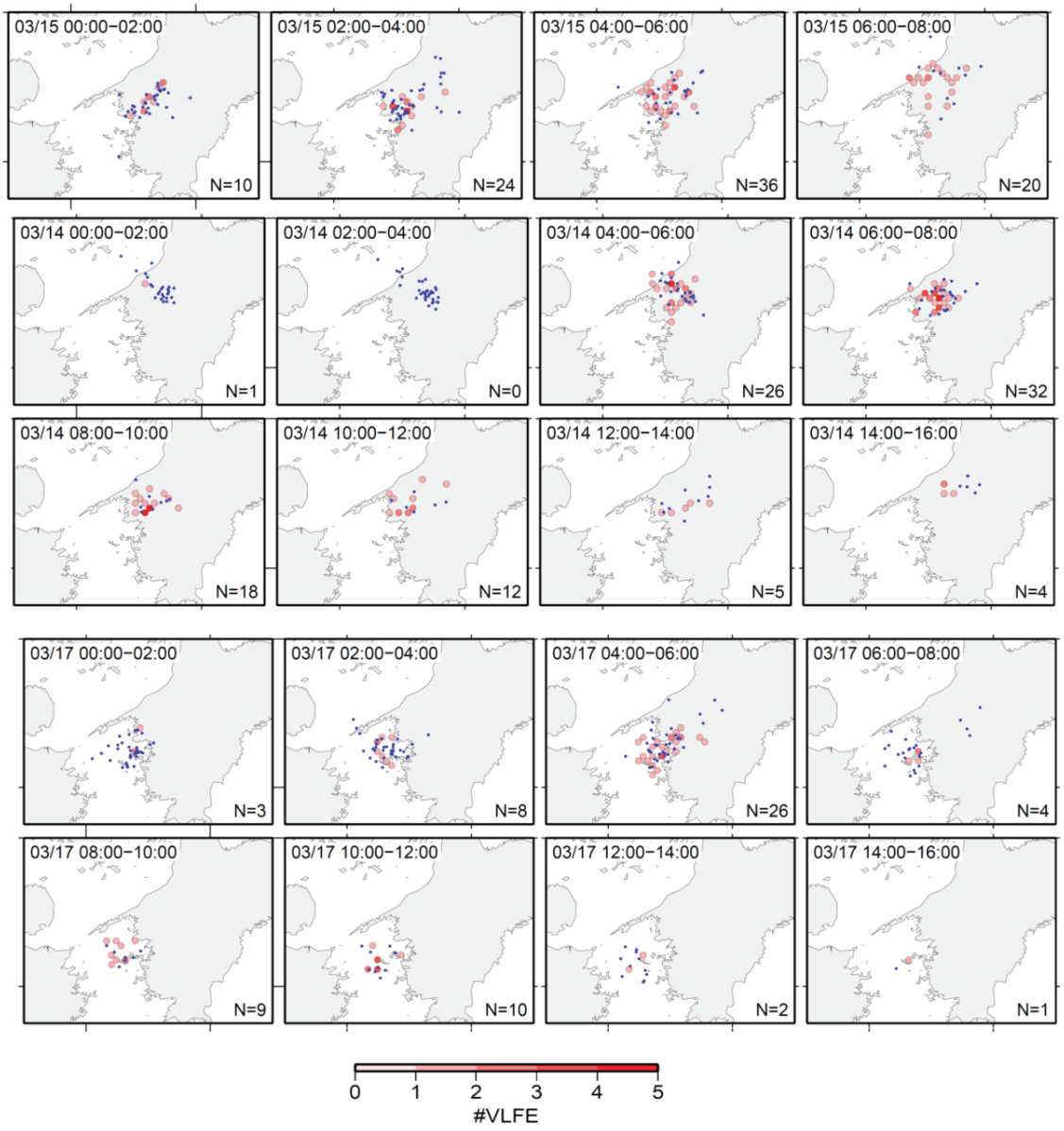

Figure 6.1: The High temporal resolution of VLFE detection with preservation of clear spatial distribution which confirms the high accuracy of this detection method. The blue circles are tremor epicenters while the red circles are VLFE epicenters. The color scale represented the VLFE detection number in the same location. Each small panel represented shikoku West map with VLFE and tremor distribution every two hours and indicating to VLFEs rapid reversal with tremor RTR (a) Data from 6 to 22 September 2006 (b) Data from 10 to 21 March 2007.

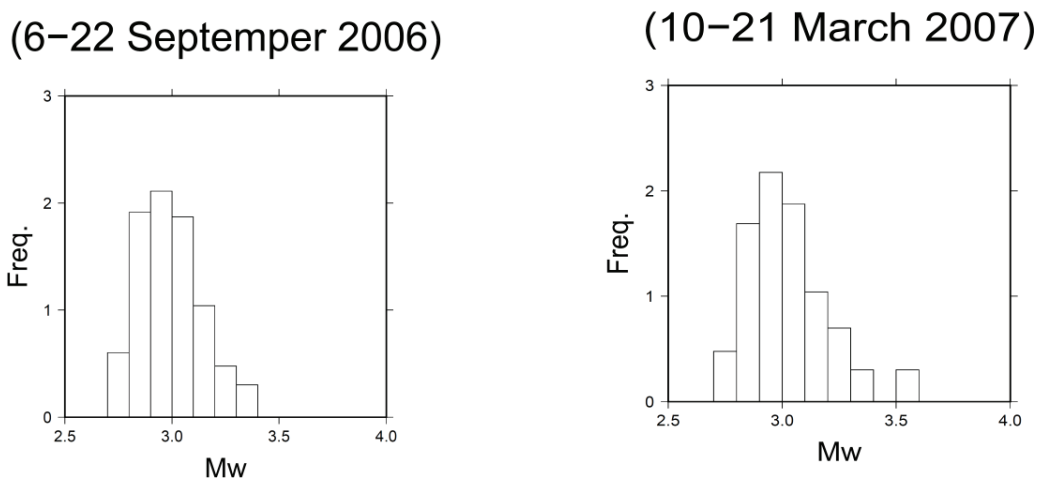

Figure 6.2: Moment magnitude-frequency relationship (a) data from 6 to 22 September 2006 (b)data period from 10 to 21 March 2007, in both results, it is noticeable that the minimum moment magnitude is about 2.7 and the average is 2.9 which is smaller than the previous studies.

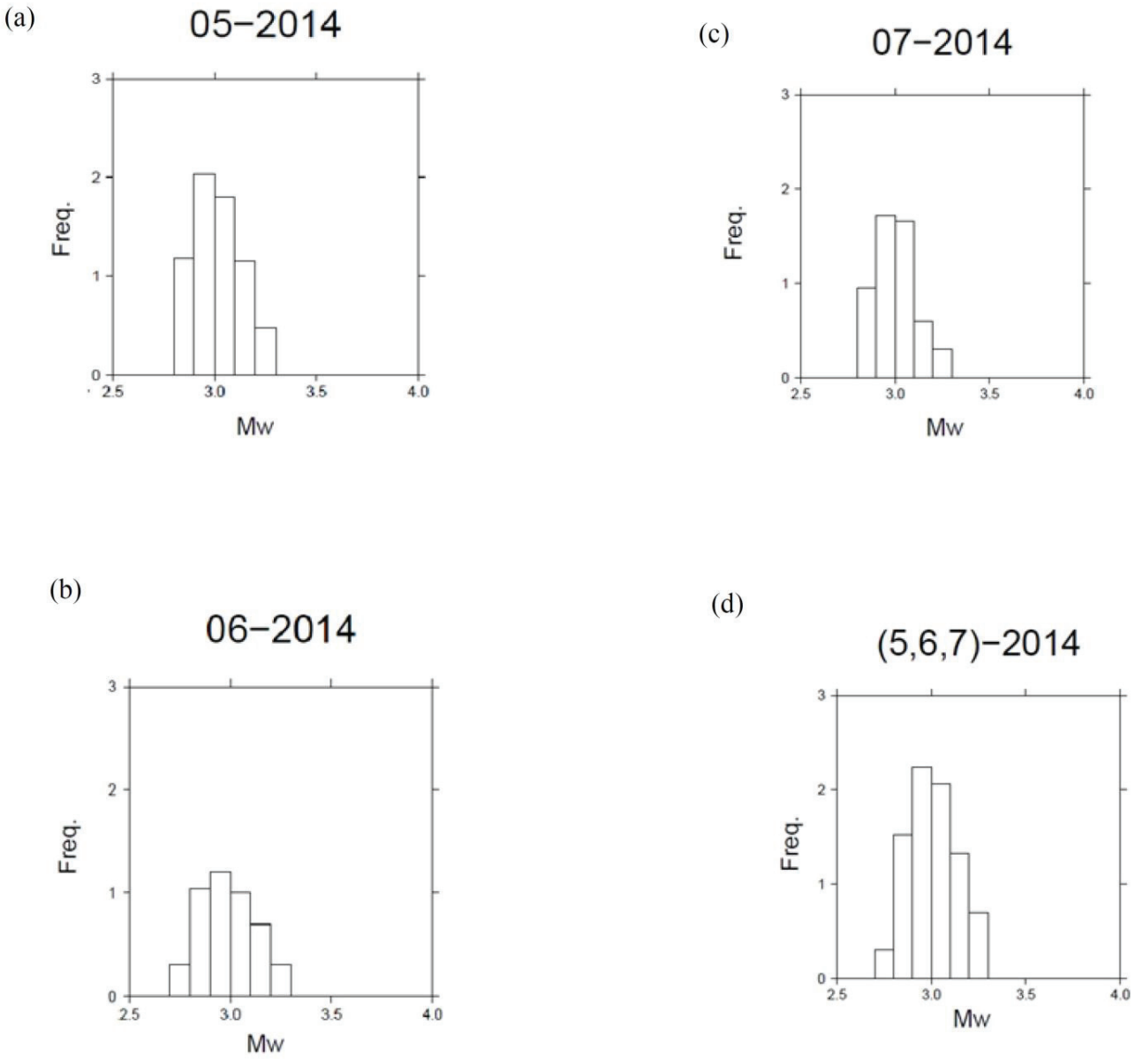

Figure 6.3: Same as Figure 6.2 but in (a) for data from 1 to 31 May 2014 (b) for data from 1 to 29 June 2014, (c) from 1 to 30 July 2014, and (d) for all the period together from May 1st to July 30th, 2014

6-2. Tremor in southwest Japan

Deep long-period tremors were recognized and located in a nonvolcanic region in southwest Japan. Epicenters of the tremors were distributed along the strike of the subducting Philippine Sea plate over a length of 600 kilometers. The depth of the tremors averaged about 30 kilometers, near the Mohorovic discontinuity. Each tremor lasted for at most a few weeks. The location of the tremors within the subduction zone indicates that the tremors may have been caused by fluid generated by dehydration processes from the slab [Obara ,2002]. Tremor occurs simultaneously with short-term slow slip events (SSEs); an SSE with simultaneous tremor is termed episodic tremor and slip (ETS) because the two phenomena are spatially and temporally coupled [e.g., Rogers and Dragert, 2003]. [Annoura, et al., 2016]. Tremor and SSE usually migrate coincidently along the strike of the subducting plate [Obara, 2010]. Tremor correlates with VLFE in space and time as previous studies showed, for example [Ito, 2007] and [Ghosh et al,2015], but a new study showed that it is possible that VLFE not correlate with tremor in both space and time [A. Hutchison et al,2016], to study the relationship between VLFEs and NVT in Nankai trough, we utilized the NVT data which are the results of the Automatic Tremor Monitoring System (ATMOS) [Suda et al, 2009].

6-3. Relationship between very low-frequency earthquake and tremor

6-3-1. Spatio-temporal distribution

6-3-1-1. Spatio-temporal correlation

We chose our data periods because the periods include episodic tremors and according to the previous findings [e.g. Ito et al., 2007] VLFEs occur when and where there is strong tremor detected, and the both phenomena have a clear spatiotemporal relationship. In this study, we found that VLFE activity occur in wide range during our data periods, although the total tremor lasted for more time and more space, but in most cases VLFE are located within and where tremors are located as the previous studies results as Figures 4.1, 4.2, 5.4, 5.5, 5.8, 5.9, 5.13 and 5.17- 23 are shown.

6-3-1-2. Very low-frequency earthquake not associate with tremor

Although it is noticeable that VLFE and NVT are correlated in space and time in most cases , but we noticed some VLFE events that not correlated with tremor activity both in space and time (small blue circles in Fig 4.1(b), Fig 4.2 (b), and in Figs 5.16-22, but this suggestion needs more analysis and interpreting in the future, if we could confirm those events as a real VLFE events, this result may change our current understanding of the clear spatiotemporal relationship between tremor and VLFE as a results issued by [Hutchison & Ghosh, 2016]. In Figs 4.1 and 4.2, although we analyzed the same data periods twice by using different virtual source grids, we noticed that some events appeared at the same time and space in both results in each time period. Yellow circles in the both figures and these events are not correlated with a tremor in space and time, therefore it is possible they are real VLFE detection.

6-3-1-3. Rapid reversals of very low-frequency earthquake and tremor

From the spatiotemporal distributions results, some features about tremors and VLFE activities could be confirmed, for example, the phenomenon called rapid tremor reversal (RTR) [Houston et al., 2011], in which the tremor migrate rapidly back in the opposite direction to the overall movement direction, which are shown by green rectangle in (a) and ellipse in (b) of Fig 4.1, green rectangle in (a) and ellipse in (b) of Fig.2, and green ellipses in Figs 5.17, 18 and 21. We also noticed that at the same time as RTR, VLFE also performed high-speed source movement in the opposite direction to the overall source movement Fig 6.1.

In the rectangle surrounded by the blue frame in Figs 4.1 (a), 4.2 (a), 5.17, 18 and 21, tremor occurs in the same cluster for a long time. In this cluster, the mode of VLFE occurrence varied depending on the activity period. In the activity in September 2006, VLFE rarely occurred in this cluster. On the other hand, in March 2007 a lot of VLFE activity was detected. Such features were seen only in this tremor cluster during this analysis period.

6-3-2. Comparison between moment release of very low-frequency earthquake and reduced displacement of tremor

Figure 6.4 (a) and (b) represents the relationship between the temporal cumulative number of VLFE seismic moment and tremor's Reduced Displacement (RD) on September 2006 and March 2007 respectively. Takeo et al. 2010 observed a correlation between VLF moment and tremor energy rate with a correlation coefficient of 0.61. From the results of this method and with respect to the scale, we noticed a linear relationship between VLFE moment tremor RD.

In Figure 6.5 (a- j) which represent VLFE moment and tremor RD from 2011 to 2015 respectively, it is noticeable that VLFEs moment very low compare of 2006 and 2007 activity, this may because artificial technique (data or parameters) or natural phenomena so we need to confirm these results in the future.

6-3-3. Comparison between moment release of very low-frequency earthquake and reduced displacement of tremor

Figure 6.6 (a) and (b) represents the hourly and the cumulative number of detections per the analysis periods of VLFE and tremor in September 2006 and March 2007 respectively, by Comparing the temporal generation pattern of VLFE and tremor, VLFE events are rapidly active in each active period compared to tremor. This is particularly noticeable in the three active periods of activity in March 2007. As well, by paying attention to the peak of each activity, we can see that the peak of VLFE is delayed with respect to tremor. this feature proves that our VLFEs results are not artificial result, the tremor detection number is larger than VLFEs, this may because of different sizes or characteristics of the two phenomena and their occurrence mechanisms.

In Figure 6.7 (a-j) which represent the VLFE and tremor detection numbers from 2001 to 2015 activity, respectively. It is noticeable that's VLFEs detection number is very low compared with 2006 and 2007 activity, this could be because of different sizes or characteristics of the two phenomena and their occurrence mechanisms.

(a)

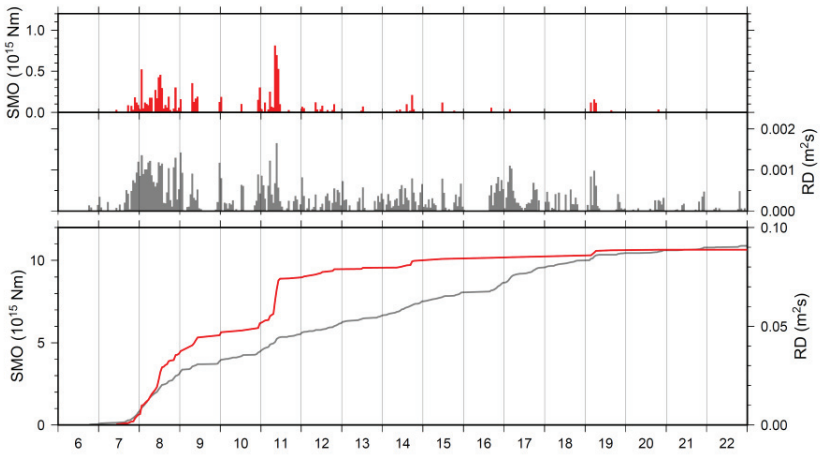

(b)

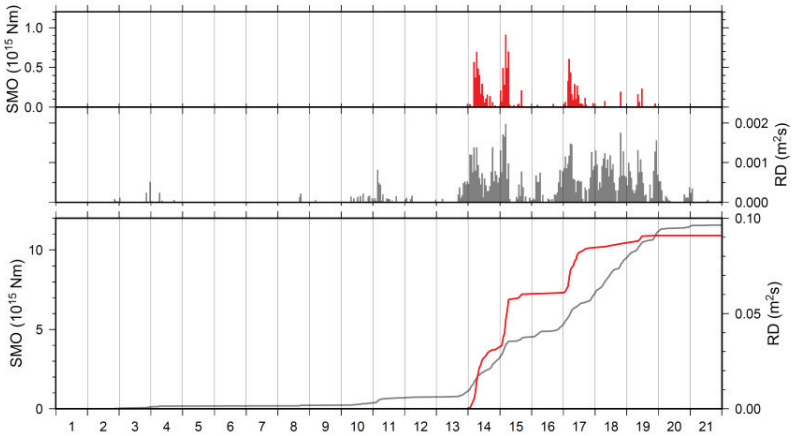

Figure 6.4: Comparison between VLFEs' seismic moment and tremors' reduced displacement(RD) (a) data from 6 to 22 September 2006, (b) data from 10 to 21 March 2007, the red line is VLFEs' moment while the gray line is tremors' RD. The bars in the upper panel represents the cumulative number in each active day while the lower panel represents the cumulative number curve for all the analysis periods.

(a)

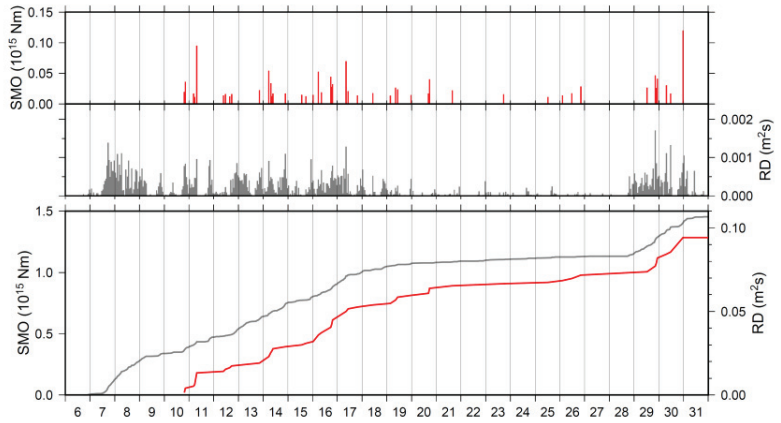
SMO (10^{15} Nm)
RD (m^2s)
SMO (10^{15} Nm)
RD (m^2s)

(b)

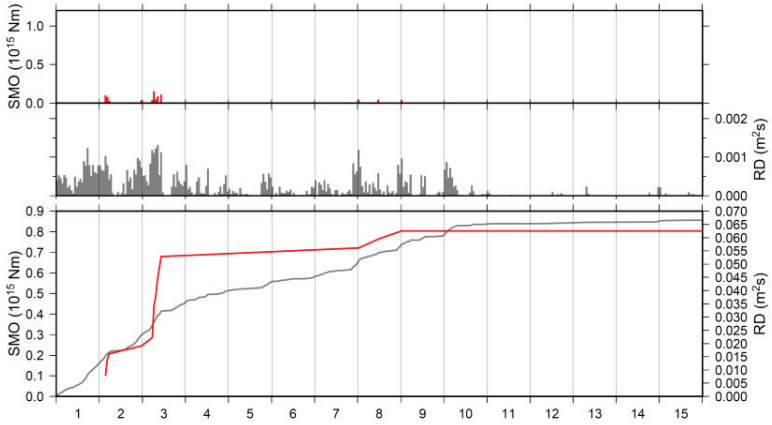
SMO (10^{15} Nm)
RD (m^2s)
SMO (10^{15} Nm)
RD (m^2s)

(c)

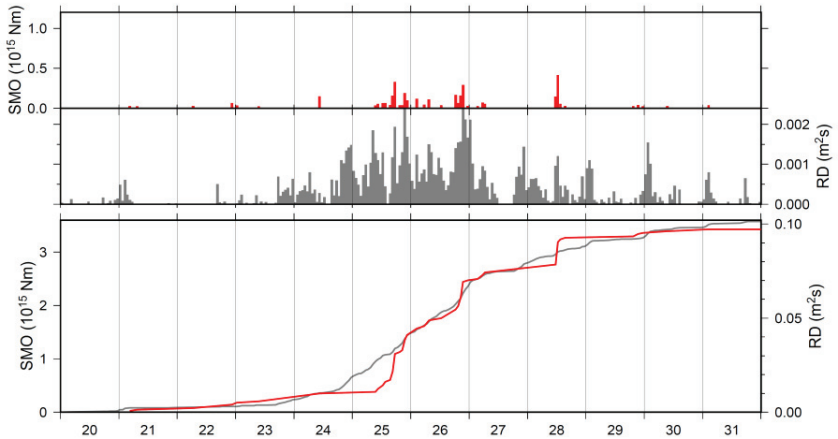
SMO (10^{15} Nm)
RD (m^2s)
SMO (10^{15} Nm)
RD (m^2s)

(d)

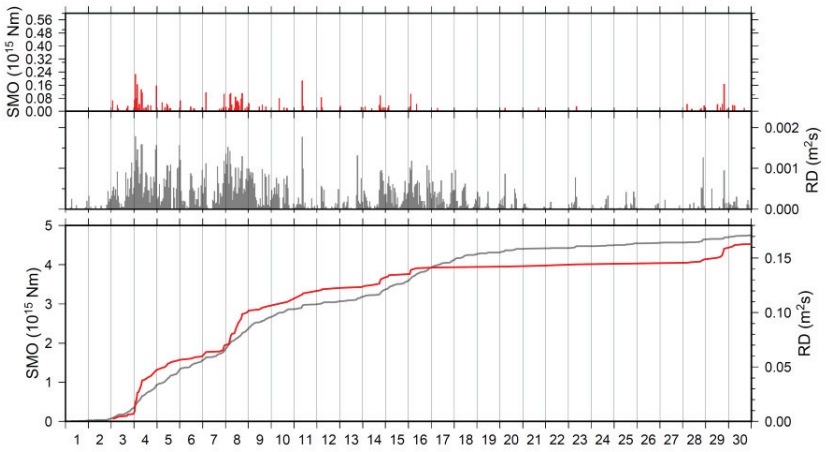
SMO (10^15 Nm)
0.56
0.48
0.40
0.32
0.24
0.16
0.08
0.00
0.002
0.001
0.000
RD (m^2s)
5
4
3
2
1
0
SMO (10^15 Nm)
0.15
0.10
0.05
0.00
RD (m^2s)
1 2 3 4 5 6 7 8 9 10 11 12 13 14 15 16 17 18 19 20 21 22 23 24 25 26 27 28 29 30

(e)

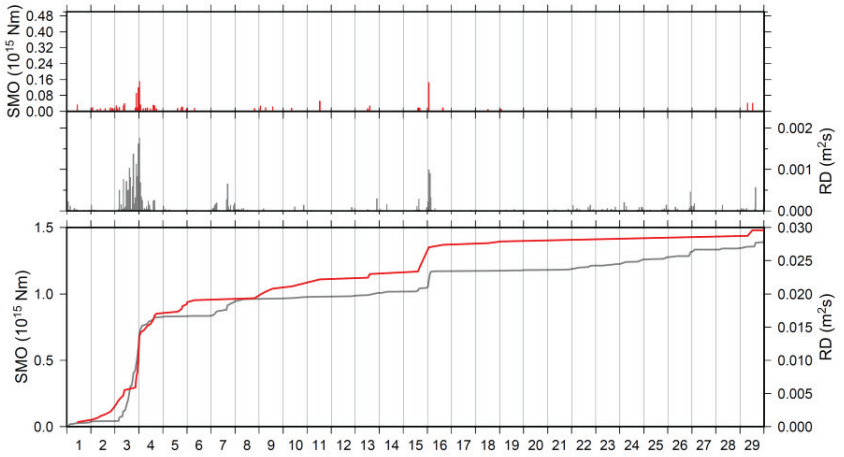
SMO (10^15 Nm)
0.48
0.40
0.32
0.24
0.16
0.08
0.00
0.002
0.001
0.000
RD (m^2s)
1.5
1.0
0.5
0.0
SMO (10^15 Nm)
0.030
0.025
0.020
0.015
0.010
0.005
0.000
RD (m^2s)
1 2 3 4 5 6 7 8 9 10 11 12 13 14 15 16 17 18 19 20 21 22 23 24 25 26 27 28 29

(f)

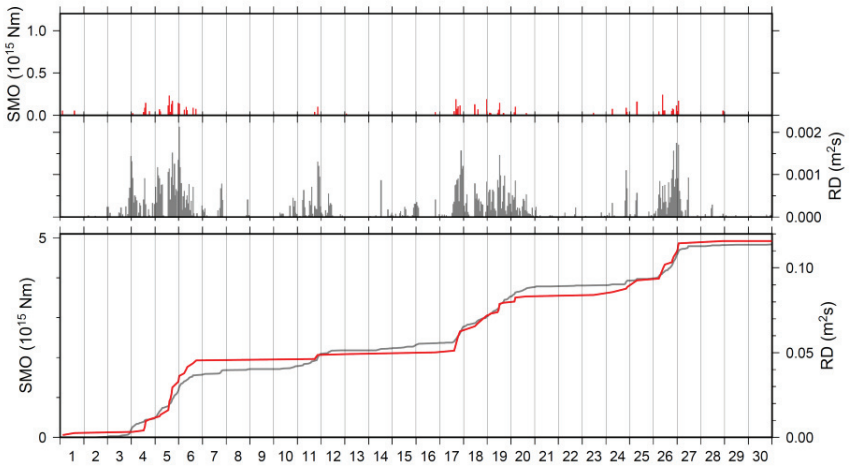
SMO (10^15 Nm)
1.0
0.5
0.0
0.002
0.001
0.000
RD (m^2s)
5
0
SMO (10^15 Nm)
0.10
0.05
0.00
RD (m^2s)
1 2 3 4 5 6 7 8 9 10 11 12 13 14 15 16 17 18 19 20 21 22 23 24 25 26 27 28 29 30

(g)

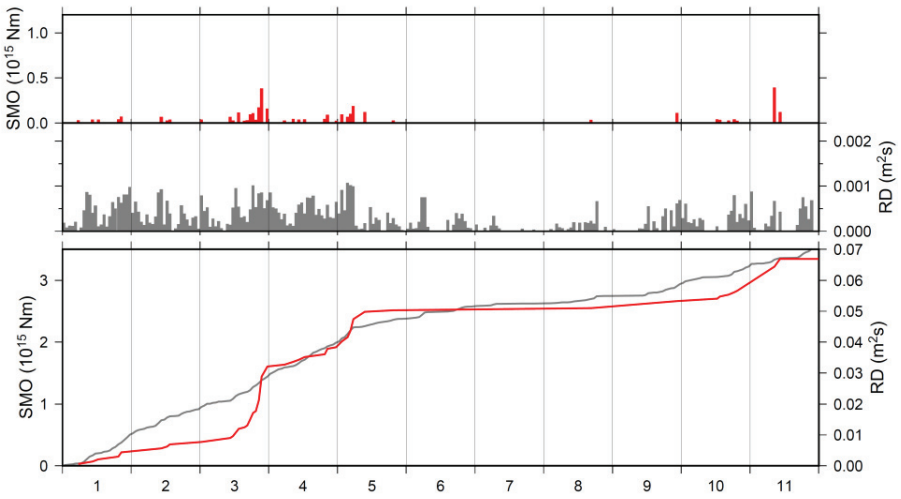

Figure 6.5: Comparison between VLFEs' seismic moment and tremors' reduced displacement(RD) (a) data from 2011, (b) data from 2012 (c) data from 2013 (d) data from May 2014 (e) data from June 2014 (f) data from July 2014 (g) data from 2015, the red line is VLFEs' moment while the gray line is tremors' RD. The bars in the upper panel represents the cumulative number in each active day while the lower panel represents the cumulative number curve for all the analysis periods.

(a)

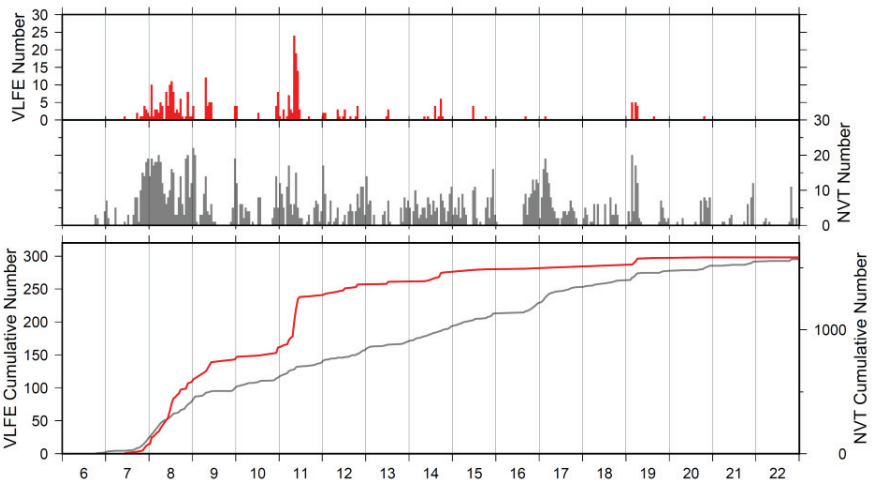

(b)

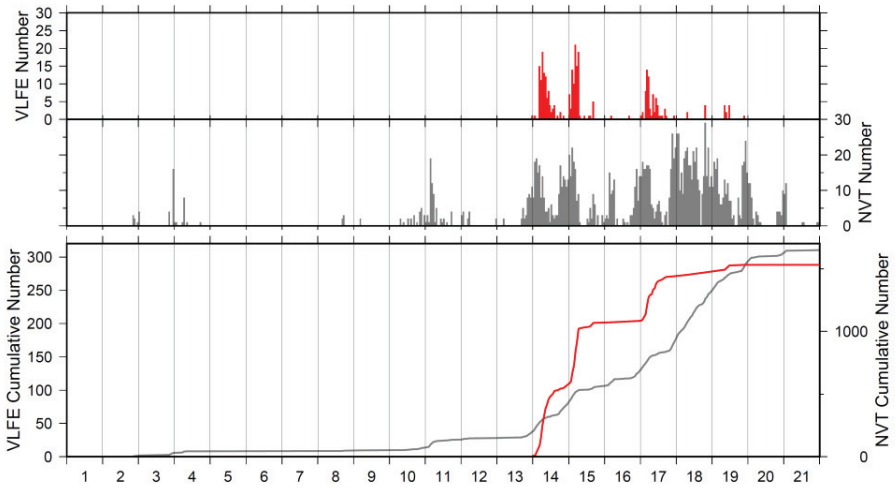

Figure 6.6: Comparison between VLFE and tremor detection number (a) data from 6 to 22 September 2006, (b) data from 10 to 21 March 2007, the red line is VLFE while the gray line is tremor cumulative detection number. The bars in the upper panel represents the cumulative number in each active day while the lower panel represents the cumulative number curve for all the analysis periods.

(a)

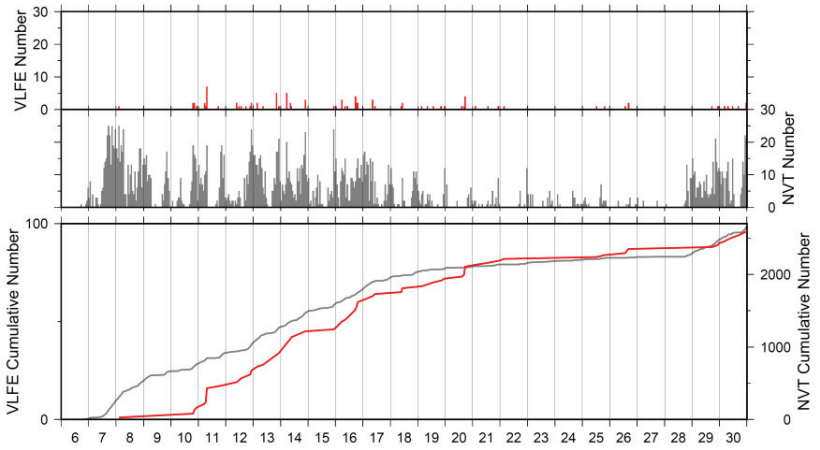
VLFE Number
NVT Number
VLFE Cumulative Number
NVT Cumulative Number

(b)

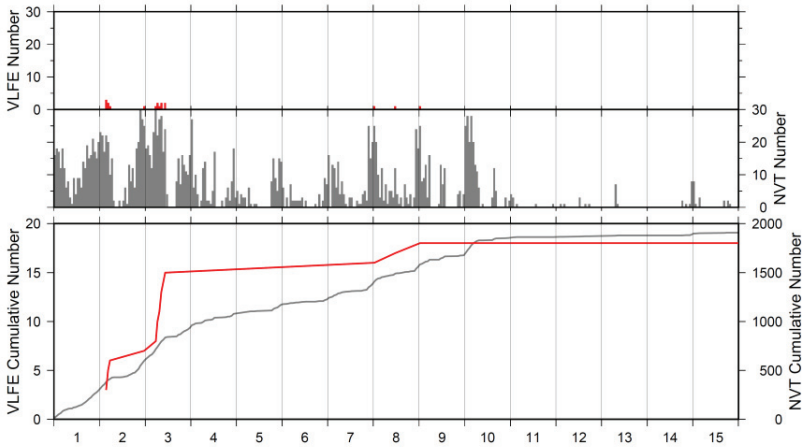
VLFE Number
NVT Number
VLFE Cumulative Number
NVT Cumulative Number

(c)

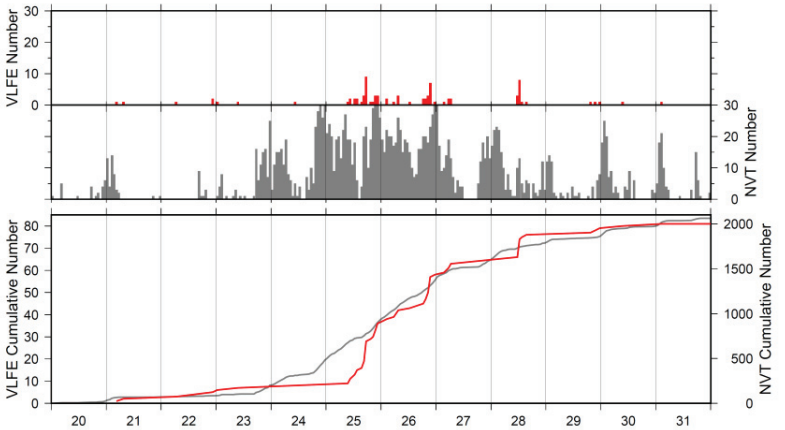
VLFE Number
NVT Number
VLFE Cumulative Number
NVT Cumulative Number

(d)

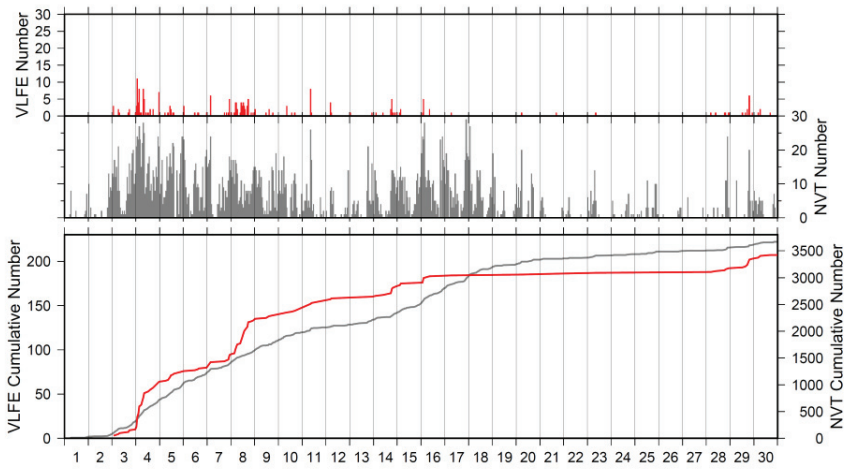
VLFE Number
NVT Number
VLFE Cumulative Number
NVT Cumulative Number

(e)

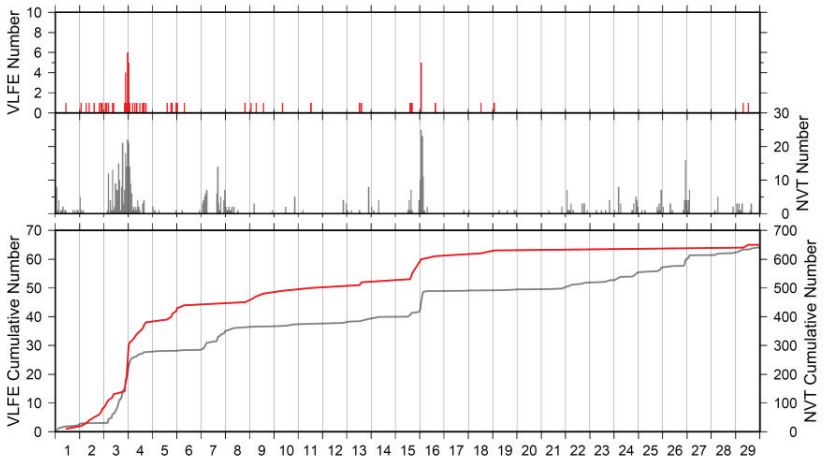
VLFE Number
NVT Number
VLFE Cumulative Number
NVT Cumulative Number

(f)

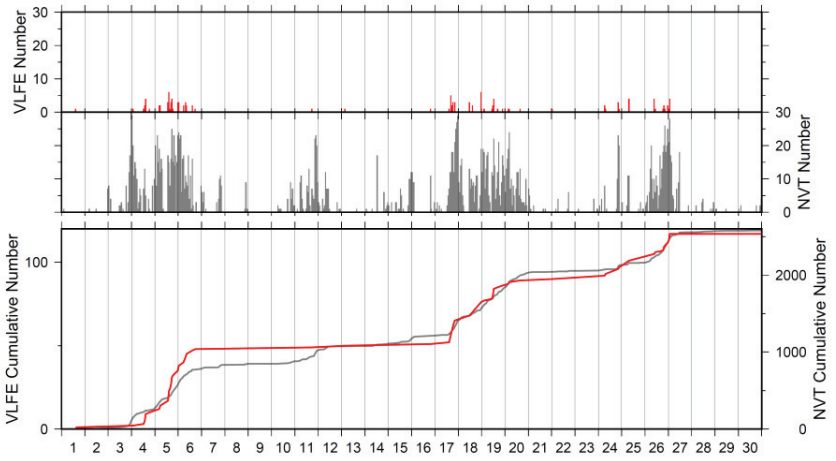
VLFE Number
NVT Number
VLFE Cumulative Number
NVT Cumulative Number

(g)

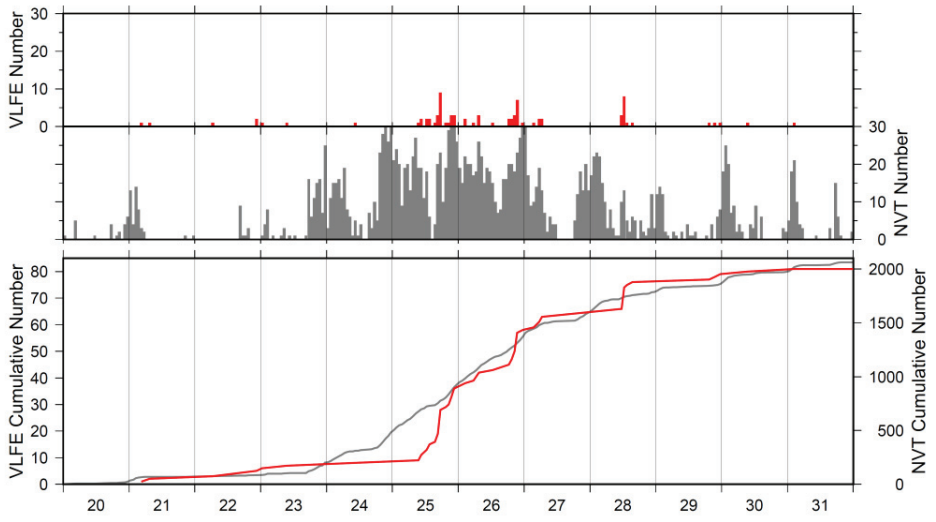

Figure 6.7: Comparison between VLFE and tremor detection number (a) data from 2011, (b) data from 2012 (c) data from 2013 (d) data from May 2014 (e) data from June 2014 (f) data from July 2014 (g) data from 2015, the red line is VLFE' while the gray line is tremor cumulative detection number. The bars in the upper panel represents the cumulative number in each active day while the lower panel represents the cumulative number curve for all the analysis periods.

Chapter 7

Discussions and Conclusions

In this study, we developed an analytical detection method for deep very low-frequency earthquakes. In this method, the virtual hypocenters assumed in advance as a reverse fault slip the upper boundary surface of the subduction Philippine Sea plate. The detection is performed by comparing the theoretical waveform obtained from the virtual source to the observed waveform. In addition, the elimination of the errors in the detection and artificial events is performed using information about the amplitude of the observed waveform and information about the occurrence of the events. The position and scale of the VLFE determined by this method were roughly in agreement with the previous studies.

It can be said that the VLFE detection accuracy of this method is significantly high accuracy compared with the previous studies, in addition to the high temporal resolution.
Although the VR value of this method is set considerably lower than that of the previous study (VR=10 for this study), we could increase detection number and the spatial distribution without increasing the artificial events number. Furthermore, we developed our method by using the dense virtual source grids (horizontal travel distance of 5 km) so we could increase the detection number and the spatial distribution compared with using travel distance of 10 km for the same method.
We tested our method for Kii, Tokai and we divided Shikoku for two areas Western and Eastern, For Kii and Tokai we could improve our results in the future by using the unlimited data and change the parameters, but as a preliminary analysis, our method could be very effective in these regions for future analysis.

For Western and Eastern Shikoku, we could save analyzing time and make the detection more accurate spatially by divide the whole Shikoku religion for two parts.
For data analysis from 2011 to 2015, the detection number of VLFE activity and their seismic moment values were very low compared with the VLFEs activity in 2006 and 2007, although we tried to improve our results by changing the parameters, we couldn't improve the results, we will do one more try as a future plan for these time periods by using F-net data instead of using HI- net data (data used in this study), if we couldn't increase the detection number we will interpret the results as a natural phenomenon which will be very important result -if we could fix- toward earthquakes prediction in Nankai trough.

From the comparison between VLFE and tremors, we found that VLFE also is a phenomenon corresponding to tremor RTR, where the VLFEs migrated rapidly back in the same time and space as the tremor rapid reversal occurred. For the spatiotemporal distribution of the two phenomena there are tremor clusters with or without VLFE depending on active phase, also VLFE is active more rapidly than tremor, as well as we noticed that VLFE activities are not correlated with tremor activity both in space and time in rare cases, although in most cases VLFE are located within the tremor area and the previous studies showed that the occurrence of the tremors just located where the tremor is located and VLFE activity is correlated with tremor activity both in space and time.

[Ghosh et al, 2015], but in another study, Hutchison and Ghosh (2016) have found that VLFE

and strong tremor activity are not spatially coincident in Cascadia. This finding challenges our current understanding of the dynamic relationship between the different types of slow earthquakes. So, we need more analysis in the future to check if these events are real VLFE events or not.

This Method could be developed to be an automatic real-time detection system for VLFE. However, in this study, we analyzed only two active periods as the main analysis and the other periods need to confirm the results in the future by using F-net data instead of Hi-net data for activity after 2011 as well we need to confirm the possibility of uncorrelated VLFE events with NVT in some cases by study this event and confirm them as a real VLFE activities. It is expected that further features on VLFEs and the relationship between slow earthquakes will be discovered by conducting analysis for several periods using this method in the same region and by examining the characteristics of individual VLFEs in detail.as well as apply this method to other regions in Nankai trough such as Tokai and kill peninsula, because as the test analysis results in this region showed possible effective results in the future. As a result, the study of VLFEs and the relationship with tremor could give a clear understanding of the characteristics of the slow earthquakes in Southwest Japan and other subduction zones around the world.

Summary

The non-volcanic seismic tremor (NVT) was discovered as well as very low-frequency earthquakes (VLFE) were observed in the Nankai Trough subduction zone southwest Japan.

In this study, we detect very low-frequency earthquakes VLFE in tremor episodic using a new method in southwest Japan and then study the spatiotemporal relationship between the two phenomena. Our method showed a high capability of detection and could detect new and small events that the conventional method could not detect, we used a dense virtual source grid and applied the new detection method of VLFE which depends on calculating the average cross-correlation (cc) between observed and Synthetic seismogram in order to increase the detection number and spatial distribution of VLFE in Shikoku region and as a first step to study and improve our understanding of the unknown relationship between VLFE and the tremor in southwest Japan.

We utilized seismic data from with 73 Hi-net seismic stations telemeter recorded in Shikoku area as the main study area and we tested the method in Kii and Tokai using 43 and 41 Hi- net stations respectively. Seismic data were filtered using 0.02–0.05 Hz band pass filter.

In the observation periods, the tremor activity occurred in 6-22 September 2006, 10-21 March 2007, 7 - 31 August 2011, 1 - 16 June 2012, 21 - 31 May 2013, 1 - 11 November 2015, 1 - 31 May 2014, 1 - 30 June 2014 and from 1to 31 July 2014 which expected to be VLFE activity periods. We used the new detection method to compare the observed and Synthetic seismogram for all the source grids by calculate average cross-correlation (cc) between them then analyzed the data for the final detection of (VLFE), virtual source grid with 5 km intervals in horizontal was used for data from 2006 and 2007 to compare with the previous results in the same periods which used grid with 10 km because, we wanted to check if we could increase the detection number and spatial distribution of VLFE by this amendment ,then we used the new dense virtual source for 2011and 2014 data analysis in order to study the relationship between VLFE and tremor. As well we tasted our method in Kii and Tokai using dense virtual source grids. In addition, we divided Shikoku area for Eastern and Western parts to check if we could increase the spatial distribution and save the analytic time.

We can say that we could increase the detection number of VLFE and the spatial distribution by using a dense grid of virtual sources. We could increase the detection number for more than 10 times compared with previous studies in Shikoku region for data in 2006 and 2007, We chose to investigate our data because the data periods include episodic tremors. We found VLFE activity in wide range during our data periods, although the total tremor lasted for more time and more space, in most cases VLFE are located within and where tremor is located, even though we noticed some VLFE events that not correlated with tremor

activity both in space and time but this suggestion needs more analysis and interpreting, if we could confirm these event as real VLFE events, this result may change our current understanding of the clear spatiotemporal relationship between tremor and VLFE as a result issued by the previous studies. we also noticed that at the same time as Rapid Tremor Reversal (RTR), VLFEs also migrate rapidly back in the opposite direction of the source movement. Furthermore, we noticed that the detection number and moment values for activity after 2011 is low compared with activity in 2006 and 2007, so we need to do more analysis in the future to confirm these results because it will be very important discovery toward earthquakes prediction in the region if the reason natural phenomena.

Although this study still need more research work in the future to confirm the new suggestion about the possible occurrence of VLFE independently from NVT in space and time ,as well to confirm the reason of the low detection number in all results after 2011 , But the current results could give a clear understanding of the characteristics of VLFE and NVT in Nankai Trough which might be important for regular small and large earthquakes prediction in the region, and that might help the scientists to develop better earthquake prediction models in the future in Nankai and other subduction zones around the world.

References

Ando, M. (1975), Source mechanisms and tectonic significance of historical earthquakes along. the Nankai trough, Japan, Tectonophysics, 27 (2), 119-140, doi: 10.1016 / 0040-1951(75) 90102-X.

Ando, M., Y. Tu, H. Kumagai, Y. Yamanaka, and C.-H. Lin (2012), Very low frequency earthquakes along the Ryukyu subduction zone, Geophys. Res. Lett., 39, L04303, doi:10.1029/2011GL050559.

Annoura, S., K. Obara, and T. Maeda(2016),Total energy of deep low-frequency tremor in the Nankai subduction zone, southwest Japan, Geophys. Res. Lett., 43, 2562–2567, doi:10.1002/2016GL067780.

Asano, Y., K. Obara, and Y. Ito (2008), Spatiotemporal distribution of very-low frequency earthquakes in tokachi-oki near the junction of the kuril and japan trenches revealed by using array signal processing, earth planets space, 60.

Baba, T., Y. Tanioka, P. R. Cummins, and K. Uhira (2002), The slip distribution of the 1946 Nankai earthquake estimated from tsunami inversion using a new plate model, Physics of the Earth and Planetary Interiors, 132(1-3), 59-73, doi: 10.1016/S0031-9201(02)00044-4.

Brown. JR, Beroza. GC, Satoshi Ide, Kazuaki Ohta, Shelly. DR, Schwartz. SY, Wolfgang Rabbel, Martin Thorwart, and Honn Kao (2009) Deep low-frequency earthquakes in tremor localize to the plate interface in multiple subduction zones, GEOPHYSICAL RESEARCH LETTERS, VOL. 36, L19306, doi:10.1029/2009GL040027.

Ghosh, A., E. Huesca-Perez, E.E. Brodsky, and Y. Ito (2015), Very low frequency earthquakes (VLFEs) in Cascadia migrate with tremor, Geophys. Res. Lett., 42, doi:10.1002/2015GL063286.

Herrmann, R. B. (2013), Computer Programs in Seismology: An Evolving Tool for Instruction and Research, Seismological Research Letters, 84(6), 1081-1088, doi:10.1785/0220110096.

Hirose, F., J. Nakajima, and A. Hasegawa (2008), Three-dimensional seismic velocity structure and configuration of the Philippine Sea slab in southwestern Japan estimated by double-difference tomography, Journal of Geophysical Research: Solid Earth, 113 (B9), B09315, doi: 10.1029/2007JB005274.

Houston, H., B.G. Delbridge, A.G. Wech, and K.C. Creager (2011), Rapid tremor reversals in Cascadia generated by a weakened plate interface, Nature Geosci, 4(6), 404-409, doi:10.1038/ngeo1157.

Hutchison, A.A., and A. Ghosh (2016), Very low frequency earthquakes spatiotemporally asynchronous with strong tremor during the 2014 episodic tremor and slip event in Cascadia, Geophys. Res. Lett., 43, 6876–6882, doi:10.1002/2016GL069750.

Ito, Y., and K. Obara (2006), Very low frequency earthquakes within accretionary prisms are very low stress-drop earthquakes, Geophys. Res. Lett., 33, L09302, doi:10.1029/2006GL025883.

Ito, Y., K. Obara, K. Shiomi, S. Sekine, and H. Hirose (2007), Slow earthquakes coincident with episodic tremors and slow slip events, Science, 315, 503–506, doi:10.1126/science.1134454.

Ito, Y., K. Obara, T. Matsuzawa, and T. Maeda (2009), Very low frequency earthquakes related to small asperities on the plate boundary interface at the locked to aseismic transition, J. Geophys. Res., 114, B00A13, doi:10.1029/2008JB006036.

Kreemer, C., W.E. Holt, and A.J. Haines (2003), An integrated global model of present-day plate motions and plate boundary deformation, Geophysical Journal International, 154(1), 8-34, doi:10.1046/j.1365-246X.2003.01917. x.

Liua, X., D. Zhaoa, L. Sanzhong (2013), Seismic imaging of the Southwest Japan arc from the Nankai trough to the Japan Sea, Physics of the Earth and Planetary Interiors, https://doi.org/10.1016/j.pepi.2013.01.003.

Matsuzawa, T., Y. Asano, and K. Obara (2015), Very low frequency earthquakes off the Pacific coast of Tohoku, Japan, Geophys. Res. Lett., 42, 4318–4325, doi:10.1002/2015GL063959

Miyazaki, S., and K. Heki (2001), Crustal velocity field of southwest Japan: Subduction and arc-arc collision, Journal of Geophysical Research-Solid Earth, 106(B3), 4305-4326, doi:10.1029/2000jb900312.

Matsuzawa, T., H. Hirose, B. Shibazaki, and K. Obara (2010), Modeling short- and long-term slow slip events in the seismic cycles of large subduction earthquakes, Journal of Geophysical Research: Solid Earth, 115(B12), B12301, doi:10.1029/ 2010JB007566.

Nakamura, M., and N. Sunagawa (2015), Activation of very low frequency earthquakes by slow slip events in the Ryukyu Trench, Geophys. Res. Lett., 42, 1076–1082, doi:10.1002/2014GL062929.

Nakajima, J., and A. Hasegawa (2007), Subduction of the Philippine Sea plate beneath southwestern Japan: Slab geometry and its relationship to arc magmatism, Journal of Geophysical Research: Solid Earth, 112(B8), B08306, doi:10.1029/2006JB004770.

Nizato. T (2014), Master thesis, Hiroshima university, 南海トラフ沈み込み帯における深部超低周波地震の自動モニタリング2014年広島大学大学院理学研究科 地球惑星システム学専攻 地球ダイナミクスグループ, 仁里 太郎

Obara, K.(2002) Nonvolcanic Deep Tremor Associated with Subduction in Southwest Japan Science, New Series, Vol. 296, No. 5573 (May 31, 2002), pp. 1679-1681

Obara, K., Y. Haryu, Y. Ito, and K. Shiomi (2004), Low frequency events occurred during the sequence of aftershock activity of the 2003Tokachi-Oki earthquake; a dynamic process of the tectonic erosion by subducted seamount, Earth Planets Space, 56, 347–351.

Obara, K., Ito, Y., (2005) Very low frequency earthquakes excited by the 2004 off the Kii peninsula earthquakes: a dynamic deformation process in the large accretionary prism. Earth Planets Space 57, 321–326.

Obara, K. (2011), Characteristics and interactions between non-volcanic tremor and related slow earthquakes in the Nankai subduction zone,

Obara.K. Kato.A. (2016), Connecting slow earthquakes to huge earthquakes, Science Online Edition: 2016/07/15 (Japan time), doi: 10.1126/science. aaf1512.southwest Japan, J. Geodyn., 52, 229–248, doi: 10.1016/j.jog.2011.04.002.

Rogers, G., and H. Dragert (2003), Episodic tremor and slip on the Cascadia subduction zone: The chatter of silent slip, Science, 300(5627), 1942–1943, doi:10.1126/science.1084783.

Schwartz, S., and J. Rokosky (2007), Slow slip events and seismic tremor at circum-Pacific subduction zones, Rev. Geophys., 45, RG3004, doi:10.1029/2006R6000208.

Sugioka, H., Okamato, T., Nakamura, T., Ishihara, Y., Ito, A., Obana, K., Kinoshita, M., Nakahigashi, K., Shinohara, M., Fukao, Y., (2012), Tsunamigenic potential of the shallow subduction plate boundary inferred from slow seismic slip. Nat. Geosci. 5, 414–418. http://dx.doi.org/10.1038/ngeo1466.

Sella, G. F., T.H. Dixon, and A. Mao (2002), REVEL: A model for Recent plate velocities from space geodesy, Journal of Geophysical Research: Solid Earth, 107(B4), ETG 11-11-ETG 11-30, doi:10.1029/2000JB000033.

Sweet, J.R., K.C. Creager, and H. Houston (2014), A family of repeating low-frequency earthquakes at the downdip edge of tremor and slip,Geochem. Geophys. Geosyst., 15, 3713–3721, doi:10.1002/2014GC005449.

Suda, N., R. Nakata, and T. Kusumi (2009), An automatic monitoring system for nonvolcanic tremors in southwest Japan, Journal of Geophysical Research-Solid Earth, 114, doi:10.1029/2008jb006060.

Takeo, A., K. Idehara, R. Iritani, T. Tonegawa, Y. Nagaoka, K. Nishida, H. Kawakatsu, S. Tanaka, K. Miyakawa, T. Iidaka, M. Obayashi, H. Tsuruoka, K. Shiomi, K. Obara (2010), Very broadband analysis of a swarm of very low frequency earthquakes and tremors beneath Kii Peninsula, SW Japan, Geophysical Research Letters, 37, doi:10.1029/2010gl042586.

Tsuruoka, H., H. Kawakatsu, and T. Urabe (2009), GRiD MT (grid-based real-time determination of moment tensors) monitoring the long-period seismic wavefield, Physics of the Earth and Planetary Interiors, 175(1-2), 8-16, doi:10.1016/j.pepi.2008.02.014.

To, A., Obana. K, H. Sugioka, E. Araki, N. Takahashi, and Y. Fukao, (2015) Small size very low frequency earthquakes in the Nankai accretionary prism, following the 2011 Tohoku-Oki earthquake http://dx.doi.org/10.1016/j.pepi.2015.04.007.

Walter, J.I., S.Y. Schwartz, M. Protti, and V. Gonzalez (2013), The synchronous occurrence of shallow tremor and very low frequency earthquakes offshore of the Nicoya Peninsula, Costa Rica, Geophysical Research Letters, 40(8), 1517-1522, doi:10.1002/grl.50213.